INFORMATION TO USERS

This manuscript has been reproduced from the microfilm master. UMI films the text directly from the original or copy submitted. Thus, some thesis and dissertation copies are in typewriter face, while others may be from any type of computer printer.

The quality of this reproduction is dependent upon the quality of the copy submitted. Broken or indistinct print, colored or poor quality illustrations and photographs, print bleedthrough, substandard margins, and improper alignment can adversely affect reproduction.

In the unlikely event that the author did not send UMI a complete manuscript and there are missing pages, these will be noted. Also, if unauthorized copyright material had to be removed, a note will indicate the deletion.

Oversize materials (e.g., maps, drawings, charts) are reproduced by sectioning the original, beginning at the upper left-hand corner and continuing from left to right in equal sections with small overlaps.

Photographs included in the original manuscript have been reproduced xerographically in this copy. Higher quality 6" x 9" black and white photographic prints are available for any photographs or illustrations appearing in this copy for an additional charge. Contact UMI directly to order.

Bell & Howell Information and Learning
300 North Zeeb Road, Ann Arbor, MI 48106-1346 USA
800-521-0600

Correlating and measuring DNA damage and mutations

by

Gopaul Kotturi
B.A.Sc., University of Alberta, 1986
M.A.Sc. University of Waterloo, 1989

A Dissertation Submitted in Partial Fulfillment of the
Requirements for the Degree of

DOCTOR OF PHILOSOPHY

in the Department of Biology

Dr. Barry W. Glickman. Supervisor (Dept. of Biology, University of Victoria)

Dr. Ben F. Koop, Departmental Member (Dept. of Biology, University of Victoria)

Dr. Johan G. de Boer, Departmental Member (Dept. of Biology, University of Victoria)

Dr. Francis E. Nano, Outside Member (Dept. of Biochemistry and Microbiology, University of Victoria)

Dr. Elliot A. Drobetsky (Centre de Recherche, Hopital Maisonneuve-Rosemont, University of Montreal)

© Gopaul Kotturi, 2000
University of Victoria

All rights reserved. This dissertation may not be reproduced in whole or in part, by photocopying or other means, without the permission of the author.

Supervisor: Dr. Barry W. Glickman

ABSTRACT

Mutations are generally thought to be targeted events. The distribution of mutations is based upon the initial original deposition of DNA damage and the fidelity and efficiency of repair of this damage. These factors are dependent on the primary site of DNA modification and the surrounding nucleotides (i.e., mutation is "context sensitive"). To better understand mutagenesis, I measured DNA damage and/or mutation at the DNA sequence level, then considered the impact of mutation location and the surrounding nucleotide environment. The selected mutagens, ultraviolet light (UV) and benzo(a)pyrene [B(a)P], were chosen because they produce well-characterized lesions and are environmentally relevant.

UVC (254nm) light-induced DNA damage is well documented. UVC produces a characteristic spectrum of mutations. The predominant UV-induced mutations are C → T transitions occurring at TC or CC sites, as well as CC → TT tandem transitions. The latter class of mutation is considered the hallmark of UV mutagenesis. Quantitatively speaking, the primary types of UV-induced DNA lesions are cyclobutane pyrimidine dimers (CPDs) and the 6-4 pyrimidine/pyrimidone (64PyPy). These are also the suspected predominant pre-mutagenic lesions. Each lesion was independently measured at the DNA sequence level in a defined region of DNA. The pattern of UVC-induced DNA damage revealed a complex induction pattern. The flanking DNA nucleotides partially influenced the pattern of damage deposition. Sites where C → T transitions and CC → TT

transitions were recovered at high frequencies were also frequently damaged. Thus, at these sites, mutation fixation was potentially more influenced by initial DNA damage than the rate of DNA repair.

Two other components of the UV spectrum [UVB (290-320 nm) and UVA (320-400 nm)] are more environmentally relevant than UVC since UVB and UVA reach the surface of the earth. The results of UVC experiments were used as a guide to interpret the results obtained using UVB since direct light absorption by DNA has been shown to be one of the main biological effect at both wavelengths. The model that was chosen for the studies was an *in vivo* transgenic rodent mutagenesis assay. The research presented in the thesis represents one of the first studies to characterize UV-induced mutation at the DNA sequence level in rodent skin. The backs of female C57Bl/6 *lacI* transgenic mice were shaved and exposed to either UVB or UVA light. UVB was found to be significantly more mutagenic than UVA. The UVB-induced mutation spectrum was characterized by C $\rightarrow$ T transitions at dipyrimidine sites, implicating CPD and/or 64PyPy lesions as premutational DNA lesions. The majority of UVA-induced mutations was C $\rightarrow$ T transitions at dipyrimidines sites and hence, as with UVB-induced mutation, attributed to CPDs and 64PyPy. In the UVA-dose response experiments, the induced mutant frequency was lower than expected at higher doses. A statistically significant increase in putative clonal expansion suggested that skin cells might have undergone cell killing followed by repopulation.

In a final study, C57Bl/6 *lacI* transgenic male mice were intraperitoneally injected with the mutagen B(a)P at doses of 0, 62.5, 125, 250, and 500 mg/kg. This resulted in a

linear increase in mutation frequency (4.8 to $53x10^{-5}$). All mutations increased at GC basepairs and not AT basepairs following B(a)P treatment. This was consistent with models suggesting guanosine adducts to be mutagenic lesions.

In conclusion, the transgenic *lacI* mouse mutagenesis model was a sensitive target for *in vivo* mutagenesis from UVB, UVA and benzo(a)pyrene exposures. The system detected class-specific mutation frequency differences and increases in cell proliferation after mutagen exposure. With a further refinement of techniques, the correlation of DNA damage and mutation will allow even more exquisite studies.

Examiners:

Dr. Barry W. Glickman, Supervisor (Dept. of Biology, University of Victoria)

Dr. Johan G. de Boer, Departmental Member (Dept. of Biology, University of Victoria)

Dr. Ben F. Koop, Departmental Member (Dept. of Biology, University of Victoria)

Dr. Francis E. Nano, Outside Member (Dept. of Microbiology and Biochemistry, University of Victoria)

Dr. Elliot A. Drobetsky (Centre de Recherche, Hopital Maisonneuve-Rosemont, University of Montreal)

Table of Contents

ABSTRACT ii

Table of Contents v

List of Abbreviations viii

List of Tables x

List of Figures xi

Acknowledgments xii

Dedications xiii

Layperson's Introduction 1

CHAPTER I – Background 9

1. FROM DNA DAMAGE TO MUTATION 9
1.1. INTRODUCTION 9
1.1.1. Ultraviolet light 9
1.1.2. Polyaromatic hydrocarbons - benzo[a]pyrene 17

2. TRANSGENIC RODENT MUTAGENESIS ASSAYS 21

CHAPTER II . DNA damage analysis using an automated DNA sequencer 31

1. INTRODUCTION 31
1.1. Development of Automated DNA Sequencers. 32
1.2. Ancillary applications of Automated DNA sequencers. 33

2. METHODS 35
2.1. Template generation 36
2.2 Internal Standards and Sequencing Reactions 39
2.3. DNA Damage Induction and Fragment Cleavage 41
2.4. Electrophoresis of DNA samples 42
2.5. Data Analysis 46
2.6. Relative Mobility of DNA fragments. 51

3. DISCUSSION 53
3.1. Developing Technologies 54

4. CONCLUSIONS 55

CHAPTER III. Correlation of UV-Induced mutational spectra and the *in vitro* damage distribution at the human *hprt* gene. 57

1. INTRODUCTION 57

2. MATERIALS AND METHODS 60
2.1. Template generation 61
2.2. Template purification 61
2.3. Internal Standards and Sequencing Reactions 63
2.4. DNA Damage Induction and Fragment Cleavage 65
2.5. Electrophoresis of DNA samples 66
2.6. Analysis of data 68

3. RESULTS 69
3.1. Distribution of UV-induced photoproducts 69
3.2. Formation of UV-induced photoproducts at particular dipyrimidine sites. 72

4. DISCUSSION 75

5. ACKNOWLEDGMENTS 81

CHAPTER IV. UVB-INDUCED MUTATIONAL SPECTRA IN THE *LACI* GENE FROM TRANSGENIC MOUSE SKIN 82

1. INTRODUCTION 82

2. MATERIALS AND METHODS 84
2.1. Exposure to UVB light 84
2.2. Mutant Frequencies 86
2.3. Mutational Spectra 87

3. RESULTS 87
3.1. Mutant Frequency at the *lacI* transgene in mouse skin 87
3.2. Mutagenic Specificity of UVB-induced and spontaneous mutations 88

4. DISCUSSION AND CONCLUSIONS 98

CHAPTER V. UVA-INDUCED MUTATIONAL SPECTRA IN THE *LACI* GENE FROM TRANSGENIC MOUSE SKIN 105

1. INTRODUCTION 106

2. MATERIAL AND METHODS 109
2.1. Exposures 109
2.2. Mutant Frequencies 109
2.3. Mutational Spectra 111
2.4. Clonal Expansion 112

3. RESULTS 112

3.1. Mutant Frequencies 112
3.2. Mutation Frequencies 113
3.3. Clonal Expansions 113
3.4. Mutational Spectra 123

4. DISCUSSION 124
4.1. UVA light is mutagenic in the skin of mice 124
4.2. Dose response in the *lacI* transgene following UVA irradiation 128
4.3. UVA-Induced Mutation Spectra 130

5. CONCLUSIONS 132

CHAPTER VI. BENZO(a)PYRENE-INDUCED DOSE RESPONSE OF THE MUTANT FREQUENCY, MUTATIONAL FREQUENCY AND MUTATIONAL SPECTRA IN THE *LACI* TRANSGENE OF BIG BLUE® C57BL/6 MALE MOUSE LIVER. 133

1. INTRODUCTION 133

2. MATERIAL AND METHODS 136
2.1. Chemicals 136
2.2. Treatment of mice 136
2.3. Liver DNA isolation 137
2.4. Screening for *lacI*⁻ mutants 138
2.5. DNA characterization of *lacI*⁻ mutants 139
2.6. Statistical Analysis 140

3. RESULTS 141
3.1. B(a)P-induced mutant and mutation frequencies in the liver of C557Bl/6 Big Blue® male mice. 141
3.2. Clonal expansion of B(a)P-induced mutagenesis 145
3.3. Class-specific mutation frequencies 145

4. DISCUSSION 157
4.1. B(a)P-induced Mutant Frequency 157
4.2. Biological Interpretation of B(a)P-Induced Mutagenesis. 161

5. CONCLUSIONS 166

CHAPTER VII. DISCUSSION AND FUTURE DIRECTIONS 167

1. GENERAL DISCUSSION 167

2. MUTATION-BASED TRANSGENIC RODENT MODELS 175

3. TUMOR TRANSGENIC RODENT MODELS 178

VIII. Bibliography 183

List of Abbreviations

64PyPy	Pyrimidine <6-4> pyrimidone photoproduct
A	Adenosine
AAF	Acetylaminofluorene
AF	*N*-2-aminofluorene
aprt	adenosine phosphoribosyltransferase
ALF	Automated laser fluorescent
ANOVA	Analysis of variance
AU	Absorbance units
B(a)P	benzo(a)pyrene
bp	Base pair
C	Cytosine
cDNA	Complementary DNA
CE	Capillary electrophoresis
CEH	Center for Environmental Health
CHO	Chinese hamster ovary
cis-DDP	*Cis*-diamine dichloroplatinum
complex	complex mutation
cos	cohesive end sites
CPD	Cyclobutane pyrimidine dimer
dbl subst	double substitution
ddH2O	distilled deionized water
ddNTP	Dideoxy nucleotide triphosphate
del	deletion
DMSO	Dimethyl sulfoxide
DNA	Deoxyribonucleic acid
dNTP	Deoxynucleotide triphosphate
DTT	Dithiotriol
dupl	duplication
E. coli	*Escherichia coli*
EMS	ethyl methane sulfonate
ES	endonuclease sensitive site
FE	Fisher's Exact test
fs	frameshift (either the insertion or deletion of 1 basepair)
FU	Fluorescent units
G	Guanosine
GCA	Generalized Cochran Armitage test
GMP	Guanosine monophosphate
H	either adenosine, cytosine, or thymidine
hprt (HPRT)	Hypoxanthine-guanine phosphoribosyltransferase

IMP	Inosine monophosphate
IS-1	Internal standard – 1
IS-2	Internal standard – 2
IS-3	Internal standard – 3
LSD	Least significant difference
MF	Mutant frequency
MnF	Mutation frequency
mRNA	Messenger ribonucleic acid
N	Normal
NER	Nucleotide excision repair
nt	nucleotide
NTS	Non-transcribed strand
PCR	Polymerase chain reaction
PE/ABD	Perkin Elmer / Applied Biosystems Division
pol	Polymerase
PRPP	5-Phosphoribose1-pyrophosphate
QPCR	Quantitative polymerase chain reaction
R	adenosine or guanosine
RFLP	Restriction fragment length polymorphism
RFU	Relative fluorescent units
RNA	Ribonucleic acid
SD	Standard deviation
SE	Standard error
SSCPA	Single strand conformation polymorphism assay
T	Thymidine
TCR	transcription-coupled repair
TDBP	Tris (2,3-dibromopropyl)phosphate
tRNA	Transfer ribonucleic acid
TS	Transcribed strand
UVA	Ultraviolet A wavelength range (320-400 nm)
UVB	Ultraviolet B wavelength range (290-320nm)
UVC	Ultraviolet C wavelength range (254 nm)
X-gal	5-bromo-4-chloro-3-indolyl-b-D-galactopyranoside
XP	Xeroderma pigmentosum
XPA	Xeroderma pigmentosum complementation group A
XPV	Xeroderma pigmentosum variant
Y	cytosine or thymidine
ΔG	Gibbs free energy of formation

List of Tables

Table I. Comparison of mutational spectra. These data are for the *lacI* gene in *E. coli*. Only the DNA binding region (nucleotide 29-206) is considered, but the data between brackets for B[*a*]P are for the whole gene. 11
Table II. Sequence context of mutational events following EMS (Pienkowska *et al.*, 1993) or UV (Schaaper *et al.*, 1987) treatment for the sites with 5% or more of the mutations. The mutated base is underlined. 12
Table III. Comparison of the numbers of mutants recovered from the *lacI* gene of *E. coli* and the *aprt* gene of Chinese hamster cells after exposure to UV and benzo[*a*]pyrenediolepoxide. 14
Table IV. Summary of the mutagenic and bypass effect obtained with site-specific and stereo-specific UV-induced DNA lesions transfected into *E. coli*. The bypass rate was calculated by percentage of vectors that were replicated when compared with controls. The percent error was determined as the ratio of plasmids carrying the altered and the original sequence. The fraction of the predominant mutation reflected the fraction of the total mutants recovered. In the case of the TT 64PyPy, 89 of 91, or 98% of the mutants were the transition, 3'T → C) 15
Table V. A list of various automated DNA sequencers and associated integration and peak identification software. 34
Table VI. Distribution of various dipyrimidine sites between the non-transcribed (NTS) and transcribed (TS) strand. 60
Table VII. The effect of the 5' nucleotide of a 5'-TC-3' dipyrimidine on the recovery of 64PyPy. 74
Table VIII. The effect of the 3' nucleotide of a 5'-TC-3' dipyrimidine on the recovery of 64PyPy (please see notes from Table VII). 74
Table IX. UVB is mutagenic in the skin of *lacI* mice. 89
Table X. *lacI* mutations in skin from untreated or UVB-treated transgenic mice. 90
Table XI. Summary of *lacI* mutations in untreated, UVB-treated or full spectrum-treated mouse skin. 96
Table XII. Sequence Specificity of GC → AT Transitions. 97
Table XIII. UVA is mutagenic in skin from *lacI* transgenic mice. 114
Table XIV. UVA mutagenicity is dose-dependent in skin of *lacI* mice. 115
Table XV. *lacI* mutations in skin from UVA-treated (800J/cm^2) or untreated transgenic mice. 116
Table XVI. Summary of possible clonal expansion effects in untreated and UVA-treated skin. 122
Table XVII. Summary of *lacI* mutations in untreated and UVA-treated skin by mutation class. 125
Table XVIII. Sequence specificity of GC → AT transitions in UVA-treated mouse skin. 126
Table XIX. Mutant frequencies (MF) in liver from untreated and B(*a*)P-treated mice. 143
Table XX. Analysis of variance testing the differences of the means of mutant frequencies from each dose of B(a)P in the liver of the C57Bl/6 Big Blue® mice. 144
Table XXI. *LacI* mutations in the liver from untreated and B(a)P-treated C57Bl/6 male mice. 146
Table XXII. Summary of relevant *lacI* mutations by class as a portion of the total mutation frequency. 158
Table XXIII. Monte-Carlo estimations of the Fisher's Exact test to determine the difference in mutational spectra. 162
Table XXIV. Contingency χ^2 analysis of background and B(a)P-induced (125mg/kg) mutational spectra of the liver of C57Bl/6 male mice. 163

List of Figures

Figure 1. Outline of the lambda LIZ vector used to generate transgenic mice and rats. 27
Figure 2. The regulation of lacZ gene expression by the Lac repressor. The Lac repressor synthesized by the *lacI* gene forms a tetramer, which binds to the lacO sequence. A) A colourless plaque is generated by an intact Lac repressor. B) A mutant Lac repressor leads to a blue plaque in the presence of the chromogenic substrate, X-gal. 28
Figure 3. Illustration of the resolution from various automated DNA sequencers and electrophoretic conditions. All frames show the same piperidine cleavage products induced by 1.2 kJ/m^2 of UV (254 nm) light in the transcribed strand of the human *hprt* cDNA. The electropherograms are the raw data from automated DNA sequencers. Frame 'a' is an electropherogram of a sample run on a PE/ABD 373A with 24 cm 'well-to-detector' plates and a 6% polyacrylamide gel and other electrophoretic conditions recommended by PE/ABD. Frames 'b-d' show data from a Pharmacia A.L.F.™ with the common conditions of: Power = 21W, Current = 34mA, Voltage = 1500V. The electropherograms are runs at 6% polyacrylamide and 25^{0}C, 6% polyacrylamide and 40^{0}C, 12% polyacrylamide and 40^{0}C for Frames 'b', 'c', and 'd', respectively. 45
Figure 4. Distribution of piperidine cleavage products induced by 1.2 kJ/m^2 of UV (254 nm) light in the non-transcribed strand of the human *hprt* cDNA. The electropherograms are the raw data from a Pharmacia A.L.F.™ automated DNA sequencer. The DNA is resolved on a 6% polyacrylamide gel with the standard electrophoretic conditions: The fluorescent units (FU) are linear arbitrary units. Cleavage products were matched with DNA sequencing termination products in adjacent lanes to determine the base position. The control experiment is shown with the decreased line intensity. Frames 'a,b,c' show different time ranges in the same experiment. Frame 'd', as an insert to frame 'c' shows the dilution series which brings the undamaged fragment (Undam. Frag.) into the range that does not have the signal attenuation. 49
Figure 5. A flow diagram of the experimental methods indicating the major steps in the protocols. 62
Figure 6. Combined relative distribution of CPD and 64PyPy in both the non-transcribed strand and transcribed strand of the human hprt gene (bp 1 to 226). Solid bars represent the relative frequency of photoproducts as determined by peak integration. Bars located above the corresponding sequence represent the CPD distribution (UV dose = 0.5kJ/m2), while bars below the sequence represent the 64PyPy distribution (UV dose = 1.2 kJ/m2). Bars are positioned between the damaged dinucleotide. All independent point mutations are positioned directly above the corresponding base. 71
Figure 7. Relative 6-4 <PyPy> formation at 5'-TC-3' sites as a function of predicted Gibbs free energy. The Gibbs free energy was determined by the program OLIGO by centering a 24 nt oligonucleotide around the 5'-TC-3' site. 76
Figure 8. Irradiance at 0.5m using the illumination system of Oriel bulb #6271 filtered by Schott filters UG5 and GG19. 85
Figure 9. Irradiance at 0.5m using the illumination system of Oriel bulb #6271 and Schott filters UG11 and WG335. 110
Figure 10. Strategy for the use of the p53 +/- and TG.AC mouse lines for short-term bioassays to identify carcinogens (adopted from Tennant et al., 1995). 182

Acknowledgments

"The man of science appears to be the only person who has something to say just now, and the only man who does not know how to say it."

- Sir James Barrie

My educational/life journey reached this stage from the love, support and immense caring of many people. The place to start is very obvious to me and it is my loving and caring parents, Susan Kotturi and Dr. Murthi Kotturi. They were a constant source of love, which I tapped often.

For love of an exceptional variety, I can think of my two wonderful children, Sante and Yasmine. They provided a beautiful framework to explore 'another education' based in unconditional love. I am deeply grateful for them for giving me this base to use as I explore other interpersonal skills. As I watched them grow, I used their interest in life and drive to master the 'simple' aspects of life to motivate myself and complete my experiments and writing.

I am grateful to Dayle for caring for our children and who showed me alternative viewpoints and a method in which to express them.

To my sister, Maya, for providing support and love when it counted the most.

My supervisor, Dr. Barry Glickman, or 'Barry' is a mentor and friend. He has provided me support and opportunities and is a teacher in his own right. In my mind, a teacher is one who transfers information, knowledge and opinion and he does this. There were several times during my 'tenure' as a graduate student, which may have caused him to doubt me, and I appreciate the time and latitude to complete my degree.

When I think of unconditional friendship, Peixoto da Cruz, Pat Steele and Pauline Tymchuk come to mind. I would be in a different mental frame if I did not have their supportive hugs and thoughts.

Johan de Boer, Dave Walsh, Jana Kangas, Ken Sojonky, Greg Stuart, James Holcroft, Haiyan Yang, Pam Warrington, and Heather Erfle provided a great 'lacI' group which were the intellectual and practical framework which allowed the labour and interesting intensive 'Big Blue' work to be possible.

Barry Ford and John Curry helped me from the start and offered practical advice throughout my studies for which I am very grateful.

I wish to express to thank my PhD committee to whom I am grateful for reading this entire thing and bearing with my self-expression.

My family friends and support network also provided a 'safety net' for me to feel secure in moving through the challenges of balancing parental and professional responsibilities. Of special note are Nigel and Judith Atkin. Nigel for his beliefs and energies and Judith for caring and statements like 'Oh well, just laugh about it and it'll feel better!'

I lastly wish to thank the Canadian education system to provide me with the opportunity of this formal education.

Dedications

This thesis is dedicated to:

My mother, **Susan,** *and my father,* **Murthi**, *for an example of what can be accomplished and for values of love and sacrifice.*

My two shining stars, **Sante** *and* **Yasmine** *who love me and continue to warm my heart.*

Layperson's Introduction

"There is no concept so difficult that it can not be explained in a simple way."
- Albert Einstein

The purpose of research described in this thesis is to explore how chemical and physical agents, such as benzo(a)pyrene and ultraviolet light, may exert deleterious effects on living organisms. Ultraviolet light has been subdivided into three classes depending on its wavelength: UVA (320-400 nm), UVB (290-320) and UVC (240-290 nm). In this thesis I do not refer to UVC as a range of wavelengths, rather as monochromatic light of wavelength (254nm). This distinction is important because the monochromatic source has a much better defined biological action. In addition UVC (254nm), or germicidal UV has been the most historically widely-used light source because it has been used to kill bacteria. In contrast UVA, which is a major component of sunlight, has received relatively little attention until recently. The use of "UVA lamps" at indoor tanning salons has led to an increased interest in studying this component of sunlight. The more intense exposure to UVA at tanning salons has raised questions as to its contribution to skin cancer and skin aging. Some "UVA lamps" may emit a small portion of UVB and also may contribute to the effects of "UVA lamps". Direct exposure to UVB light has been considered to be more of a health concern than exposure to UVA light. However, the impact of UVB from sunlight is mitigated because UVB is largely filtered by the ozone layer. UVC from sunlight is not a concern because it is vastly

reduced. However, in the future, UVB may become more of a concern if the ozone layer continues to thin because the more UVB will reach the surface of the earth and create a greater risk to organisms.

The increased risk can be explained by the different biological absorption patterns of UVA and UVB. One of UV light characteristics is its ability to directly act on DNA. Different wavelengths have different efficiencies of energy absorption by DNA. DNA absorbs light relatively efficiently at shorter wavelengths up until 280 nm and less efficiently between 280 and 300 nm. However, as the wavelength of UV light increases beyond 300 nm, absorption drops logarithmically. At the UVA / UVB border (320 nm) DNA still directly absorbs a small amount of energy. At light wavelengths greater than 340 nm DNA does not absorb appreciable energy. Ozone effectively filters light below 320 nm. As the ozone layer is depleted, shorter wavelength light at the crucial UVA/UVB border will not be filtered. Since DNA absorption is affected logarithmically by light near this border, a small change in light flux may have tremendously increased biological consequences.

Environmental mutagens such as UV light may have many types of effects on organisms. In this thesis, two major endpoints were studied that relate to the information storage banks (DNA) of cells. Specifically, these endpoints are DNA damage and DNA mutation. DNA damage is any change or modification to the molecular structure of the genetic material (DNA). For example when DNA absorbs energy from UV light, new chemical bonds may be formed which disrupt the normal three-dimensional structure of the DNA. The distortion of the DNA double helix may lead DNA repair enzymes to

recognize the damage. These enzymes will hopefully correct the alterations. If the DNA damage is not repaired before it is time to create a new copy of the DNA for the daughter cells, the DNA damage may have a structure which causes an error in the DNA copying. If the error does not get noticed and corrected, the change may be permanent (i.e., the mutation becomes fixed).

A heritable mutation is a change in the DNA sequence of a germline cell (e.g., spermatocyte). A somatic mutation is a change in DNA sequence of a tissue other than germ cells. Mutations are permanent changes in the DNA sequence. If by chance a mutation occurs at a point where critical information of a cell is stored, the cell may have an altered function. Over a period of time these mutations accumulate and they can cause a wide variety of effects such as cell death or uncontrolled growth. Cancer may occur as a result of uncontrolled growth, although there are many other factors. Thus understanding DNA damage, the mechanisms that have evolved to remove the DNA damage (e.g., DNA repair systems) and mutations are all important as this may contribute to understanding important diseases such as cancer. All the processes from the initial DNA damage through repair to mutation fixation are extremely complicated and interesting to research.

Chapters II to V describe two general studies which, together, may illuminate one of the key processes involved in cancer development. The studies involved: 1) comparing the distribution of initial DNA damage from UV light with the distribution of UV-induced mutations; and 2) determining the nature of UV-induced mutations recovered in the skin. In the first study, DNA damage was measured at individual positions in a gene and compared to the number of mutations occurring at that position. The relationship

between the DNA lesions and mutations has many facets. It is assumed that if sites with the highest level of DNA damage are identical to sites of the most frequently recovered mutations, then the high initial DNA damage was an important first step of the mutagenic process. After the high initial DNA damage, DNA repair enzymes presumably were unable to repair all of the damage at these sites. The remaining DNA damage may predispose these sites to mutations at during the copying or replication of the DNA.

For example, UVC(254nm)/UVB induces many types of DNA damage but two kinds predominate: 1) pyrimidine <6-4> pyrimidone photoproducts (64PyPy); and 2) cyclobutane pyrimidine dimers (CPD). Each of these lesions was measured individually to determine the distribution of DNA damage along a segment of DNA. The individual distributions were compared to location and frequency of mutations recovered along the same segment. If only one type of DNA damage was frequently recovered at mutated positions, it might infer that only this type of DNA damage may be responsible for the replications errors. A sunscreen could be designed to preferentially eliminate that type of DNA damage which could be a practical result of this research. In the DNA segment there were two frequently mutated positions among many other sites with only one or a few mutations. Each of the frequently mutated sites was correlated with high initial DNA damage. However, CPDs were predominantly measured at one site and 64PyPy were most frequent at the other site. Thus a high frequency of DNA damage may have lead to a high recovery of mutations, and each type of DNA damage can potentially play a role in UVC-induced mutation.

In Chapters IV and V, the UV experiments were extended to an animal (rodent)

model to investigate *in vivo* mutagenesis. This mouse model is transgenic (i.e., the mice have an extra piece of DNA in every nucleated cell). This extra piece of DNA, or the transgene, is derived from a bacterial virus known as lambda phage. The lambda phage DNA can be efficiently recovered, and screened for mutations. The mutations are counted and further characterized by DNA sequencing. The transgenic rodent mutagenesis assay has the great advantage of measuring mutations in every tissue, which was not possible before this assay was developed. The ability to detect of somatic mutations in every tissue means that a vast amount of knowledge can be gained about the nature and distribution of mutations, and how they may be involved in cancer.

The transgenic rodent mutation assay was implemented to study the *in vivo* mutagenic effects of UVA and UVB light in the skin of mice. Chapter IV describes the results of UVB exposure to the skin of mice. UVB proved to be a potent mutagen and induced mutations that have been historically associated with UV. These predominant mutations are C $\rightarrow$ T transitions at dipyrimidine sites (i.e., CT, CC or TC) and tandem CC $\rightarrow$ TT transitions. The latter are virtually exclusively found after exposure to UV light. In fact, these normally rare mutations were commonly identified in a key cancer-related gene recovered from isolated skin cancer biopsies. After UVB exposure (9.0 J/cm^2), both the C $\rightarrow$ T transitions at dipyrimidine sites and CC $\rightarrow$ TT transitions were recovered at levels significantly above background. Since these UVB-induced mutations were easily detected and delineated from spontaneous events, the transgenic rodent skin may be useful model to test sunscreens and topical agents.

Chapter V describes results from a study where mice skin was exposed to UVA light. UVA constitutes a much greater fraction of sunlight than either UVB or UVC but has traditionally been thought to be relatively harmless. This was assumed because DNA does not efficiently absorb UVA. Recently however, studies have shown UVA to be mutagenic, and these results were confirmed by recovering hallmark mutations of UV-induced mutagenesis. UVA light appeared to induce cell proliferation because a significant number of animals each had a high than normal number of identical mutations. If, for a given animal, it has two or more identical mutations, there are two main possibilities. First, the site and type of the mutation may be very susceptible to the type of treatment. Second, one of the identical mutations may have arisen and that particular cell may have divided and increasing the number of that same identical mutation. These identical mutations are usually a small minority of the total number of mutations. Whenever they occur the assumption is the second cause is more probably. This phenomenon of multiple identical mutations from the same animal is called 'clonal expansion'. Only in the animals exposed to UVA was there an increase in clonal expansion. It was hypothesized that the increase in clonal expansion may have been a result of cell death followed by repopulation of the cells that had been exposed to UVA. This hypothesis was further supported by the type of mutations which comprised the clonal events. The clonal, or identical, mutations had a statistical increase in the number of UV-characteristic mutations (i.e., C $\rightarrow$ T transitions at dipyrimidine sites). UVA light has been shown in cell culture to induce cell death through a process called apoptosis. Apoptosis is a method the body uses to rid itself of cells in a controlled manner. The

results presented in Chapter V are consistent with the induction of apoptosis followed by a cell proliferation to repopulate the skin. Further work with experiments designed to monitor apoptosis during the animal exposures is needed to confirm these interesting results.

In Chapter VI, another classical mutagen, benzo(a)pyrene, was studied with the transgenic rodent mutagenesis assay which was described above. Benzo(a)pyrene was chosen because, similar to UV light, a great deal of data has been generated studying this compound. With the wealth of information available, it can be utilized in an in-depth analysis of the mutagenic effects of this chemical compound. UV light is primarily direct acting, however benzo(a)pyrene is not very reactive. It needs to be partially metabolized before it can react with DNA. A majority of the enzymes that transform benzo(a)pyrene into a mutagenic compound are found in the liver. A dose-response experiment was performed using liver as the target tissue. The mutant frequency and the mutational spectrum were determined in the benzo(a)pyrene treated and untreated liver of the transgenic mouse. A mutational spectrum is a collection of mutants that are characterized at the DNA sequence level. By combining the information of the mutant frequency and the mutational spectrum, and applying analysis tools, the mutation types induced by benzo(a)pyrene were determined. Only mutations that occurred at GC basepairs were recovered as a result of benzo(a)pyrene treatment. Reports of benzo(a)pyrene-induced mutations at AT basepairs were not confirmed. New statistical analysis tools were compared to existing statistical tools. The newer tools appeared to better analyze the data and provided a method to better interpret the results of the transgenic rodent mutgenic

assays.

Finally, Chapter VII presents a general discussion of the previous chapters and a discussion of the future of transgenic animals used in bioassays. The transgenic model used in these studies has a mutation endpoint. The transgenic rodent mutagenesis model showed its utility by being used to elucidate *in vivo* mutagenic processes. Two other newer transgenic models have a tumor endpoint. They have been engineered to predispose the animals to the development of tumors. Since cancer is associated with a tumor endpoint, these 'next generation' models may prove to be extremely useful. Also it should be considered that these two models could be crossed. With both tumor and mutation endpoints, more information could be obtained from a single animal. New transgenic models are rapidly increasing, as the technology for creating these animals becomes more accessible. The bioassay of the future may contain aspects of the current models or be superceded by an, as yet, uncreated, animal model.

CHAPTER I – Background

1. FROM DNA DAMAGE TO MUTATION

1.1. INTRODUCTION

Examining the effects of environmental mutagens requires an understanding of the basic mechanisms of mutation. This section describes how mutational specificity can be a useful tool for understanding the nature of mutation. It can be especially powerful when accompanied by some knowledge of the potential DNA lesions. Ultimately, for the examination of weak mutagens, or exposures to low levels of mutagens, the comparisons of mutational spectra of background versus exposed organisms will likely prove to be extremely important.

1.1.1. Ultraviolet light

Several studies have been carried out on the mutational specificity of UV light. Early indications from the study of nonsense mutations in the *E. coli lacI* gene suggested that G:C→A:T mutations predominated at dipyrimidine sites (Coloundre and Miller, 1977). A similar conclusion was reached in one of the first sequencing studies using the single-strand bacteriophage M13 as the target (Brandenburger *et al.*, 1981). The first extensive study of UV-induced mutational specificity involving the sequencing of mutations in the *lacI* gene was that of Schaaper *et al.* (1987) in which mutation was

examined in both a repair proficient (Uvr^+) and a repair deficient ($UvrB^-$) strain of *E. coli*. While the induced-mutation frequency per unit dose was 3-4 fold greater in the $UvrB^-$ strain, the distribution of mutations in both strains was rather similar. About 80% of the recovered mutations were base substitutions, 10% were frameshifts and 5% deletions.

The vast majority of mutations recovered in the *lacI* gene were G:C→A:T transitions at dipyrimidine sites (Table I and Table II). Tandem double events (i.e., CC→TT transitions) were also recovered. This later type of mutation is considered to be the hallmark of UV-mutagenesis, as it almost exclusively been recovered from UV-induced mutations. Numerous studies in different systems have reported an increase in G:C→A:T, or tandem CC→TT events at dipyrimidine sites following UV treatment (Armstrong and Kunz, 1990; Armstrong and Kunz, 1992; Drobetsky *et al.*, 1987; Drobetsky *et al.*, 1989; Drobetsky *et al.*, 1994; Ivanov *et al.*, 1983; McGregor *et al.*, 1991; Wang *et al.*, 1993; Vrieling *et al.*, 1992).

An important observation concerns the preferential repair of lesions along the transcribed strand of active genes. This occurs in both bacterial and mammalian systems, and reflects the coupling of transcription to nucleotide excision repair (NER) (Mellon *et al.*, 1987; Mellon and Hanawalt, 1989). The preferential repair of lesions along the transcribed strand (TS) is reflected in the specificity of mutation, since UV-induced mutations, in transcribed genes occur primarily due to photoproducts located on the

Table I. Comparison of mutational spectra. These data are for the *lacI* gene in *E. coli*. Only the DNA binding region (nucleotide 29-206) is considered, but the data between brackets for B[*a*]P are for the whole gene.

Class	Spontaneous[1] %	B[*a*]P[2] %	UV[3] %	EMS[4] %
GC->AT	33.3	4.8 (2.6)	56.9	97.9
AT->GC	9.2	0	9.7	0.6
GC->TA	5.6	23.8 (15.6)	8.3	0.4
GC->CG	2.9	4.8 (2.6)	6.9	0
AT->TA	8.5	19.0 (6.5)	6.9	0.3
AT->CG	11.7	0 (1.3)	1.4	0.2
+1 fs	0	0	0	0
-1 fs	4.4	19.0 (27.3)	4.2	0.4
del	16.7	0 (15.6)	5.6	0.1
ins	7.8	9.5 (22.1)	0	0
complex	0	19.4 (6.5)	0	0
Total #	412	21 (77)	72	1129

[1] Schaaper and Dunn (1991).
[2] Bernelot-Moens *et al.* (1990).
[3] Schaaper *et al.* (1987).
[4] Pienkowska *et al.* (1993).

Table II. Sequence context of mutational events following EMS (Pienkowska *et al.*, 1993) or UV (Schaaper *et al.*, 1987) treatment for the sites with 5% or more of the mutations. The mutated base is underlined.

EMS-Induced Mutants

Position	5'-		- 3'
42	TAA	C	GTT
56	GTC	G	CAG
57	TCG	C	AGA
75	TCT	C	TTA
92	TCC	C	GCG
93	CCC	G	CGT
120	TTT	C	TGC

UV-Induced Mutants

Position	5'-		- 3'
75	GTT	T	CCC
89	GTT	T	CCC
90	TTT	C	CCG
120	TTT	C	TGC

non- transcribed strand (NTS). If no time is allowed for transcription-coupled repair, such as irradiating normal human fibroblasts in early S-phase, mutations biased towards the transcribed strand (McGregor *et al.*, 1991). However, if the same cells were irradiated in in G_1 phase, there was an opportunity for repair by transcription-coupled repair and mutations primarily were recovered in the NTS (McGregor *et al.*, 1991).

The premutational lesions for UV light remain are not definitely known. However, two lesions are suspected because of their high abundance after exposure to UV. These two primary lesions are the cyclobutane pyrimidine dimer (CPD) and the (6-4) pyrimidine-pyrimidone (64PyPy). Early studies concentrated on the potential role of the CPD in UV-mutagenesis (Haseltine, 1983). The recognition that the 64PyPy photoproduct which is produced at 5-10% the rate of CPD may also be a premutagenic lesion has stirred considerable interest (Haseltine, 1983). Data from *E. coli*, indicate that the 64PyPy could be an important contributor to UV-mutagenesis (Glickman *et al.*, 1986). However, a broad range of UV-induced lesions have been shown to be mutagenic in engineered plasmid vectors transfected into *E. coli* though to differing degrees (see Table IV). Other factors contributing to UV-mutagenesis include the deamination of cytosine Tessman and Kennedy, 1991) and the possible photoreactivation of CPDs and 64PyPy that can occur at significant rates (Tessman and Kennedy, 1991). The contribution of the different DNA lesions to the overall UV induction of mutation remains controversial. The hallmark mutations of UV-induced mutagenesis has clearly been established as the G:C→A:T transition at dipyrimidine sites and the tandem CC→TT transitions.

Table III. Comparison of the numbers of mutants recovered from the *lacI* gene of *E. coli* and the *aprt* gene of Chinese hamster cells after exposure to UV and benzo[*a*]pyrenediolepoxide.

Class	UV		B[*a*]P	
	aprt CHO[1]	*lacI E.coli*[2]	*aprt* CHO[3]	*lacI E. coli*[4]
GC->AT	17	41	1	2
AT->GC	1	7	0	0
GC->TA	0	6	13	12
GC->CG	4	5	3	2
AT->TA	2	0	2	5
AT->CG	0	1	0	1
+1 fs	1	0	1	0
-1 fs	0	3	1	21
del/dupl	0	0	0	29
dbl subst	7	0	0	0
complex	0	0	0	5
Total #	32	63	21	77

[1] Drobetsky *et al.* (1987)
[2] Schaaper *et al.* (1987) (DNA binding region only, nucleotides 29-206)
[3] Mazur and Glickman (1988)
[4] Bernelot-Moens *et al.* (1990) (Entire *lacI* gene, Uvr$^-$, Deletions/duplications includes +/- 4 bp hotspot)

Table IV. Summary of the mutagenic and bypass effect obtained with site-specific and stereo-specific UV-induced DNA lesions transfected into *E. coli*. The bypass rate was calculated by percentage of vectors that were replicated when compared with controls. The percent error was determined as the ratio of plasmids carrying the altered and the original sequence. The fraction of the predominant mutation reflected the fraction of the total mutants recovered. In the case of the TT 64PyPy, 89 of 91, or 98% of the mutants were the transition, 3' T → C).

Photoproduct	Percent Bypass	Percent Error	Predominant Mutation
TT (64PyPy, UVC)[1]	22.1%	91%	3'T→C (89%)
TT (64PyPy, UVB)[1]	12.3%	53%	3'T→C (25%)
TC (64PyPy, UVC)[2]	24.5%	34%	C→T (28%), T→A (5%)
TC (64PyPy dewar, UVB)[2]	12.5%	79%	C→T (36%), T→A (15%)
TT *cis-syn* CPD[3]	19%	6%	3'T→A (5%)
TT *trans-syn* CPD[4]	29%	11%	5'T→A (2.5%)
OT (O=abasic site)[5]	7%	50%	5'T→A (23%), 5'T→C (18%)
TO (O=abasic site)[5]	5%	23%	3'T→C (14%)
UU *cis-syn* (uracil-uracil CPD)[6]	19%	5%	UU→TA (3.3%)
UU *trans-syn* (uracil-uracil CPD)[6]	9%	15%	UU→CT (8.8%) UU→AT (3.9%)

[1] (LeClerc *et al.*, 1991)
[2] (Horsfall and Lawrence, 1994)
[3] (Banerjee *et al.*, 1988)
[4] (Banerjee *et al.*, 1990)
[5] (Lawrence *et al.*, 1990)
[6] (Gibbs *et al.*, 1993)

Sequence context plays a major role in the deposition of DNA damage. Using naked DNA, the relative formation of UV-induced cyclobutane dimers at different dipyrimidine sites has been estimated by Mitchell *et al.* (1992) as TT>TC≈CT>CC in the ratio of 52:21:19:7 for UVB light (280-320 nm) and (68:16:13:3) for UVC light (240-280 nm). The different range of wavelengths was specified by Mitchell *et al.* (1992) and is not the generally accepted range. In general, there is a trend towards increased levels of UV-induced damage in regions rich in pyrimidines (Koehler *et al.*, 1991; Brash *et al.*1987) and significant site-to-site variation is observed (Brash *et al.*, 1987; Koehler *et al.*, 1991; Kotturi and Glickman, unpublished; Pfeifer *et al.*,1991; and Sage *et al.*,1992). There is a good correlation between the high frequency of CPD and 6-4 photoproducts at 5'-TCC-3' sites and the G:C→A:T transition mutational hotspots in the adenine phosphoribosyltransferase (*aprt*) locus in Chinese hamster ovary (CHO) cells (Drobetsky and Sage, 1993).

One reason for the lack of clarity is the possibility that both lesions are capable of contributing to UV mutagenesis. While the initial deposition of damage within a DNA sequence can be determined, a second consideration is that DNA repair is both strand and sequence specific. Indeed, the current models for mutagenesis and carcinogenesis suggest that the rate of repair at a given site is often more important than the initial amount of DNA damage (Tornaletti and Pfeifer, 1994; Kunala and Brash, 1992). In studies at moderately cytotoxic UV fluences (20 J/m^2) (Tornaletti and Pfeifer, 1994; Gao *et al.*, 1994) measured the rate of repair in the human *p53* and *PGK*1 genes and found that the site-to-site variation in the rate of excision of CPD lesions could be as great as 15-fold.

Although no definite rules can yet be formulated to predict the sites of slow repair, considerable data from the studies of mutational specificity indicate the relevance of repair rates to mutagenesis (Kunala and Brash, 1992).

1.1.2. Polyaromatic hydrocarbons - benzo[a]pyrene

The first documented case of induced cancer derive from the description of scrotal cancers in chimney sweeps (Pott, 1775) and the polycyclic aromatic hydrocarbons (PAHs) were soon recognized as the likely source of the elevated risk of this cancer. Typical PAHs include such compounds as benzo[*a*]pyrene (B[*a*]P), methylchrysene and dimethylbenz[*a*]anthracene (DMBA).

PAHs require activation to their ultimate mutagenic form, and these mutagenic forms of two PAHs, B[*a*]P and DMBA, has been shown to be potent carcinogens (Mane *et al.*, 1990). Activation results in dihydrodiol epoxides of these compounds that react and form bulky adducts primarily with exocyclic amino groups of guanine (N^2) and adenine (N^6) which opens the epoxide ring.

Benzo[*a*]pyrene is converted into its reactive metabolites, the diol epoxides (Weinstein *et al.*, 1976), by the enzymatic action of P-450's and epoxide hydrolase (Thakker *et al.*, 1985). The racemic mixtures of the diol epoxide stereoisomers that have the potential to bind to DNA are: 1) (±)-*r*-7,*t*-8-dihydroxy-9,*t*-10-epoxy-7,8,9,10-tetrahydro-benzo[*a*]pyrene (BPDE-I); 2) (±)-*r*-7,*t*-8-dihydroxy-9,*c*-10-epoxy-7,8,9,10-tetrahydro-benzo[*a*]pyrene (BPDE-II); and 3) (±)-*r*-9,*t*-10-dihydroxy-7,*c*-8-epoxy-7,8,9,10-tetrahydro-benzo[*a*]pyrene (BPDE-III) (Tang *et al.*, 1992). These epoxides

alkylate nucleic acids and predominantly (95% of the adducts) form a covalent bond to the exocyclic N^2 amino group of guanine (Sayer *et al.*, 1991). Adducts to the N^6 position of adenine are formed, but to a lesser degree (Sayer *et al.*, 1991; Cheng *et al.*, 1989; Harvey, 1979). Other minor adducts form at N^7 amino group of guanine (King *et al.*, 1979). deoxycytosine bases (Meehan *et al.*, 1977) and those which are present due to alkylation of denatured DNA (Sayer *et al.*, 1991).

The various reactive diol epoxides have different mutagenic potentials and much effort has been devoted to their study. Each of the three racemic diol epoxides can form four optically active isomeric forms. The reaction with DNA can result in either *cis* or *trans* addition to one of the two enantiomers. Thus a wide spectrum of different stereostructural adducts is possible. The (+) enantiomer of BPDE-I is considered the most mutagenic in mammalian cells and only this adduct was shown to be carcinogenic when applied to mouse skin (Buening *et al.*, 1978; Slaga *et al.*, 1979). On the other hand, the (-) enantiomer is more mutagenic in bacteria, when similar levels of adduct formation are compared (King and Brookes, 1984; Carothers *et al.*, 1988; Stevens *et al.*, 1985; Wood *et al.*, 1977).

The complexity introduced by the range of possible adducts coupled with the variation in repair rate complicates the problem of deducing which adducts form and where. A novel approach is the replication of genetically engineered plasmids with a specific type of adduct at a given location because this allows the recovery of mutations induced by a defined lesion. Mackay *et al.* (1992) determined the mutagenic specificity of the (+)-enantiomer of BPDE-I, by incorporating the (+)-*anti*-BP-N^2-Gua adduct as part of

the sequence 5'-CTGCA-3' in a plasmid. Replication resulted in almost exclusively (57/58) GC->TA transversions (Mackay *et al.*, 1992). When the 5' flanking T was replaced with any other base, the contribution of GC->TA decreased to 65% (Rodriguez and Loechler, 1993b). This change in spectrum was attributed to "adduct structural polymorphism", in which the adduct conformation is modulated by the local sequence context. Other bulky adducts have been shown to adopt different conformations such as the AAF-C^8-Gua adduct (Belguise-Valladier and Fuchs, 1991; Veaute and Fuchs, 1991). The influence of local sequence context adduct conformation was further investigated by Rodriguez and Loechler (1993a) by comparing the mutational spectra of an (+)-*anti*-BPDE-I adducted plasmid by varying the 5' base and the adducted plasmid treatment prior to transformation. The mutational alteration at 5'-TG-3' sequences was predominantly G:C→T:A transversions (27/29) while 5'-GG-3' sequences consistently yielded a lower percentage of G:C→T:A mutations (31/52). This indicated two possible adduct conformations. An interesting observation was made regarding the mutational pattern of one of the 'hotspots' for base substitution, at a single 5'-CG-3' site (5'-CG_{115}-3'). Before heating the adducted plasmid, the mutational pattern resembled that of 5'-TG-3' sequences, predominantly G:C→T:A mutations (13/15). After heating the pattern shifted to that of the 5'-GG-3' sequence context resulting in only 15/33 G:C→T:A transversions. Heating had no statistical effect on the mutational pattern of 5'-TG-3', or 5'-GG-3' sites. Further investigation revealed that AP sites were not formed at an appreciable rate concurrent with the shift in mutational spectra (Drouin and Loechler, 1993). The

difference in mutational specificity seemed to result from adduct conformation which was influenced by both heat and local sequence context.

The results obtained with both defined adducts and the *in vivo* mutational spectra indicate the importance of B(a)P-induced adducts and mutations at G:C basepairs. The sequence specificity of adduct formation has been examined in polymerase arrest studies with modified T7 DNA polymerase (Thrall *et al.*, 1992). Polymerase pause sites are taken as an indication of adduct formation. Such sites predominantly involve G:C basepairs, especially at runs of two or more guanines. Differences at the various guanine residues indicate sequence specific context effects which may reflect either sequence-specific properties or the presence of different conformations of the bulky adduct (Rodriguez and Loechler (1993a). The effect of sequence context of B(a)P-induced mutation is an important question addressed later in this thesis.

Consistent with the importance of G:C sites as targets for adduct formation is the observation that the G:C→T:A transversion is the hallmark of B[*a*]P-induced mutation. This transversion represents about 60% of the induced base substitutions (Bernelot-Moens *et al.*, 1990; Chen *et al.*, 1990; Mazur and Glickman, 1988; Rodriguez and Loechler, 1993b; Yang *et al.*, 1987). However, the complete mutational spectrum is quite complex, much more so than for example, after treatment with an alkylating agent such as EMS (Table I). Following B[*a*]P treatment mutations such as G:C→A:T transitions, G:C→C:G transversions and frameshifts also occur (Mazur and Glickman, 1988; Rodriguez and Loechler, 1993a; Zhu *et al.*, 1994). The specificity of B[*a*]P is quite

similar in both mammalian and bacteria systems with some cases of an increased recovery of G:C→C:G transversions in mammalian cells.

Base substitutions recovered in the *lacI* gene of *E. coli* (Bernelot-Moens *et al.*, 1990) following BPDE treatment were predominantly G:C→T:A transversions (Table III). However, 50% of the mutations recovered were -1 bp frameshifts which occurred mostly in runs of guanines. BPDE induced mutations have also been analyzed in the *aprt* gene of CHO cells by Mazur and Glickman (1988). Again, the predominant mutations were found to be G:C→T:A transversions (Table III). Further analysis suggested that their occurrence was biased towards runs of guanines, especially when flanked 5' by adenine. BPDE also induced frameshift mutations in runs of guanine in the human *aprt* gene (Zhu *et al.*, 1994) and in the *E. coli lacI* gene in a transgenic mouse model by Kohler *et al.* (1991).

It is not surprising considering the overall similarity of mutational spectra in bacterial and mammalian systems that following exposure to B[*a*]P the Ha-*ras* mutations recovered from animal tumours were consistent with expectations for this mutagen (Bizub *et al.*, 1986; Quintanilla *et al.*, 1986).

2. TRANSGENIC RODENT MUTAGENESIS ASSAYS

The correlation of a particular mutation, found in a tumor, to a particular treatment (Bizub *et al.*, 1986; Quintanilla *et al.*, 1986) was one of the motivating forces to develop *in vivo* transgenic rodent models (Gossen *et al.*, 1989, Kohler *et al.*, 1990; Kohler

et al., 1991; Boerrigter *et al.*, 1995; Nohmi *et al.*, 1996). These models have the potential to tremendously increase our knowledge about *in vivo* mutagenesis and the role of mutagenesis in tumor development. The main advance these models facilitated was the ability to study *in vivo* tissue-specific events. The transgenic rodents have a mutational reporter within a shuttle vector in every nucleated cell. The shuttle vector permits any target gene to be used for mutation screening and the use of a manageable prokaryotic host to screen a large number of cells (Kohler *et al.*, 1990).

The transgenic loci (*lacI* and *lacZ* lambda-phaged based) were selectively or genetically neutral (Cosentino and Heddle, 1996). Neutrality minimized the influences on *in vivo* mutation. Thus mutations accumulated with increased treatments without deleterious effects to the whole organism. The mutagenic effects were additive (Cosentino and Heddle, 1996) which may facilitate the statistical detection of these effects above background endogenous levels. All transgenic rodent models may not have genetically neutral transgenes. The transgenic *lacZ*-plasmid rodent model which is able to detect large mutations (Boerrigter *et al.*, 1995), may not be entirely neutral because a native locus located near the transgene may be deleted along with along with a portion of the transgene. If the native locus was involved in regulation of cell growth, the cells with the mutated transgene and deleted native locus may have a selective advantage or disadvantage.

While neutrality gave rise to certain benefits such as cumulative mutagenic effects, the properties of the transgenes, which resulted in the neutrality, needed to be analyzed. The transgenes were concatemers of prokaryotic genes (e.g., bacteriophage or

plasmid). Eukaryotic promoters were not inserted in the transgene constructs. None of the transgenes were actively transcribed or expressed. Without transcription, the transgenes were not subject to transcription-coupled repair (TCR; Mellon and Hanawalt; 1989). TCR preferentially removes or repairs DNA damage from the transcribed DNA strand (Tomaletti and Pfeifer, 1992). With reduced DNA damage in the transcribed strand fewer mutations are recovered (Chen et al., 1990; McGregor et al., 1991; Kunala and Brash, 1992). The total size of the concatemers was approximately 1 megabase for the lambda-*lacI* transgenic system and was assumed to have a negligible replication burden on the cell compared to the entire mammalian genome.

Prokaryote loci have a higher GC content than endogenous mammalian loci (Baker and Allen, 1982). Of particular interest was the relatively higher number of CpG sites in the bacterial transgenes. The CpG sites were assumed to be methylated in the bacterial transgenes (Wyborski *et al.*, 1996). A high proportion of the mutations recovered from the untreated animals were located at CpG sites (de Boer and Glickman, 1998). Methylation of the 5'-cytosine and subsequent spontaneous deamination was proposed to be the mechanism responsible for the large contribution of GC $\rightarrow$ AT transitions of background, or spontaneous, mutation spectra (de Boer *et al.*, 1997). The differences between prokaryote and eukaryote loci did not prevent the use of these models. They only need to be considered since the bacterial transgenes are surrogate markers for endogenous loci.

A further consideration of the application of these transgenic rodent mutagenesis assays to detect *in vivo* mutagenic processes was their sensitivity. For these mutagenesis

assays the sensitivity is defined by the fold increase of the induced mutagenic response over background levels. In a wide variety of tissues, the background or spontaneous mutant frequency was approximately 2-5 $x10^{-5}$ (de Boer and Glickman, 1998). When compared spontaneous mutant frequency of endogenous loci, and especially *hprt*, the transgenic loci have a higher background (Skopek *et al.*, 1995, 1996). The transgenic and endogenous loci appeared to respond the same absolute amount of induced mutant frequency to a similar acute treatment (Tao *et al.*, 1993; Skopek *et al.*, 1995, 1996). Thus a small increase in induced mutant frequency may be detected at an endogenous loci and not at the bacterial transgene. However the induction may become significant by increasing the number of treatments. In addition, the mutants can be characterized by DNA sequencing and shifts in mutational spectra can aid in the detection of mutagenic processes. A small increase in the induced mutant frequency was further corroborated to be treatment-induced [i.e., tris(2,3- dibromopropyl)phosphate] as a significant shift in mutational spectra was observed (de Boer *et al.*, 1996).

Two of the most widely used transgenic models have incorporated lambda phage shuttle vectors into the genome of a rodent but each model with a different reporter gene. The two target genes are the *lacI* (Kohler *et al.*, 1991) and *lacZ* (Gossen *et al.*, 1989) genes. These transgenic targets primarily reported point mutations, frameshifts and small insertions or deletions (de Boer *et al.*, 1997). Other systems included one, which uses the *gpt* gene, a bacterial homolog to the *hprt* gene, and *spi*, a native locus to bacteriophage lambda (Nohmi *et al.*, 1996). The *gpt* transgene was used to detect similar types of mutations as the *lacI* or *lacZ* transgenes. Larger deletions were detected by the *spi* loci

which provided the 'delta-gpt' transgenic model the ability to detect both point mutations and large deletions in one system. Another system, which was designed to detect large deletions, was the *lacZ*-plasmid model (Boerrigter *et al.*, 1995). As with the lambda-based systems, the *lacZ*-plasmid model has concatemers of a transgenic plasmid. The plasmids are recovered by performing a restriction digest to reduce the viscosity of the DNA and allow the individual copies of the plasmid to be recovered. Point mutations can be detected with a similar technique to the lacZ-lambda model but the restriction digest of the genomic DNA does not constrain the boarder between the transgene and the native DNA. If the portion of the transgene that contains the restriction site is deleted, the recovered plasmid will contain a portion of the transgene and a portion of the genomic endogenous DNA. The size of the delection could be achieved by characterization of the endogenous DNA around the transgene insertion site.

The lambda-*lacI* and lambda-*lacZ* transgenic rodent mutagenesis assays are more widely used because they were the first developed and were commercialized early. Technically, these transgenic models were based on the insertion of head-to-tail concatemers of bacteriophage lambda. The concateremers increase the number of mutational targets per cell and allow the use of smaller tissue samples than would have been possible with single-copy transgenes. The transgenes were extracted by cell-free packaging extracts from the mammalian genomic DNA by recognizing and packaging the lambda DNA into proheads. At the junction of the concatemers were cohesive end sites (*cos*). The *cos* sites are the recognition sequence for the phage enzyme terminase (Emmons 1974; Feiss and Campbell, 1974). After recognition of the *cos* site, terminase

bound the prohead and cleaved at the *cos* site (Feiss and Becker, 1983). Packaging the DNA into the prohead was a complicated ATP-dependent process. Wild-type phage have a length of 46 kb and the packaging efficiency was relatively constant between 78 and 105% of the wild-type length (Feiss and Becker, 1983). Above this limit, the energy requirements to insert the extra DNA into the prohead were presumed insurmountable. Lambda genomes below 78% were presumed missing genes, which resulted in low growth rates.

Relative to the *E. coli lacZ* gene, the *E. coli lacI* gene has been extensively characterized as a mutational target (Coloundre and Miller, 1977; Farabaugh *et al.*, 1978; Schaaper *et al.*, 1987; Schaaper and Dunn, 1987). Figure 1 shows the lambda phage shuttle vector with the primary mutational target gene, *lacI* and a secondary target gene, *cII*. The *cII* gene was recently described as a mutational target (Jakubczak *et al.*, 1996) and could be used because it was native to the lambda phage. The construct used in the lambda-*lacI* (Big Blue®) transgenic rodents is shown in Figure 1. The lambda-*lacI* system represented a major focus of the latter parts of this thesis.

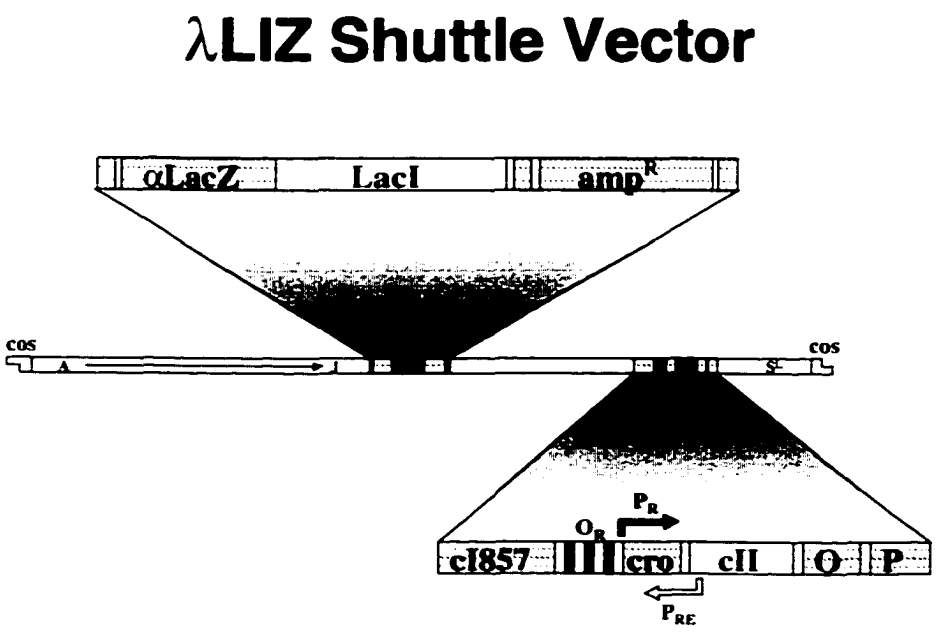

Figure 1. Outline of the lambda LIZ vector used to generate transgenic mice and rats.

The ability to screen for *lacI* mutations is based on how mutant LacI protein interferes with the normal function of the lac operon. The lac operon regulates the production of proteins required to metabolize lactose. The LacI repressor functions as a tetramer and binds to the *lacO* or lac operator. In the presence of lactose, the inducer, the LacI repressor changes conformation and can not bind the lac operator. Transcription of the lacZ gene occurs and metabolism of lactose occurs. The use of this system as a forward mutation assay has been possible because lactose-analogues have been found which did not induce the lac operon. An example of such an analogue is 5-bromo-4-chloro-3-indolyl-b-D-galactopyranoside (X-gal).

In the transgenic rodent system, the presence of X-gal and a wild-type LacI repressor leads to the generation of colourless plaques (see Figure 2). Defective LacI protein allows the transcription of the *β-galactosidase* or *lacZ* gene, and the LacZ protein metabolizes X-gal to form a blue compound. Mutations in the *lacI* target gene are detected by the presence of a blue plaque. The ratio of blue to colourless plaques represents a measure of the mutant frequency. The regulation of the lac operon is illustrated in Figure 2.

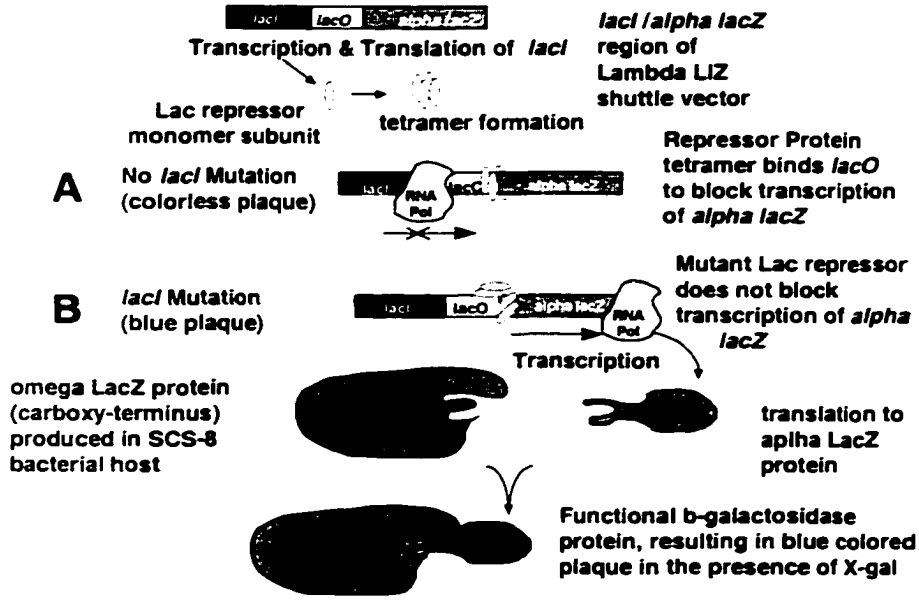

Figure 2. The regulation of lacZ gene expression by the Lac repressor. The Lac repressor synthesized by the *lacI* gene forms a tetramer, which binds to the lacO sequence. A) A colourless plaque is generated by an intact Lac repressor. B) A mutant Lac repressor leads to a blue plaque in the presence of the chromogenic substrate, X-gal.

The application of this system as a short-term mutagenesis assay relies primarily on being able to detect an increase in mutant frequency (MF) or mutation frequency (MnF) and, to a lesser extent, on detecting a difference in mutational spectra (de Boer *et al.*, 1996). The lambda-*lacI* transgenic rodent mutation assay has been tested in greater than 100 test compounds, and a large database of *lacI* mutations. The database is available on the internet (http://darwin.ceh.uvic.ca/bigblue/bigblue.htm).

Validation of transgenic rodent mutation assays consisted, in large part, of the identification of major sources of variation through the development of statistical tools, which can be applied to study design. (Piegorsch *et al.*, 1994, 1995, 1997; Carr and Gorelick, 1994; Carr and Gorelick, 1995; Callahan and Short, 1995; Carr and Gorelick, 1996; Fung *et al.*, 1997; Winegar *et al.*, 1997). The key sources of MF variance appear to be the number of animals per treatment group and the number of (plaque forming units) per animal (Piegorsch *et al.*, 1995). For the *lacI* and *lacZ* phage-based models, a doubling of mutant frequency is detected with a power of 0.80 and a 95% confidence interval with 125,000-300,000 plaque forming units (pfu) / animal and 5-10 animals per treatment group. This assumes the spontaneous mutant frequency is approximately 2-4 x 10^{-5}. The lacZ-plasmid mouse model can detect a 50% increase above the background mutant frequency of 4-7 x 10^{-5} with a power of 0.8 and 95% confidence interval using three animals per group and 350,000 pfu/animal (Boerrigter and Vijg, 1997). These statistical approaches are based on the Generalized Cochrane-Armitage method which can allow the animals to be used as the experimental unit (Carr and Gorelick, 1995). The result is well-

standardized assays with good analysis tools to aid in the detection of a mutagenic effect of test compounds.

The lambda-*lacI* transgenic rodent is focused on the detection of mutations, however, the precursor to a mutation or genetic alteration is DNA damage. DNA damage may be repaired and/or lead to a mutation. The deposition of DNA damage and the rate of DNA repair is nucleotide sequence specific; therefore DNA context plays a significant role in the fixation of mutation. The next two chapters describe the measurement and biological significance of DNA damage. The former of the two chapters explains, in detail, the methodology used. The latter provides an overview of the method but primarily interprets the results of the experiments.

CHAPTER II . DNA damage analysis using an automated DNA sequencer

Gopaul Kotturi, Wolfgang C. Kusser and Barry W. Glickman

Centre for Environmental Health, Department of Biology, University of Victoria, Victoria, B.C., Canada, V8W 2Y2

published in: Technologies for Detection of DNA damage and mutations, Ed. G.P. Pfeifer, Plenum Press, New York., pp185-196.

Abstract

This chapter reviews the state of the art of applying automated DNA sequencers to the analysis of the distribution of DNA damage. The use of both the Perkin Elmer / Applied Biosystems Division (PE/ABD) 373A and Pharmacia Biotech Automated Laser-Fluorescent (A.L.F.™) instruments is reviewed along with the software for the analysis of the data. Data obtained on the A.L.F.™ using UVC-irradiated DNA is used to illustrate this approach. The practical advantages and inherent difficulties are discussed in detail. We conclude that these instruments provide sufficient sensitivity and speed to justify their use for this non-DNA sequencing application. The automated analysis of DNA damage can be expected to have applications in both studies of environmental toxicology as well as drug design and development.

1. INTRODUCTION

Advances in bictechnology and molecular genetics have made possible a better understanding of the molecular nature of mutation. For example, the discovery of genetically altered proto-oncogenes and tumor suppressor genes in cancerous cells has led to a better understanding of the links between mutation and cancer. Similarly, the ability to study mutation and mutational specificity *in vivo* and *in vitro* has led to an increased appreciation of the mechanisms of mutation and the role that DNA damage and DNA repair plays in determining the specificity of mutagenesis. In turn, differences in both the cellular metabolism of exogenous chemicals and DNA repair can at least in part explain

tissue, gender, and species specificity of carcinogenesis. We remain however, a long way off from being able to predict the individual risks implicated with the mutagenic potential of chemical and physical agents. A part of this problem reflects our lack of knowledge of how individual lesions are handled in different tissues and different species genetic against the make-up of an individual.

In the past few years, an increasing amount of sequence data has confirmed that the mutational specificity of mutagenic agents appears specific for each agent, providing a mutational "fingerprint", if you will. It is also clear that the mutational fingerprint is a composite image with at least three components. These are 1) the ability of the genetic target to reveal mutation (the target filter which is related to the product and the mutation selection criteria); 2) the distribution of DNA damage; and, 3) the specificity of DNA repair. The importance of the latter two factors can be emphasized by the realization that the initial distribution of DNA damages will contain clues as to the relevance of the different types of lesions to the mutational process; and, finally, that it is the absence of repair or misrepair of lesions that will determine their biological potency. It is from these origins that the distribution of DNA damages in DNA derives its importance. This chapter describes an automated approach to the study of the distribution of DNA damage.

1.1. Development of Automated DNA Sequencers.

'Automated DNA sequencers' is a term currently used to describe instruments that utilize fluorescent chromophores instead of radioactive isotopes to detect DNA fragments. Fluorescence of the labelled molecules generated during dideoxy-mediated

DNA sequencing reactions is recorded in real-time during gel electrophoresis (Smith *et al.*, 1985; Sanger *et al.*, 1977). The fluorescent signal is directly converted into a digital signal which can be acquired, stored and processed into sequence information 'automatically' by a computer (Smith *et al.*, 1986). Compared to standard autoradiographic techniques several steps are eliminated and human handling greatly reduced. These steps include: 1) precise timing of the electrophoresis; 2) drying the gel; 3) exposing of the film, and waiting one or more days before developing the autoradiogram; and 4) generation of the DNA sequence data. Table V lists the various automated DNA sequencers and the ancillary software required to perform DNA damage experiments. We have no experience with the Licor Biotechnology automated DNA sequencer and do not report on this system here although it can be similarly applied to the study of DNA damage distribution.

1.2. Ancillary applications of Automated DNA sequencers.

Since highly fluorescent chromophores and laser-induced fluorescence are employed, the detection limits can be extremely low, in the order of $3x10^{-18}$ to $1x10^{-16}$ M (Ansorge *et al.*, 1987; Smith *et al.*, 1985). In addition to their high sensitivity, these instruments can be designed to have a wide dynamic range of detection. This represents a dramatic improvement over conventional autoradiograms and should facilitate the adaptation of automated DNA sequencers to non-sequencing applications. These supplementary applications were not initially recognized, particularly the subsequent requirement for ancillary downstream software to perform peak integration, data analysis

Table V. A list of various automated DNA sequencers and associated integration and peak identification software.

Company	Model	Ancillary Software
Pharmacia Biotech (Piscataway, New Jersey, USA)	A.L.F. Blue™	1) Fragment Manager™ 2) ALF2SMA™ and SMART™ Manager
	A.L.F. Express™	
Perkin/Elmer Applied Biosystems Division (Foster City, CA, USA)	373A™	1) Genescan™ 2) Genotyper™
	377™	
Licor Biotechnology Division (Lincoln, Nebraska, USA)	4000™	1) RFLP Scan (from Scanlytics)
	4000 LX™	

and data presentation. An early study relied on the correlation of peak height to DNA quantity (Koehler *et al.*, 1991) largely because of the lack of downstream software. The first software to become available still required extensive input from the user (Shoukry *et al.*, 1991). Current analysis software, listed in Table V, greatly increases the flexibility of automated DNA sequencers.

The use of automated DNA sequencers to determine the sequence specificity of DNA damaging agents was established using approaches such as cleavage techniques (Shoukry *et al.*, 1993; Koehler *et al.*, 1991; Shoukry *et al.*, 1991), or DNA polymerase and DNA polymerase 3'→5' exonuclease activity (Sage *et al.*, 1992). Several other techniques that can be adapted are single strand conformation polymorphism analysis (SSCPA) (Iwahana *et al.*, 1994), mismatch determination (Verpy *et al.*, 1994), T-cell receptor clonality (Segurado and Schendel, 1993), and quantitative polymerase chain reaction (QPCR) analysis (Porcher *et al.*, 1992).

2. METHODS

As outlined above, the techniques involved in utilizing an automated DNA sequencer do not differ in any fundamental way from conventional sequencing protocols. There are a few modifications and precautions which appear to be more relevant to fluorescently-tagged DNA and these are discussed in detail. In order to illustrate the transition to fluorescent technology, we describe the detection of UVC (254nm) - induced DNA damage. These techniques have been widely applied using radioactive-based

protocols both *in vitro* (Drobetsky and Sage, 1993; Brash *et al.*, 1987) and *in vivo* (Wei *et al.*, 1995; Gao *et al.*, 1994; Tornaletti and Pfeifer, 1994; Kunala and Brash, 1992; Pfeifer *et al.*, 1991). UVC light induces lesions which are predominantly the cyclobutane pyrimidine dimers (CPDs) and 6-4 pyrimidine-pyrimidone photoproducts (64PyPy). The sequence-specificity of both these photoproducts is determined by distinct cleavage techniques at the site of the photoproduct which includes: 1) the treatment with hot alkali for cleavage at 64PyPy (Lippke *et al.*, 1981); and 2) the enzymatic T_4 endonuclease V cleavage at CPDs (Gordon and Haseltine, 1982). Thus the length of the cleaved DNA fragment reveals the position of the damage and quantitating the peak determines the amount of damage at that DNA site. What follows is a description of the procedure to determine the distribution of 64PyPy, starting with DNA amplification through to the analysis and presentation of the data.

2.1. Template generation

It is essential to generate pure full-length DNA template for the DNA damage experiment because after UV irradiation greater than 80% of the DNA fragments remain undamaged (Goodisman and Dabrowiak, 1992). This ensures that, on average, a 'single hit' or 1 adduct per DNA molecule occurs. In a 300 bp fragment with approximately 100 possible sites of damage, each peak represents about 0.05% to 3.0% of the total quantity of DNA. Any non-specific DNA fragments from the amplification severely impacts the accuracy of the experiment if they result in a peak.

2.1.1. Amplification

In vitro studies use template DNA generated by PCR which facilitates the incorporation of a fluorescent label since the primers are labelled on the 5' end with fluorescein phosphoamidite. The first decision that must be made concerns the position and length of the primer sequence. Computer programs such as OLIGO® (National Biosciences, Hamel, MN, USA) greatly facilitate primer design. The PCR conditions can be optimized by adjusting the magnesium concentration, annealing temperatures and invoking a 'touchdown' protocol to minimize the formation of non-target fragments.

The specific target sequence used in this example was the first 230 bp of the human *hprt* cDNA. Flanking regions of 30-50 bp are added to each end of the target sequence for several reasons. Interference of any undesired ssDNA ends is reduced. Since the primer peak from a sequencing reaction is ≈40 bp wide and sequencing reactions are used to determine peak positions, no peak positions can be determined until after the primer peak is past the detector. The total length of the fragment is 297 bp and is amplified using the following PCR conditions. In a 100 µl reaction volume the following components are added: 10-100 pg of plasmid DNA (containing the human *hprt* cDNA), 2µl of 25 pmol/µl of each primer, 1µl of 5U/µl of AmpliTaq (Perkin Elmer, Norwalk, CT, USA), 10 µl of 10X buffer (600 mM KCl, 150 mM Tris-HCl pH 8.9, 27.5 mM $MgCl_2$); 2µl of 25mM of each dNTP (Pharmacia Biotech, Pistacaway, NJ, USA); and ddH_20 to volume. Depending on the DNA strand being studied, the appropriate primer is 5'-labelled fluorescein phosphoamidite (Pharmacia Biotech). The 297 bp fragment is

amplified with a Perkin-Elmer 9600 GeneAmp PCR system using 30 cycles of: 1) 94°C for 1 min; 2) 57.5°C for 30 s and; 3) 72°C for 1 min. The primer sequences are:

HPRT-21F: 5'-CCTGAGCAGTCAGCCCG-3'

HPRT-255R: 5'-ATCACTATTTCTATTCAGTGC-3'

2.1.2 Template purification

Our method of choice to reduce the non-specific fragments generated by PCR is to use a low melting point (LMP) agarose gel followed by phenol/chloroform extraction of the excised band. This yields a product of sufficient quantity and purity to perform DNA damage experiments. Specifically, the PCR fragment is loaded on a 4.0% low-melting point agarose gel (FMC BioProducts, Rockland, ME, USA) **without** ethidium bromide (EtBr). Although in the absence of EtBr, some DNA may be lost, this protocol **avoids** the exposure of the DNA to EtBr and UVB light which may introduce nicks. All lanes of a 70 ml gel (10 cm x 10 cm) are loaded with the PCR mixture and electrophoresed at 50 V for 16-18h. To localize the desired band a longitudinal slice is cut form the from the edge of the gel, soaked in a 0.1 μg/ml EtBr solution for 10 min and visualized with a UV transilluminator. The gel slice is cut such that its length reveals the position of the predominant band. Using the truncated gel slice repositioned in the gel tray, the remainder of the appropriate DNA band is excised. The excised gel band is melted at 60°C in 2 volumes of TE buffer (50 mM Tris-HCl pH 7.6, 1 mM EDTA) and the DNA is extracted using phenol, phenol/chloroform (50/50) and chloroform/iso-amylalcohol (24:1). The product is ethanol precipitated. The PCR product is resuspended in H_2O to

yield a final DNA concentration of ≈ 30 ng/μl and stored at -20 °C until required. DNA concentrations are determined using Hoechst 33258 intercalation and measuring the fluorescence on a Hoefer Fluorimeter TK100 (Hoefer Scientific Instruments, San Francisco, CA, USA). The fluorescein label of the PCR fragment contributes ≈ 3 % of the signal and this minor systematic error is ignored.

To avoid exposing the DNA to phenol, the DNA in the gel band could have been recovered by dialysis, but usually the yields of DNA are much lower compared to the phenol extraction protocol. Control experiments for damage inducing agents such as UVC light, benzo[*a*]pyrene diol epoxide and coriandrin, reveal no significant background damage (unpublished results).

2.2 Internal Standards and Sequencing Reactions

Internal standards are required to compare the results from separate runs. The design of the automated DNA sequencer determines the number and type of controls required. Our laboratory's earlier efforts relied on the PE/ABD 370/373A system (Foster City, CA, USA) (Sage *et al.*, 1992; Koehler *et al.*, 1991; Shoukry *et al.*, 1991). More recently we acquired Pharmacia Biotech A.L.F.™ DNA sequencers (Piscataway, NJ, USA) and applied them to the study of sequence-specific DNA damage (Kotturi *et al.*, unpublished).

In the case of the Pharmacia A.L.F.™ three fluorescein-labelled internal DNA standards are employed. The first internal standard (IS-1) monitors the degradation of the

fluorescein from chemical reactions and the recovery of DNA after DNA precipitations. The IS-1 standard is added to the DNA sample following UVC radiation. The length of IS-1 is 317 bp. Its length is 20 bp longer than the full-length fragment because the width of the undamaged peak is equivalent to about 20 bp of sequence. The second and third standards (IS-2 and IS-3), 322 and 347 bp, respectively, are required specifically for the Pharmacia A.L.F.™ because this instrument has 40 fixed photodiodes and the DNA may not migrate directly in front of the photodiode. The IS-2 and IS-3 standards are required in order to ascertain that each photodiode is responding in a like manner. All three internal standards are prepared and purified as described above.

Sequencing reactions are added as external controls which are used to align the damage related peaks with the corresponding sequence position. Cycle sequencing is usually employed because of modest template requirements compared to T_7 polymerase-based sequencing. For the PE/ABD 373A, cycle sequencing using dye-labelled dideoxyterminator or dye-labelled primers protocols can be used effectively. One of the four nucleotide reactions with the dye most distinct from the labelled template can be added in the same lane to accurately determine the peak position. For the experiments with the Pharmacia A.L.F.™, the following cycle sequencing protocol is used: A master mixture of 2.6 µl of 10X sequencing buffer [300mM Tris/HCl pH 9.0, 300mM KCl, 50mM $MgCl_2$], 1.5 µl of the appropriate labelled primer at 2.5 pmol/µl (Dalton Chemicals, North York, Ont., Canada), 125 ng of *hprt* cDNA, 1.2 µl of 5U/µl AmpliTaq (Perkin-Elmer, Norwalk, CT, USA) as combined with double-distilled H_2O to a volume

of 26 µl. The labelled primer is identical to the labelled primer used to amplify the PCR fragment. Six µl of the master mixture is aliquoted into one of four PCR tubes. Four µl of one of the termination mixes (A, C, G, or T) is added into one of 200 µl thin-walled PCR tubes (Perkin Elmer). The final concentration of the dNTP and ddNTP in each of the termination mixture is: 1) 60 µM for each dNTP and; 2) 'A' and 'T' RXNs: 0.8 mM ddATP, 'C' RXN: 0.4 mM ddCTP, 'G' RXN: 0.08 mM. The sequencing reactions are carried out in a Perkin-Elmer Thermocycler 9600 programmed for the following cycles: 1) 94°C - 2 min and then 2) 25 cycles of the following: 94°C - 10s; 50°C - 20s; 72°C- 30s. After the reaction is completed, 6 µl of deionized formamide (USB, Cincinnati, OH, USA), 5 mg/ml Dextran Blue 2000 dye (Pharmacia Biotech) is added. The dye facilitates loading and is excluded from the gel. At this point the samples are either stored at -20 °C until required or are denatured for 2 min at 95 °C and 8-10 µl are loaded onto the gel. Another practical advantage of utilizing a fluorescein-based assay is that the sequencing reactions can be made up in bulk and stored at -20 °C for several months without degradation.

2.3. DNA Damage Induction and Fragment Cleavage

Aliquots of 300 ng of the purified PCR fragment in ≈ 10 µl drops are placed in a sterile petri dish. The petri dish is placed in wet ice and the distance from the 8-watt Sylvania germicidal lightbulb (UVC, 254 nm) is adjusted such that the dose rate is 8 J/m^2s as calibrated by using chemical actinometry (Murov, 1973). To detect 64PyPy a

dose of 1.2 kJ/m^2 is used. Prior to the addition of piperidine, 1 µl of the first internal standard (IS-1) is added to estimate the recovery of the fluorescently-tagged DNA after the cleavage treatments. The DNA is treated with 1M piperidine at 90 °C for 30 min in a total volume of 100 µl, followed by an ethanol precipitation to recover the DNA. The DNA is dried overnight under vacuum without the application of any further heat to remove traces of piperidine. Typically there is a loss of 40% of the fluorescent signal attributed to the degradation of the fluorescein during the piperidine treatment.

2.4. Electrophoresis of DNA samples

Following the cleavage procedure, the samples consist of fragmented DNA of varying length. The full length fragment corresponds to the undamaged template while the smaller fragments reveal sites of cleavage and hence, DNA lesions.

2.4.1. Sample Dilution

Several dilutions of the sample are usually required because the photodiode signal is attenuated. Peaks with attenuated tops can not be accurately quantitated. Based on an initial starting quantity of 300 ng, four dilutions (1.0, 0.5, 0.1, and 0.05) consistently allowed both the damage peaks to be accurately quantitated as well as bringing the concentration of the undamaged fragment below the level of attenuation. The DNA is lyophilized until it is ready to be examined at which time the sample is resuspended into 16.5 µl of H_2O. A final volume of 10 µl was maintained. The IS-2/IS-3 mixture is added (1.0 µl), as well as a further 5.0 µl of deionized formamide containing Dextran Blue

2000. The final volume to be loaded is 16 µl. Samples can be stored at - 20°C or are heated to 94 °C for 2 min and immediately placed onto wet ice to cool. Liquid loss due to condensation is reversed as the water droplets are spun down in a microfuge and replaced into the ice until loaded.

2.4.2. Lane Assignments

Sequence lane assignments of the samples requires some preplanning. There are forty lanes available on the Pharmacia A.L.F.™ In comparison, the PE/ABD 373A may allow either 24 or 36 lanes and may have 2 samples per lane. Usually there is enough space on the gel to have several different 'exposed' samples. In the case of the Pharmacia A.L.F.™, the forty lanes are arranged into 10 clones. Sequencing reactions used to determine the sequence position of the peaks associated with the DNA damage must be loaded in the correct 4 lanes to automatically process the data into sequencing information. Three sequencing reactions (4 lanes each) are loaded and are usually located in clones 3, 5 and 8 or lanes 9-12, 16-20 and 29-32, respectively. Up to three lanes are used for internal standards to determine the quantity of IS-1 without loss of yield (lanes 38-40). This leaves 25 lanes or sufficient space for 3-5 exposed samples plus the control sample based on 4 dilutions per sample. Some partial sequencing reactions are loaded into lanes to concentrated samples where the best results are expected. This facilitates peak alignment between damage-induced peaks and DNA sequence reactions and minimizes problems due to bleeding by spacing concentrated samples. The dilutions are grouped together and the most dilute samples are loaded into lanes 1-6.

2.4.3. Preparation of the polyacrylamide gel

The cleaning and assembly of the gel cassettes can be accomplished by following the detailed manufacturer's instructions. The gel quality is of prime importance when using an automated DNA sequencer. We presently use 6% polyacrylamide, 19:1 polyacrylamide / *bis*acrylamide (5%C) Ready Mix gels (Pharmacia Biotech) which provide good reproducibility. Other gels that provide good separation are the recently developed Hydrolink Mutation Detection Enhancement™ or Longranger™ gels (AT Biochem, Malvern, PA, USA).

2.4.4. Electrophoresis conditions

Once the gel is warmed, wells are prewashed with electrophoresis buffer from the top reservoir to ensure that any salts such as urea do not cause a stacking effect which shifts the DNA bands. The electrophoresis conditions which can be adjusted are temperature, and electrical settings. In addition, the polyacrylamide concentration can also be altered. Reducing the laser power from the default 3 W to 2 W decreases the background fluorescence which increases the effective dynamic range of the instrument. Figure 3 shows the resulting resolution with a variety of gel conditions. Results from the standard PE/ABD 373A configuration are also shown in Figure 3a. This configuration has a 'well-to-detector' distance of 24 cm. Plates with a 'well-to-detector' distance of 34 and 48 cm are also available. As seen in Figure 3c, the resolution under standard conditions used for DNA sequencing is not optimal. The high temperature and short 'well-to-detector' distance of 19 cm are the major reasons. Typical run times are 5-6 h, in fact,

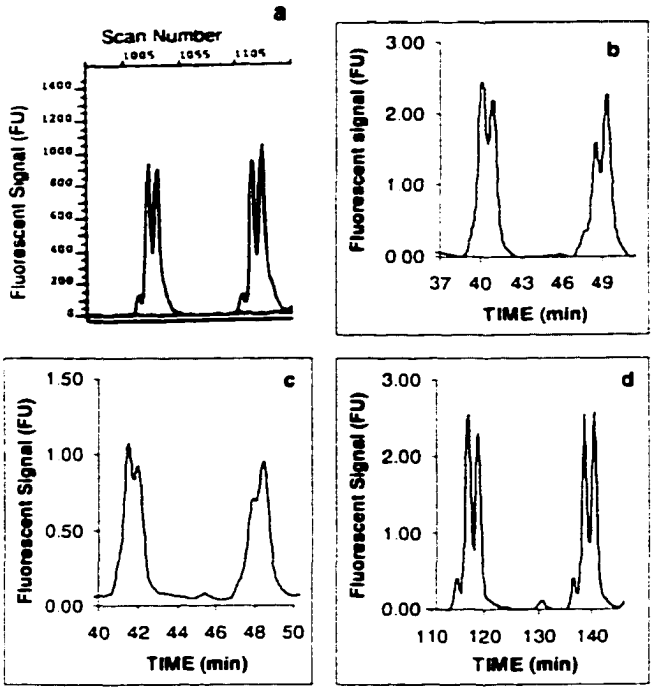

Figure 3. Illustration of the resolution from various automated DNA sequencers and electrophoretic conditions. All frames show the same piperidine cleavage products induced by 1.2 kJ/m^2 of UV (254 nm) light in the transcribed strand of the human *hprt* cDNA. The electropherograms are the raw data from automated DNA sequencers. Frame 'a' is an electropherogram of a sample run on a PE/ABD 373A with 24 cm 'well-to-detector' plates and a 6% polyacrylamide gel and other electrophoretic conditions recommended by PE/ABD. Frames 'b-d' show data from a Pharmacia A.L.F.™ with the common conditions of: Power = 21W, Current = 34mA, Voltage = 1500V. The electropherograms are runs at 6% polyacrylamide and 25^{0}C, 6% polyacrylamide and 40^{0}C, 12% polyacrylamide and 40^{0}C for Frames 'b', 'c', and 'd', respectively.

diagnostic information is possible after 2-3 h. Herein lies another significant advantage of using the automated DNA sequencer. Optimal resolution is obtained with a 12% gel (see Figure 3d) but the electrophoresis time is increased to 13h.

2.5. Data Analysis

After the end of the electrophoresis run, the data are stored in a digital format on a hard drive. The analysis of data from the PE/ABD 373A is performed with the 672 Genescan™ software which is different from the DNA sequencing software. Because the DNA sequence of the DNA sequencing reactions can not be calculated, it is more time consuming to determine the DNA bases which are damaged.

Before the electrophoresis run is started, a sample sheet is completed and this information is used to automatically detect the samples across the width of the gel. Also in the setup, the user can define which of the different dyes will be present. After the run is complete, the software automatically scans for the maximum intensity of the peaks in the width dimension and tracts any 'bent' lanes. This is a valuable procedure which can compensate for any defects in the gel. If the lane autodetection misses a lane, or if the lane 'bending' algorithm does not accurately tract the lane, it is possible to make adjustments. The user can go into the view of the electropherogram which is in two dimensions, time and fluorescent intensity. The time units are only displayed in 'scans' which represents the number of times the laser has scanned across the gel. Alternatively, if a PE/ABD size standard such as GENESCAN-500™ was run on the gel, the scans can be converted to 'base pairs'. The assignment of size is only a rough estimate because the

DNA fragment may migrate at a slightly different rate. The best alignment is achieved by running partial sequencing reactions in the same lane.

The parameters which define how the program will integrate the data are chosen. The baseline is automatically generated and the area under the peaks is integrated. Unfortunately, the baseline cannot be edited to account for baseline drifts near the primer peak. Raw data from the electropherogram can not be formatted and readily imported into a spreadsheet program to generate a custom plot. Electropherograms can be saved as graphic files (e.g., PICT files) and imported into a graphics program but it is difficult and time consuming to properly format and annotate the plot in a manner which displays the data efficiently. Peak tables can be exported directly to a spreadsheet program. The Genotyper™ software has the same limitations for peak quantitation but does allow the user to analyze data from various experimental runs.

In the case of the Pharmacia A.L.F.™, before proceeding with peak quantitation software data from sequencing reactions are processed and the DNA sequence is calculated. Any migration anomalies related to the particular DNA sequences such as GC compressions are determined and facilitate peak alignment. For the Pharmacia A.L.F.™ there are 2 data analysis programs. The first program which is similar to the PE/ABD 672 Genescan software is called Fragment Manager™. This Windows™-based program displays electropherograms quickly and is very good for quantitating results from experiments that have <5 peaks and have a narrow size distribution (< 30 bp). The user is somewhat limited by the number of parameters that can be adjusted to calculate the area

under the peaks. The most difficult noise to accommodate occurs when the salt front pass the detector because there is a large shift in the baseline. This is significant because at the trailing edge of the salt front, the DNA fragments start to pass the detector. As shown in Figure 4, the fluorescent signal of the salt front (< 50 min) is mostly compensated to subtract the background fluorescence. If integration is performed using this electropherogram, the area of the peak labelled 'TC23' would be too large. Unless these effects to the baseline can be appropriately compensated, errors in integration occur.

Our experience indicates that the most effective software for peak quantitation is a program developed to evaluate data from a Pharmacia SMART™ system. To utilize this software, a Pharmacia A.L.F.™ file is converted to a format which can be imported into the Pharmacia SMART™ Manager software. The conversion software is called ALF2SMA™. The software translates raw data generated by Pharmacia A.L.F.™ Manager up to and including version 2.5. The ALF2SMA™ program is a simple one line command executed from an OS/2 window that selects the lanes and time interval that will be converted. Once the file is converted, the relevant lanes or 'curves' are opened in the SMART™ Manager. Of primary interest are the baseline and peak integration calculations. Both have several parameters which allow the user to change the baseline to overcome problems. The parameters which can be chosen are: shortest baseline segment; noise window; maximum baseline level; and highest acceptable slope. While the units of the abscissa remain in minutes, the ordinate units are absorbance (AU) because the SMART™ Manager is primarily designed to run with a UV spectrophotometer. The

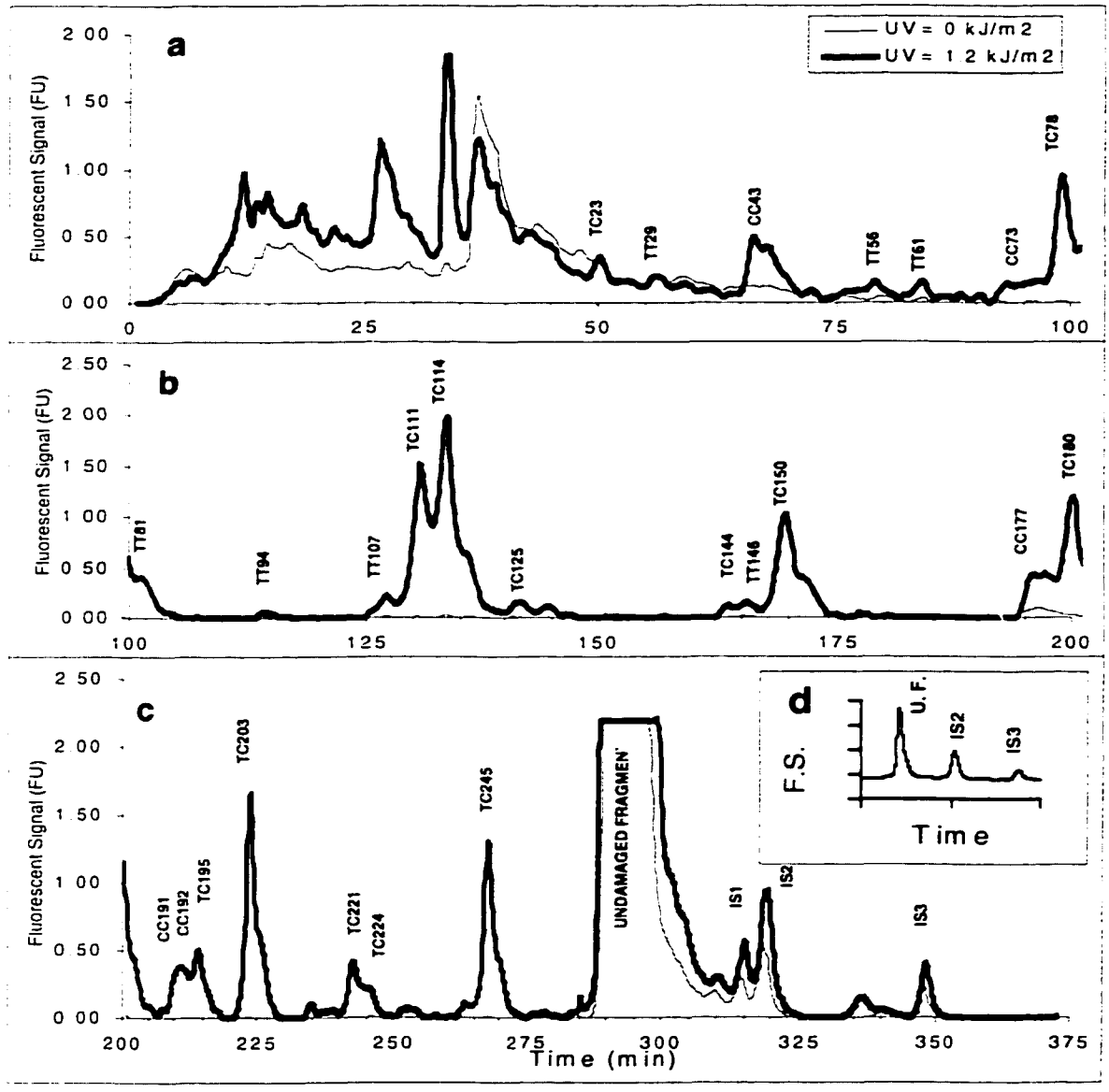

Figure 4. Distribution of piperidine cleavage products induced by 1.2 kJ/m^2 of UV (254 nm) light in the non-transcribed strand of the human *hprt* cDNA. The electropherograms are the raw data from a Pharmacia A.L.F.™ automated DNA sequencer. The DNA is resolved on a 6% polyacrylamide gel with the standard electrophoretic conditions: The fluorescent units (FU) are linear arbitrary units. Cleavage products were matched with DNA sequencing termination products in adjacent lanes to determine the base position. The control experiment is shown with the decreased line intensity. Frames 'a,b,c' show different time ranges in the same experiment. Frame 'd', as an insert to frame 'c' shows the dilution series which brings the undamaged fragment (Undam. Frag.) into the range that does not have the signal attenuation.

ordinate is scaled from the ALF™ Manager software from 0-100% of full scale to 0 to 4.095 AU in the SMART™ Manager program. Usually to produce the correct baseline for the region of the electropherogram with a rapidly decreasing baseline, the two parameters that are changed are the highest acceptable slope and shortest baseline segment. Values suggested by the program are 0.006-0.008 AU/min and 8-10 min, respectively, while values that are more appropriate are 0.015-0.025 AU/min for the highest slope and 2-5 min for the shortest baseline segment. By changing the parameters too drastically smaller peaks, especially later in the electrophoretic run, when the peaks broaden, may be confused with noise. If this occurs, the baseline can be manually edited by adding or deleting 'baseline points' to problem segments of the curve and recalculated. The recalculation is very 'robust' and accurately redraws the baseline consistent with the new baseline points which even cause large discontinuities in the previous baseline. Infrequently, a systematic noise is present in both the control and exposed experimental results which must be taken into consideration before peaks are quantitated. This may be a result of inadequate purification of the full length fragment. To compensate for this problem, curves can be subtracted. All anomalies are usually accounted for at this point and the area under the curve can be integrated and a peak table is generated. To reject peaks that represent noise, similar to the other software, it is possible to set minimum peak height, width and area and the maximum number of largest peaks. The peak table from the SMART™ Manager contains useful calculations such as peak width at one-half height, which the user can use to judge the quality of the data. Peak area and retention

time are used to correlate a peak to the DNA sequence. At this point it is usually most efficient to export the peak table into a spreadsheet program. In the example using UVC light, each peak is in turn is analyzed with exposed DNA sample and the 'T' and 'C' reaction being displayed to assign sequence position to the DNA damage. If the DNA lesion remains on the 3'-end of the fluorescently-labelled DNA fragment there may be a retention time shift (Comess *et al.*, 1992). But with the aforementioned 30-50 bp flanking regions, this effect is minimal. Finally, the electropherogram can be exported into a spreadsheet format. The number of data points selected should be between 1300-1800 points. After the electropherogram curve is imported, the data can be formatted and annotated to a much greater degree than is possible in other peak quantitation programs. An example of typical experimental results is shown in Figure 4.

2.6. Relative Mobility of DNA fragments.

One complication using automated DNA sequencers is that DNA molecules are moving past the detector during the real-time collection of data. This manifests itself as shorter DNA fragments elute with sharper peaks and, as the size of the fragments increase, peaks broaden which results in a lower peak height to area ratio. Peak spreading is due to the effects of diffusion and the difference in relative velocities. Diffusion does not affect the accuracy of the integrated area but it does impact the peak resolution, or the ability to separate two peaks.

A more important problem is the ability to determine the relative mobilities or velocities of two DNA fragments of different size. Smaller DNA fragments pass the

detectors at a faster rate or velocity than larger fragments. If a fluorescent molecule passes the detector more slowly it will generate a greater fluorescent signal. The average velocity from 'well-to-detector' is not accurate because the velocity of the fragments (< 300 bp) changes during the course of the electrophoretic run. The important place to determine the relative velocity is as the molecules pass the detector. Commercial products such as size standards (e.g., SIZER 50-500™, Pharmacia; GENESCAN-500™, PE/ABD) with equimolar DNA fragments at about every 25-50 bp can be obtained. Integration of data electrophoresed from these products could quickly determine the function of relative mobilities because the area should increase with DNA fragment size. However, our experience is that the actual concentration of each of the components in the SIZER 50-500™ varies considerably. To date, we have not determined the accuracy of the GENESCAN™ products. While the quantity of each of the components in the SIZER 50-500™ is not precisely 5 fmol/μl, the size is accurate. From a plot of retention time (time to reach the detector) as a function of DNA fragment size, an exact linear relationship is evident (R^2 =0.9996). This relationship is only valid for DNA fragments from 50 to 500 bp under the conditions used. Thus the velocities of the fragments at the detector are a linear function of DNA size within this range. Smaller fragments do not travel linearly until they approach the detector. By using the retention times of larger fragments (e.g., 400, 450 and 500 bp), an accurate relationship for velocity of the DNA fragments at the detector can be determined. Since the large fragments do not travel significantly in the part of the electrophoresis, the average velocity equals the velocity at the detector. The velocity at the

detector for the shorter fragments is extrapolated with the knowledge of the above linear relationship. The function can be easily applied to the table of integrated areas based on either retention time or DNA size to correct for the different mobilities. The function can be easily applied to the table of integrated areas based on either retention time or DNA size to correct for the different mobilities. The function for the velocity at the detector is:

$$\text{Velocity} = 9.75 \times 10^{-2} \text{ cm/min} - 9.61 \times 10^{-5} \text{ cm/(min bp)} * [\text{DNA size}],$$

where the DNA size is in bp. The velocity of a 50 bp fragment is 0.093 cm/min compared to a 300 bp fragment with a velocity of 0.69 cm/min. The ratio of the velocities is 0.75, therefore if the area of a 50 bp fragment is used a basis for calculation, the integrated area for the 300 bp must be reduced by 25% in order to compare the relative amounts of DNA damage. We want to emphasize that this calculation should be repeated periodically if retention times shift from experiment to experiment or if different electrophoretic conditions are used. Peaks integrated from Figure 4 are corrected in a similar manner. The area for the amount of 64PyPy at peak 'TC78' is 500 FU*min and the area of peak 'TC203' is 880 FU*min. The velocities of the fragments are 0.088 and 0.076 for the 100 (TC78) and 225 bp (TC203) fragments, respectively. The area of the 'TC203' peak is reduced by 14% to 760 FU*min to be able to compare equivalent amounts of damage.

3. DISCUSSION

Associated with any technology there are trade-offs which have to be weighed. Automated DNA sequencers have a demonstrated advantage over radioactive-based apparatus. There are clear benefits: 1) elimination of radioisotopes; 2) data are obtained in

5-7 h or by the following morning; 3) samples can be stored for months; 4) data are in a digital form; and 5) the possibility of automation for screening and risk analysis. In terms of throughput, the use of automated DNA sequencers only becomes an advantage when ancillary software is available even for their primary use of DNA sequence analysis. Sequence assembly software in which the data can be easily aligned, edited and checked by viewing the electropherograms facilitated this advancement. In terms of utilizing automated DNA sequencers for applications other than sequencing, the manufacturers first had to recognize the potential possibilities and develop suitable products. The main advantages of using the fluorescent based technology is that fluorescence of molecules such as fluorescein and rhodamine have extremely low detection limits and have a potentially wide dynamic range of response which can span several orders of magnitude. This is tempered with the realization that the technical design of the fluorescence detection system must be capable of producing a linear response over a large range.

3.1. Developing Technologies

Another technology that is being applied to DNA sequencing and which offers great potential is use of capillary electrophoresis (CE). This technology uses linear polyacrylamide and replaces urea with formamide to increase the stability of the gel. The linear acrylamide formation allows the replacement of the gel after each run. Higher applied voltages generate better separations and increased speeds (Khrapko *et al.*, 1994; Huang *et al.*, 1992; Chen *et al.*, 1991; Karger *et al.*, 1991). Typical conditions on the CE generate 400 bp of sequence information in 0.5 h. The main limitation appear to be the

number of parallel capillaries that an instrument can carry. In order for the capillary electrophoresis instrument to be a practical improvement over the conventional automated DNA sequencers a large number of capillaries must be run simultaneously. Naturally, much will depend upon the lifetime of a capillary used repetitively. Problems such as lane bending will be eliminated since all the sample passes in front of the detector. However, at present the injection of material into the capillary is either done by applying pressure or electrokinetically. The variability in the quantity of injected DNA is sufficiently small to generate DNA sequence information. However, our preliminary experience suggests that this is not sufficiently precise to utilize in DNA damage experiments unless an internal standard is introduced.

4. CONCLUSIONS

The application of DNA sequencing technology to other endpoints is being facilitated by the development of ancillary products and appropriate software. Here we have reviewed the application of these technologies for assessing the distribution of DNA damage. This application can be expected to have two major uses. The first is the analysis of DNA damage caused by environmentally relevant agents. The distribution of DNA damage and the analysis of its repair can be expected to have significant impacts on our understanding of the origins of cancer in humans. A second likely application is in the design of drugs targeted to specific DNA sequences. Such drugs may be used to target virus specific sequences, or human sequences amplified during the course of a disease. The automation of the analysis of DNA sequence specificity of drug binding will be of

practical assistance to the development of these types of drugs.

Acknowledgements

The authors wish to express their gratitude to Christian Ooste for his support in the performance of the experiments on the Beckman P/ACE 5000 CE system, Michael Ashwood-Smith for his many helpful comments regarding the coriandrin experiments, and Paul Romaniuk and Steve Hendy for their cooperation and assistance using the PE/ABD 373A and Genescan™.

CHAPTER III. Correlation of UV-Induced mutational spectra and the *in vitro* damage distribution at the human *hprt* gene.

G.(Paul) Kotturi, Johan G. de Boer, Ben F. Koop and B.W. Glickman

Centre for Environmental Health, Department of Biology, University of Victoria
Victoria, B.C. - V8W 2Y2

published in Mutation Research (1998) 403:237-248.

Abstract

We have determined the *in vitro* DNA damage distribution induced by 254 nm UV in the human *hprt* gene. The sequence-specific nature of the DNA damage for both main classes of UV-induced photoproducts, i.e., cyclobutane pyrimidine dimers (CPDs) and the pyrimidine <6-4> pyrimidone photoproducts (64PyPy), was evaluated. Utilizing an automated DNA sequencer plus auxiliary software, semi-automated analyses were performed for peak quantitation and retention-time to sequence-position correlation. 64PyPy were predominantly formed at 5'-YTC-3' sites ($p<0.02$; where Y=C,T). The effect of the 3' flanking nucleotide was 3'-T formed at lower frequencies compared to 3'-A,C ($p<0.03$). No effect of flanking nucleotides was detected for CPDs recovered at 5'-TT-3' sites.

Sites of mutations in the *hprt* gene were compared to the sites of DNA damage. Two regions of frequently mutated nucleotides corresponded to sites of high deposition of damage. The two sites either had a high frequency of CPDs or 64PyPy, which implicated both types of photoproducts as premutagenic lesions.

1. INTRODUCTION

Knowledge of the preferred sites of mutation 'fixation', when combined with information about the incidence of DNA damage allows insight into both the nature of premutagenic lesions and the effects of DNA repair. In the case of 254nm ultraviolet light (UV), mutations were typically characterized by single and tandem C→T transition at dipyrimidine sites (Hoffmann *et al.*, 1991; Drobetsky and Sage, 1993; Menichini *et al.*, 1991; Vrieling *et al.*, 1991; Drobetsky *et al.*, 1987; McGregor *et al.*, 1991; Vrieling *et al.*, 1992; Tornanen and Pfeifer, 1992). The two main UV-induced photoproducts are the

pyrimidine <6-4> pyrimidone photoproduct (64PyPy) and cyclobutane pyrimidine dimer (CPD). Research on the sequence-specific nature of UV-induced DNA damage has focused on these two suspected premutational lesions (Brash *et al.*, 1987; Koehler *et al.*, 1991; Kunala and Brash, 1992; Pfeifer *et al.*, 1991; Tornanen and Pfeifer, 1992; Sage *et al.*, 1992; Drobetsky and Sage, 1993; Tornaletti *et al.*, 1993; Tornaletti and Pfeifer, 1994; Gao *et al.*, 1994). Determination of the damage distribution of other photoproducts such as thymine glycol (Yamane *et al.*, 1967), cytosine hydrate (Kittler and Lober, 1977; Boorstein *et al.*, 1990) and rare dimers (Bose *et al.*, 1983; Gasparro and Fresco, 1986) has not been possible because of their low formation rates.

Correlation of mutational spectra (Schaaper *et al.*, 1987) and initial deposition of UV-induced DNA damage distributions in *E. coli* have revealed the importance of local DNA sequence context (Koehler *et al.*, 1991; Sage *et al.*, 1992). In stretches of pyrimidines with high levels of mutations, CPDs and 64PyPy were both recovered. The high frequency of DNA lesions at dipyrimidines on both strands at another frequently mutated site implicated a role for closely-opposed photoproducts in mutagenesis. In a rodent system, an *in vitro* DNA damage distribution determined that high frequencies of both CPDs and 64PyPy corresponded to mutational "hotspots" at 5'-TCC-3' sites (Drobetsky and Sage, 1993). In comparison, the initial deposition of UV-induced DNA damage was not correlated with a mutational spectrum using the *supF* tRNA gene in a shuttle vector (Brash *et al.*, 1987) or with C→T mutations characterized in human skin cancers (Tornanen and Pfeifer, 1992; Tornaletti *et al.*, 1993). A better correlation was determined between sites of CPD

which were slowly repaired, and frequently mutated positions in both *E. coli* and human cells (Kunala and Brash, 1992; Tornaletti and Pfeifer, 1994). This suggests that the rate of repair may be more important than the initial deposition of DNA damage. However, considering the number of different repair backgrounds in the above studies, the results remain inconclusive. In addition, while the 64PyPy were repaired quickly (Wang *et al.*, 1993), the rate of repair of 64PyPy at the nucleotide level has not been taken into consideration.

The present study focuses on the distribution of *in vitro* UV-induced CPDs and 64PyPy in the first 230 nt of the human hypoxanthine (guanine) phosphoribosyltransferase (*hprt*) cDNA gene. The approach chosen utilizes an automated DNA sequencer. The *hprt* gene is an important mutational target reflected by the > 1000 mutations recovered from human *in vivo* and *in vitro* sources (Cariello and Skopek, 1993) including several studies of UV-induced mutagenesis (Dorado *et al.*, 1991; Keohavong *et al.*, 1991; Lichtenauer-Kaligis *et al.*, 1995; McGregor *et al.*, 1991; Wang *et al.*, 1993). Because *hprt* has become such a well-studied target, we felt it important to have a parallel study in which the distribution of UV-induced damage was also studied. The selected region was chosen because it contains the frequently mutated run of six guanines (nt 207-212) and a wide distribution of dipyrimidine sites in both the transcribed (TS) and non-transcribed (NTS) strand (see Table VI). Our data confirm the high variability of photoproduct deposition at similar sequences. We found that 64PyPy at 5'-TC-3' sites flanked by a 5' pyrimidine form with a higher than expected frequency. Also, two mutational hotspots for C→T transitions were both

frequently damaged. In one case, there was a high frequency of CPDs, and the other a high frequency of 64PyPy.

Table VI. Distribution of various dipyrimidine sites between the non-transcribed (NTS) and transcribed (TS) strand.

Dipyrimidine Site	DNA Strand		TOTAL
	NTS	TS	
CC	11	19	30
CT	14	12	26
TC	10	21	31
TT	20	10	30
TOTAL	55	62	117

2. MATERIALS AND METHODS

The specific target sequence selected was the first 230 nt of the human *hprt* cDNA. This target was extended 30-50 nt on either side of the region of interest. The introduction of the flanking region reduces the possible interference of any undesired ssDNA ends. Also, the primer peak from a sequencing reaction was ≈40 nt wide and as sequencing reactions were used to determine peak positions, peak positions can not be determined until after the primer peak completely passes the detector. The length of the fragment was 297 nt and was amplified using the following PCR conditions. A more

detailed protocol and analysis methods were presented elsewhere (Kotturi *et al.*, 1996) A flow diagram of the following method was presented in Figure 5.

2.1. Template generation

In a 100 µl reaction volume the following components were added: 10-100 pg of plasmid DNA (containing the human *hprt* cDNA, ATCC 57056), 2µl of 25 pmol/µl of each primer, 1µl of 5U/µl of AmpliTaq (Perkin Elmer, Norwalk, CT, USA), 10 µl of 10X buffer (600 mM KCl, 150 mM Tris-HCl pH 8.9, 27.5 mM $MgCl_2$); 2µl of 25mM of each dNTP (Pharmacia Biotech, Piscataway, NJ, USA); and ddH_20 to volume. Depending on the DNA strand being studied, the appropriate primer was 5'-labelled with fluorescein phosphoamidite (Pharmacia Biotech). The 297 nt fragment was amplified with a Perkin-Elmer 9600 GeneAmp PCR system using 30 cycles of: 1) 94°C for 1 min; 2) 57.5°C for 30 s and; 3) 72°C for 1 min. The primer sequences were:

HPRT-21F: 5'-CCTGAGCAGTCAGCCCG-3'

HPRT-255R: 5'-ATCACTATTTCTATTCAGTGC-3'

2.2. Template purification

Our method of choice to reduce the non-specific fragments generated by PCR was to use a 4% low melting point (LMP) agarose gel (FMC BioProducts, Rockland, ME, USA) without ethidium bromide followed by phenol/chloroform extraction of the excised band. This produces a product of sufficient yield and purity to perform DNA damage experiments. The product was ethanol precipitated. The PCR product was resuspended in

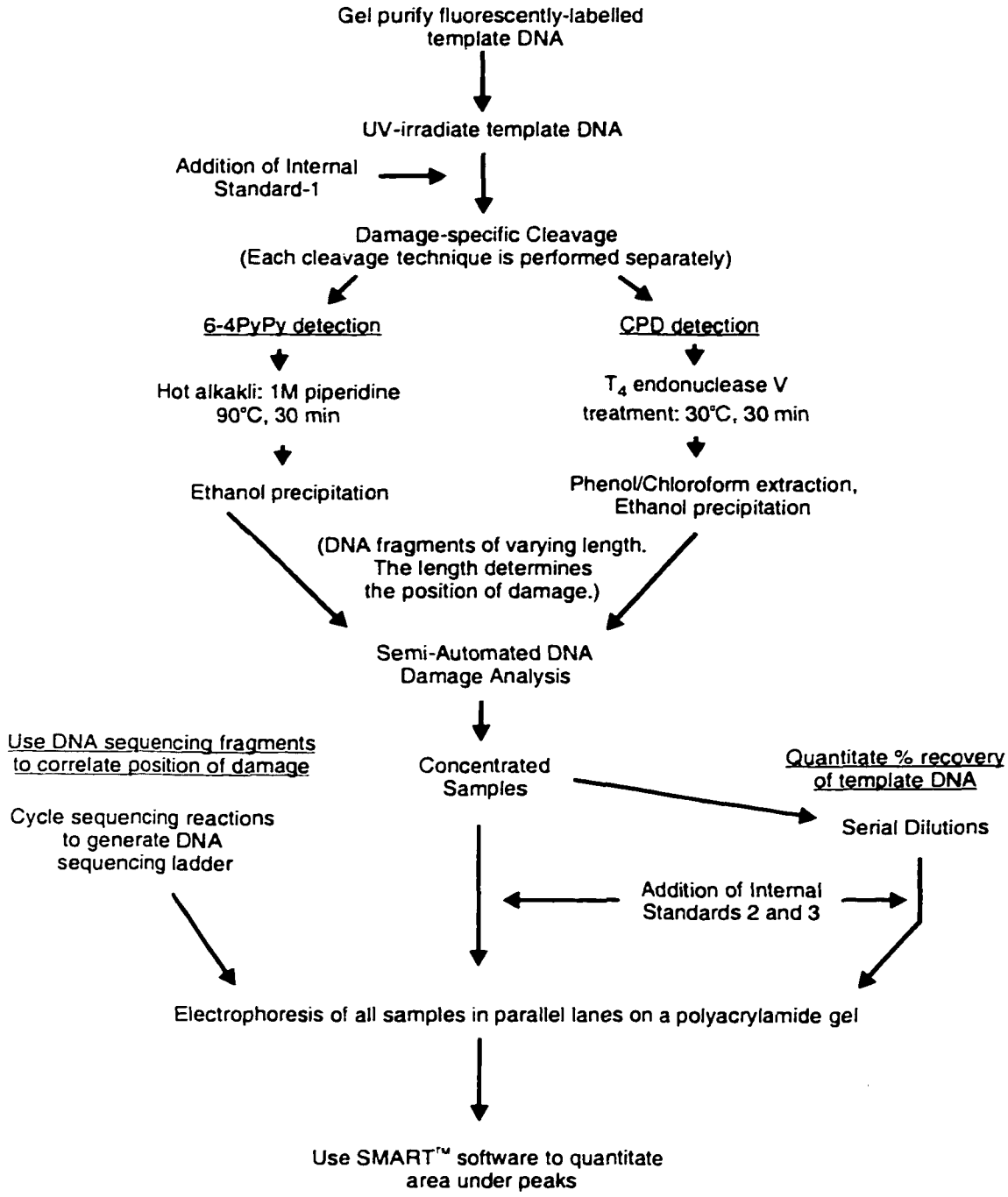

Figure 5. A flow diagram of the experimental methods indicating the major steps in the protocols.

H_2O to yield a final DNA concentration of ≈ 30 ng/μl and stored at -20 °C until required. DNA concentrations were determined using Hoechst 33258 intercalation and measuring the fluorescence on a Hoefer Fluorimeter TK100 (Hoefer Scientific Instruments, San Francisco, CA, USA). The fluorescein label of the PCR fragment contributes ≈ 3 % of the signal and this minor systematic error was ignored.

2.3. Internal Standards and Sequencing Reactions

Internal standards were required to compare the results from separate runs. Three fluorescein-labelled internal DNA standards were employed. Each of the three internal standards was a unique PCR product, which was individually prepared, as described in Chapter II. The first internal standard (IS-1) monitors the degradation of the fluorescein from chemical reactions and the recovery of DNA after DNA precipitations. The IS-1 standard was added to the DNA sample following UVC radiation as shown in Figure 5. The length of IS-1 was 317 nt. Its length was 20 nt longer than the full-length fragment because the width of the undamaged peak was equivalent to about 20 nt of sequence. The second and third standards (IS-2 and IS-3), 322 and 347 nt, respectively. The sizes IS-2 and IS-3 were chosen to not interfere with the signal of IS-1. The analysis and data recovery was facilitated by the use of an automated DNA sequencer. The physical design of the automated DNA sequencer included 40 individual lanes with 40 corresponding photodiodes. The output of the photodiodes was attenuated necessitating the serial dilution of samples to determine the quantity of large fluorescent signals. Quantifying the area under the peaks was possible because the photodiode signal was linear with concentration

(Porcher *et al.*, 1992). The IS-2 and IS-3 standards were used to correct for any differences in photodiode response and the non-linear migration of the DNA, in the horizontal axis, past the center of the photodiode. Thus, the three internal standards were added to each sample and loaded into a lane of a polyacrylamide gel to: 1) calculate the recovery of the template DNA from the cleavage treatments; 2) correct for lane wandering or non-linear migration of the DNA fragments in the direction of the electric field; 3) determine differences in the gain of individual photodiodes; 4) determine the area of the undamaged full length fragment from a series of dilutions; and 5) compare results from different experiments.

Sequencing reactions were added as external controls which were used to align the damage related peaks with the corresponding sequence position. The following cycle sequencing protocol was used: a master mixture of 2.6 µl of 10X sequencing buffer [300mM Tris/HCl pH 9.0, 300mM KCl, 50mM $MgCl_2$], 1.5 µl of the appropriate labelled primer at 2.5 pmol/µl (Dalton Chemicals, North York, Ont., Canada), 125 ng of *hprt* cDNA, 1.2 µl of 5U/µl AmpliTaq (Perkin-Elmer, Norwalk, CT, USA) as combined with double-distilled H_2O to a volume of 26 µl. The labelled primer was identical to the labelled primer used to amplify the PCR fragment. Six µl of the master mixture was aliquoted into one of four PCR tubes. Four µl of one of the termination mixes (A, C, G, or T) was added into one of 200 µl thin-walled PCR tubes (Perkin Elmer). The final concentration of the dNTP and ddNTP in each of the termination mixture was: 1) 60 µM for each dNTP and; 2) 'A' and 'T' RXNs: 0.8 mM ddATP and ddTTP, 'C' RXN: 0.4 mM

ddCTP, 'G' RXN: 0.08 mM ddGTP. The sequencing reactions were carried out in a Perkin-Elmer Thermocycler 9600 programmed for the following cycles: 1) 94°C - 2 min and then 2) 25 cycles of the following: 94°C - 10s; 50°C - 20s; 72°C- 30s. After the reaction was completed, 6 µl of deionized formamide (USB, Cincinnati, OH, USA), 5 mg/ml Dextran Blue 2000 dye (Pharmacia Biotech) was added. The dye facilitates loading and was excluded from the gel. At this point the samples were either stored at -20 °C until required or were denatured for 2 min at 95 °C and 8-10 µl were loaded onto the gel. Another practical advantage of utilizing a fluorescein-based assay was that the sequencing reactions can be made up in bulk and stored at -20 °C for several months without degradation.

2.4. DNA Damage Induction and Fragment Cleavage

2.4.1. UV-irradiation of DNA

Aliquots of 300 ng in ≈10 µL drops were placed in a sterile petri dish. The petri dish was placed in wet ice. The dose rate of the 8-watt Sylvania germicidal lightbulb (254 nm) was 8 J/m^2s as calibrated by using chemical actinometry (Murov, 1973). Prior to the cleavage of the damaged DNA, the first internal standard (IS-1) was added to estimate the recovery of the fluorescently-tagged DNA after the cleavage treatments.

2.4.2. Piperidine/Hot alkali cleavage

The DNA was treated with 1M piperidine at 90 °C for 30 min followed by an ethanol precipitation to recover the DNA.

2.4.3. T_4 endonuclease V treatment

Approximately .015 μg of T_4 endonuclease V (Dr. Stephen Lloyd) was added to 300 ng of DNA in 25 mM NaH_2PO_4 (pH 6.8), 100 μg/ml BSA (Pharmacia Biotech). The DNA was digested for 45 min at 30 °C. The DNA was purified with phenol, phenol/chloroform (50/50), and chloroform/isoamyl alcohol (24:1) extractions.

2.5. Electrophoresis of DNA samples

Following the cleavage procedure, the samples consist of fragmented DNA of varying length. The full length fragment corresponds to the undamaged template while the smaller fragments reveal sites of cleavage and hence, DNA lesions. Piperidine cleaves immediately 3' of the 64PyPy lesion and therefore piperidine-cleaved fragments aligned with the 3' nucleotide of the dipyrimidine of a DNA sequencing reaction. T_4 endonuclease V cleaves immediately 5' of the lesion and these fragments were aligned with the nucleotide position immediately 5' to the dipyrimidine site.

2.5.1. Sample Dilution

Several dilutions of the sample were usually required because the photodiode signal of the automated DNA sequencer can be attenuated and peaks with attenuated tops

can not be accurately quantitated. Based upon an initial mass of 300 ng, four dilutions (1.0, 0.5, 0.1, and 0.05) consistently allowed both the damage peaks to be accurately quantitated as well as bringing the concentration of the undamaged fragment below the level of attenuation. The DNA was lyophilized until it was ready to be examined at which time the sample was resuspended into 16.5 µl of H_2O. A final volume of 10 µl was maintained. The IS-2/IS-3 mixture was added (1.0 µl), as well as a further 5.0 µl of deionized formamide containing Dextran Blue 2000. The final volume to be loaded was 16 µl. Samples can be stored at - 20^{0}C or were heated to 94 °C for 2 min and immediately placed onto wet ice to cool. Liquid loss due to condensation was corrected as the water droplets were spun down in a microfuge. The tubes were held on wet ice until loaded.

2.5.2. Preparation of the polyacrylamide gel and electrophoresis conditions

The cleaning and assembly of the gel cassettes can be accomplished by following the detailed manufacturer's instructions. We presently use 6% polyacrylamide, 19:1 polyacrylamide / *bis*acrylamide (5%C) Ready Mix gels (Pharmacia Biotech) which provide good reproducibility.

Once the gel was warmed, wells were prewashed with electrophoresis buffer from the top reservoir. The electrophoresis conditions were 40C, 21W, 1000V 34mA.

2.6. Analysis of data

The Pharmacia ALF2SMA™ software translated the raw data generated from the Pharmacia A.L.F. Manager™ version 2.2 program. The new file format was importable into the Pharmacia SMART™ Manager software. Once the data file was in the SMART™ Manager format, typical analytical techniques were available to quantitate the peak height and area. Electropherograms from UV-exposed DNA were aligned with sequence data to determine the position of DNA damage. Photoproduct frequencies were reported in arbitrary units of Relative Fluorescent Units * min or RFU*min.

The effects of immediate 5' and 3' flanking nucleotide on the photoproduct frequency were determined by the following procedure. A one-way analysis of variance using Statistica version 5.0 (Statsoft Inc., Tulsa, OK) was performed using groups defined on the basis of sequence context. A separate analysis was performed for each type of dipyrimidine (e.g., 5'-TC-3') and for each of the 5' or 3' flanking nucleotide. All sites, including those for which no photoproducts were observed, were used in the analysis. Tables of photoproduct frequency and flanking nucleotide were generated and tested for trends. Thus, the means of the photoproduct frequency for a given data set (e.g., 5' nucleotide of the 64PyPy) were tested for a trend or significant effect. An effect is a statistical difference in the means of the photoproduct frequency for a flanking nucleotide. Next the variances of the means were tested to ensure the data was not biased. If no bias was observed in the variances, post-hoc comparisons were performed. The two types of post-hoc analyses that were performed were the least significant difference (LSD) and

Neuman-Keul test. A matrix of probabilities was generated, which is final format of the analysis. Values with $p < 0.05$ were determined statistically different.

To determine if the surrounding sequence context influenced photoproduct deposition in a more general manner than the effect of the nearest neighbour, a method to calculate the local melting temperature was used. By taking into consideration nearest neighbour effects of adjacent bases over the length of a short oligonucleotide (Rychlik and Rhoads, 1989), a general estimate of the effect of local sequence context was established. The 'localized' Gibbs free energy of formation, ΔG, estimated the strength of the DNA interstrand bonds. The ΔG for a small DNA sequence is analogous to the melting temperature. The ΔG analysis may give an indication of the degree to which the local DNA sequence can rotate to accommodate an UV-induced DNA lesion based on its stability of the duplex structure (Rychlik and Rhoads, 1989). Short oligonucleotides with the photoproduct at the center were used to calculate the ΔG. The ΔG of oligonucleotides of varying length were plotted against the photoproduct frequency and trends were observed.

3. RESULTS

3.1. Distribution of UV-induced photoproducts

The DNA damage distribution from both DNA strands and both the detection of CPDs and 64PyPy was shown in Figure 6. The relative error associated with detecting the area under a peak was 5-7%, as determined by varying the concentration of IS-1 while maintaining the concentration of IS-2. A further 10-15% error was associated with

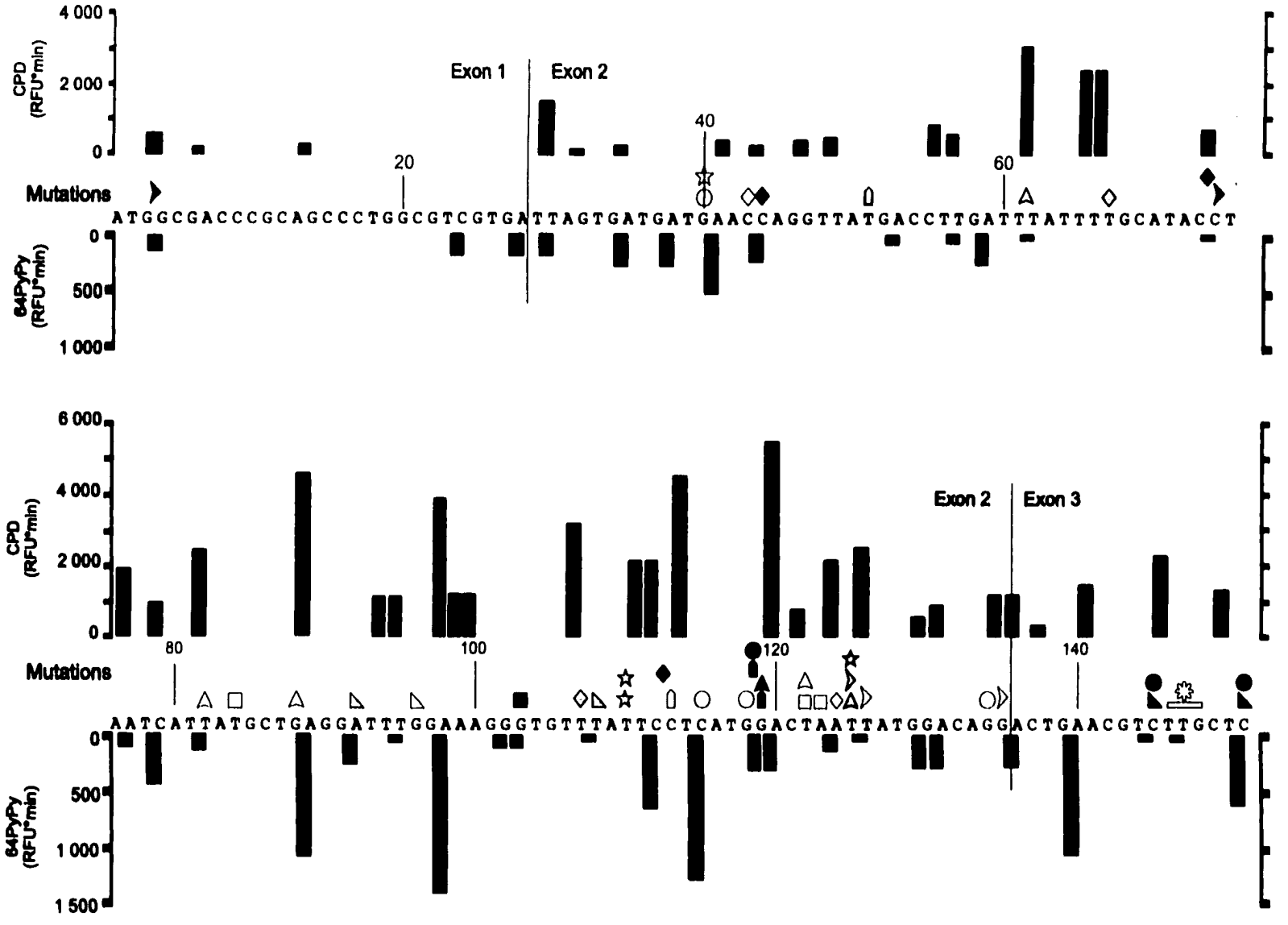
CPD (RFU*min)
4 000
2 000
0
Exon 1
Exon 2
20
40
60
Mutations
ATGGCGACCCGCAGCCCTGGCGTCGTGATTAGTGATGATGAACCAGGTTATGACCTTGATTTATTTTGCATACCT
6-4PyPy (RFU*min)
0
500
1 000
6 000
4 000
2 000
0
Exon 2
Exon 3
80
100
120
140
Mutations
AATCATTATGCTGAGGATTTGGAAAGGGTGTTTATTCCTCATGGACTAATTATGGACAGGACTGAACGTCTTGCTC
6-4PyPy (RFU*min)
0
500
1 000
1 500

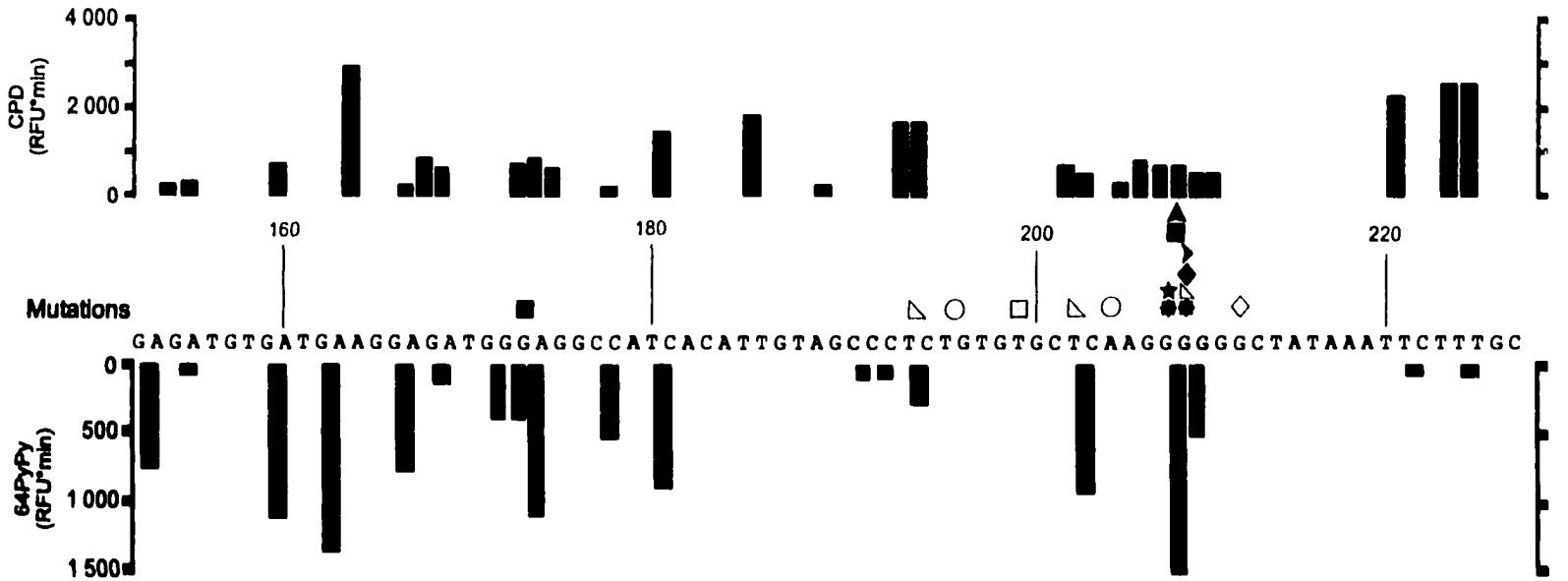

Figure 6. Combined relative distribution of CPD and 64PyPy in both the non-transcribed strand and transcribed strand of the human *hprt* gene (bp 1 to 226). Solid bars represent the relative frequency of photoproducts as determined by peak integration. Bars located above the corresponding sequence represent the CPD distribution (UV dose = 0.5kJ/m^2), while bars below the sequence represent the 64PyPy distribution (UV dose = 1.2 kJ/m^2). Bars are positioned between the damaged dinucleotide. All independent point mutations are positioned directly above the corresponding base. Tandem mutations are positioned between the mutated bases. A complex mutation of a 3 bp substitution is represented by a long open bar (bp 146-148).C→T and CC→TT transitions are shaded black; T→A and TT→AA tranversions are shaded grey. Any other base substitution is shown by an open symbol. The shape of a symbol represents the cell line from which it was recovered. If a mutation was derived from a synchronized population of cells, a distinct shape was also used as follows: ◇ normal human fibroblasts -G_1; □ normal human fibroblasts-S; △ XPA fibroblasts-G_1; ▷ XPA fibroblasts-S; (McGregor et al., 1991); ▯ SV40 transformed XPA fibroblasts (Dorado et al., 1991); ◺ XP variant fibroblasts-G_1; ○ XP variant fibroblasts-S (Wang et al., 1993); ✿ TK6 B lymphoblasts (see text for details; Keohavong et al., 1991); ☆ TK6 lymphoblastoid (Lichtenauer-Kaligis et al., 1995).

calculating a peak area for a cleavage experiment. The distribution of damage at various dipyrimidine sites was very diverse ranging from no observable photoproducts at numerous sites to the highest amount of damage of CPDs at $TC_{119-120}$ and of 64PyPy at $CC_{208-209}$. The possible sources of the diversity are discussed below.

3.2. Formation of UV-induced photoproducts at particular dipyrimidine sites.

The relative induction of CPDs at different 5'-PyPy-3' sites was determined for the entire fragment to be TT=48% > TC=29% > CT=16% > CC=7% which compared to the UVC-induced damage of TT=68% > TC=16% > CT=13% > CC=3% (Mitchell *et al.*, 1992). A similar calculation was performed for 64PyPy and it was determined that the ratio of formation was TC=76% > CC=20% > TT=4% >> CT=0%. By determining the average deposition per type of dipyrimidine (e.g., all 5'-TT-3' sites), it was quite evident there was considerable variation from site to site. CPDs at 5'-TT-3' sites formed on average (with standard deviation) 1500 ± 1100 RFU*min per site, and 64PyPy at 5'-TC-3' formed 550 ± 450 RFU*min. The standard deviation does not represent a measurement error. Rather, it was a consistent variation dependent on factors associated with the inherent nature of the DNA such as local sequence context. As expected, the damage deposition was strand independent after correcting for the number and type of dipyrimidine sites in each DNA strand (Table VI).

Various analyses were performed to determine the source of the variation. First, by using the most frequently damaged dipyrimidine of the 64PyPy (i.e., 5'-TC-3') and the CPDs (i.e., 5'-TT-3'), the effect of flanking nucleotides on photoproduct deposition was

determined. With respect to the effect of the 5' nucleotide on the deposition of 64PyPy at 5'-TC-3' dipyrimidines, the summary of effects was significant ($p < 0.002$). This indicated there was a significant influence of the 5' nucleotide on the 64PyPy frequency. Since the homogeneity of variance indicated the variances were the same ($p = 0.12$), no biases in the data were observed and post-hoc comparisons could be used to determine the source of the differences. Both the LSD and Neuman-Keul test were used to determine a statistically different induction between 5' pyrimidines and 5' purines (see Table VII). From Table VIII, a marginally significant decrease in the frequency of 64PyPy with the 3'-T compared to a 3'-C or 3'-A was observed. This decrease was very marginal since the summary of effects was on the borderline of statistical relevance ($p=0.044$). No observable patterns if both the 5' and 3' flanking nucleotides were analyzed together probably because there were too few sites of each of the 16 possible combinations within the target region. There appeared to be no influence of either the 5' or 3' nucleotide on the induction of CPDs since the summary of effects was $p= 0.99$ and 0.99 for the effect of 5' and 3' nucleotide, respectively. The homodimeric nature of the 5'-TT-3' dipyrimidine may have introduced some error in assigning the photoproduct frequency in runs of thymine because, for the larger fragments, the gel resolution may not have been sufficient to fully separate adjacent peaks. However, this did not affect the analysis with respect to flanking cytosine, guanine and adenine. Subsequent analyses were performed to determine the influence of surrounding sequences of dipyrimidine sites influenced photoproduct frequency. One such analysis focused on the surrounding sequences of 64PyPy at 5'-TC-3' sites. The ΔG for oligonucleotides of varying

Table VII. The effect of the 5' nucleotide of a 5'-TC-3' dipyrimidine on the recovery of 64PyPy.

	5' nucleotide of the 5'-TC-3' dipyrimidine			
	A	C	G	T
Mean Value[Ψ]	400.	840.	230.	890.
Number of Sites[†]	10	8	8	5
A		.011	.28	.014
C	.011[‡]		.0011	.80
G	.28	.0011		.0019
T	.014	.80	.0019	

[Ψ] Mean value of 64PyPy frequency at the corresponding 5' nucleotide. All sites, including sites with no observable photoproducts, were included in the mean.

[†] Number of sites for a given trinucleotide (e.g., there were 10 5'-ATC-3' sites in the target DNA sequence.

[‡] Underlined values are statistically independent. An interpretation of this cell in the table is that 64PyPy at 5'-CTC-3' sites form at a statistically different frequency than at 5'-ATC-3' sites. In this case, the 64PyPy frequency is statistically higher at 5'-CTC-3' sites than at 5'-ATC-3' sites.

Table VIII. The effect of the 3' nucleotide of a 5'-TC-3' dipyrimidine on the recovery of 64PyPy (please see notes from Table VII).

	3' nucleotide of the 5'-TC-3' dipyrimidine			
	A	C	G	T
Mean Value	690.	640.	380.	130.
Number of Occurrences	14	8	4	5
A		.75	.16	.0088
C	.75		.28	.027
G	.16	.28		.34
T	.0088	.027	.34	

lengths from L= 6 to 42 nt at 6 nt intervals was calculated for every 5'-T<>C-3' site with the dimer located in the middle of the sequence. For example, the oligonucleotide of length 6 at 5'-TC_{23-24}-3' is 5'-CG**TC**GT-3' and its ΔG value is -11.4kcal/mol. A plot of photoproduct frequency as a function of ΔG indicated a possible sinusoidal pattern, as shown in Figure 7. The pattern was noticeable for all oligonucleotide lengths from 6 to 42 nt and it was most predominant at the length of 24 nt. A second analysis to identify an effect of surrounding sequences investigated the effect of the DNA helix periodicity on the 64PyPy formation. This was accomplished by dividing the sequence position by 10.3 and plotting the 64PyPy formation against the remainder of the division. The resulting random pattern indicated that the position of the 64PyPy was not affected by its location in the DNA helix.

4. DISCUSSION

We determined the distribution of the two main UV-induced photoproducts by treatment with hot alkali or piperidine (Murov, 1973) and by enzymatic T_4 endonuclease V cleavage (Mitchell *et al.*, 1992). The target gene was the first 230 nt of the human *hprt* cDNA. The validity of comparing the *in vitro* irradiation of cDNA to the *in vivo* irradiation of the endogenous gene was justified by several observations. 1) The initial deposition of UV-induced DNA damage within exons is similar in purified DNA and intact cells (Mitchell *et al.*, 1992; Tornanen and Pfeifer, 1992). 2) All CpG sites are unmethylated in the 5' region in the active human *hprt* gene (Lippke *et al.*,1981; Pfeifer *et al.*, 1992), thus the frequency of 64PyPy was not altered by the methylation patterns of cytosine at

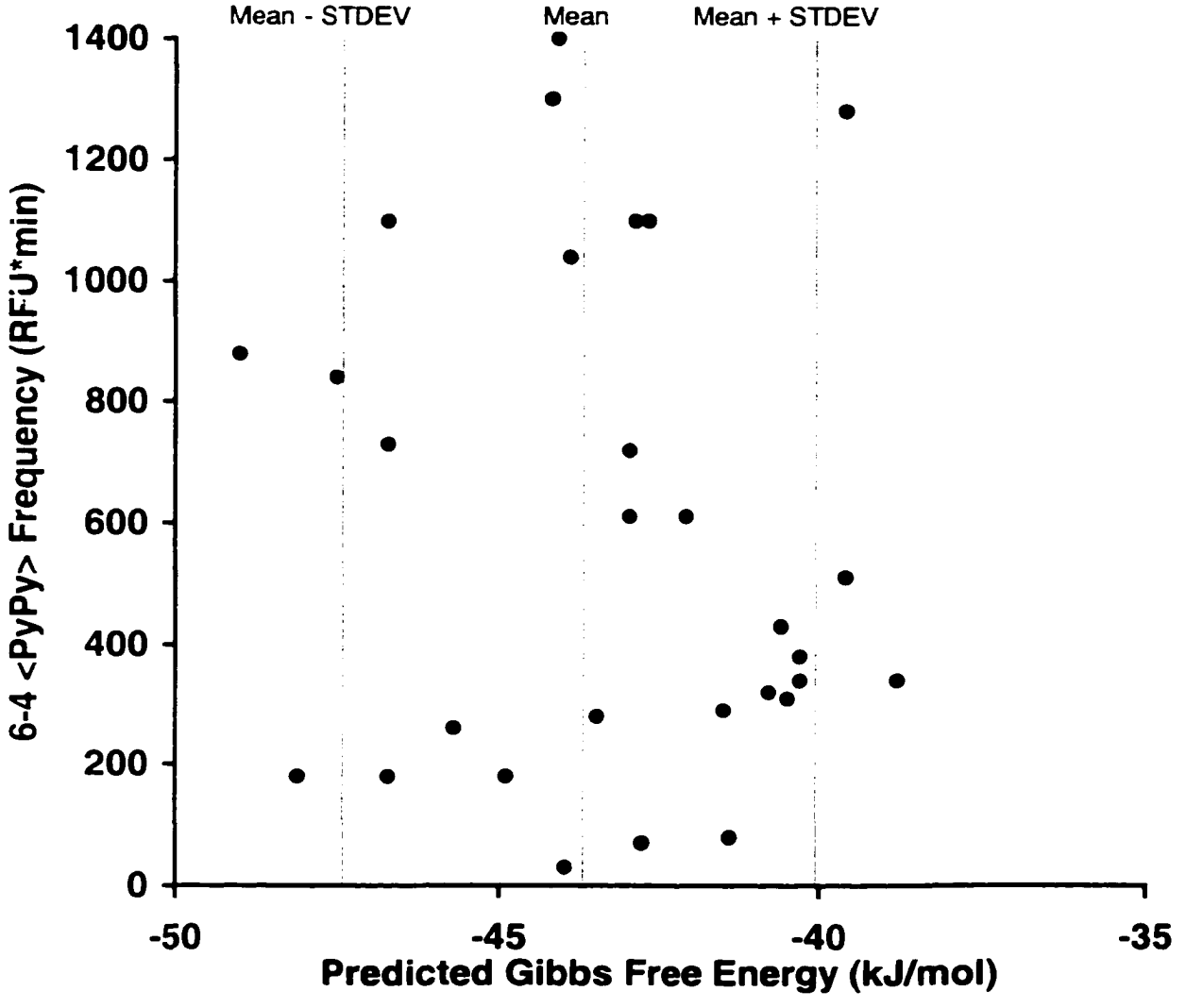

Figure 7. Relative 6-4 <PyPy> formation at 5'-TC-3' sites as a function of predicted Gibbs free energy. The Gibbs free energy was determined by the program OLIGO by centering a 24 nt oligonucleotide around the 5'-TC-3' site.

5'-Py- CG-3' sites. 3) Comparable mutational spectra were obtained after UV irradiation whether the mutations were recovered from the endogenous *hprt* loci, or an *hprt* cDNA integrated on a retroviral vector at different genomic locations (Litchenauer-Kaligis *et al.*, 1995). Thus indicating that local chromosome structure may not significantly influence the pattern of DNA damage deposition. A higher mutation frequency of the integrated DNA was observed and was attributed to a decrease in the repair of the cDNA genes with the retroviral promoter rather than the increased initial deposition. 4) Dipyrimidine sites that overlap exon boundaries were not included in the correlation of DNA damage to mutational events because the flanking sequences of the cDNA are not representative of the genomic DNA.

The analysis of the *in vitro* UV-induced sequence-specific damage deposition of both 64PyPy and CPDs was performed and the results compared against all the known UV-induced mutations in the first 230 nt of the human *hprt* cDNA gene assembled from a variety of sources . Of 58 mutations, 24 originated from excision repair-proficient cell lines. The data from repair-proficient strains includes a TK line, 'TK6', and human diploid fibroblasts, 'N' . The 34 mutations recovered in repair deficient cells were split equally between two strains. Xeroderma pigmentosum complementation group A ('XPA') cells, which are defective in nucleotide excision repair (McGregor *et al.*, 1991; Dorado *et al.*, 1991; Petinga *et al.*, 1977; van Duin *et al.*, 1989) and XP variant ('XPV') cells, which have normal rates of repair, are both UV sensitive and hypermutable (Wang *et al.*, 1993).

Mutations were distributed throughout the *hprt* gene with some clustering in two regions. The first region contained the mutational "hotspot" positioned at 208-209 nt of the target gene where eight mutations were found. Seven of these 8 mutations were either C→T or CC→TT transitions, which are the "signature" of the UV mutagenesis. In addition, at least one of these mutations was recovered from each of the cell types. This position and the surrounding sequence of six cytosines was characterized by the greatest amount of 64PyPy damage and moderate CPD deposition. This would suggest that the 64PyPy was the pre-mutational lesion as has been observed in prokaryotic systems.

A clustering of C→T transitions occurred at one other position besides 208-209, (i.e., position 118-119). As in the case of the former hotspot, the recovery of UV "signature" mutations was adjacent to a highly damaged site (position 119-120). In the absence of information about the rate of repair at this specific sequence and with only a moderate amount of 64PyPy damage at this site, the CPD at $TC_{119\text{-}120}$ was implicated as the premutagenic lesion.

The sequence surrounding position 119-120 may be described as a hypermutable region. Twenty mutations from both repair proficient and deficient cells were recovered at thirteen pyrimidine locations between position 106 and 126. UV-induced DNA damage was also relatively high in this region with four sites of high CPD formation and one site with high 64PyPy deposition. With the sequence context of dipyrimidine sites in alternating DNA strands, the high DNA damage deposition was unexpected. In general, runs of

pyrimidines were considered to be more prone to UV-induced damage (Koehler *et al.*, 1991).

A correlation was expected between highly damaged sites and mutations recovered from XPA cells because XPA cells are nucleotide excision repair (NER)-deficient. CPD damage at dipyrimidine sites was ranked and the sites of high damage were compared with position of XPA-mutations. The top 10/60 sites with detectable CPD damage contained 9/18 mutations. By using a two-tailed Fisher's exact test, XPA mutations were biased towards sites of high CPD formation ($p<0.01$). A similar analysis for sites with 64PyPy damage, revealed no bias since 3/18 mutations were recovered at the top 10/55 positions with detectable 64PyPy damage. Thus, in the absence of NER, there was a better correlation between damage and mutation for CPD compared to 64PyPy formation. CPDs form approximately at 5-10 fold greater frequency than 64PyPy per unit energy of UV light [35] and it appeared that the higher incidence of CPDs significantly influenced this correlation.

The last analysis did not directly consider that DNA damage may be sequence context dependent and the local sequence context may greatly influence the intrinsic mutability of a lesion. The only sequence-specific pattern evident from a statistical analysis was that 64PyPy were formed preferentially at 5'-PyTC-3' sites. This was contrary to a correlation between the high frequency of both CPD and 64PyPy at TC sites with the sequence context of 5'-TCC-3' and the G:C→A:T transition mutational "hotspots" at the chromosomal Chinese hamster ovary adenine phosphoribosyltransferase locus (Drobetsky and Sage, 1993). We were unable to detect a statistically higher induction of either CPDs or

64PyPy at TC or CC sites with the context of 5'-TCC-3'. While 64PyPy deposition at TC sites with a flanking 3'C, on average, occurred at a high frequency (580 RFU*min), damage at 5'-TCA-3' sites was higher (690 RFU*min). Investigation of other patterns of DNA damage deposition revealed a lack of correlation of 64PyPy formation at 5'-TC-3' with periodicity of the DNA helix. To assess the influence of larger sequence segments context, the ΔG was used to indicate the degree of DNA intrastrand binding energy surrounding 5'-TC-3' sites. A sinusoidal curve emerged which suggested that a 64PyPy formation at 5'-TC-3' sites may have been associated to the ΔG in a complicated relationship, although the results could not be explained.

In conclusion, the initial DNA deposition appeared to be influenced by the flanking DNA sequence. The most significant pattern was associated with 64PyPy and the 5' nucleotide of a 5'-TC-3' dipyrimidine. The initial photoproduct distribution of both the CPD and 64PyPy lesions may have influenced the clustering of characteristic UV-induced mutations at two frequently mutated sites. Repair deficient cells showed a good correlation between initial CPD frequency and mutant recovery. In general, there was no correlation with CPD or 64PyPy formation and mutation recovery in repair proficient cells. DNA repair or other DNA lesions must influence mutant recovery to a greater degree than initial CPD and 64PyPy deposition. Repair rates of CPDs at individual nucleotides were extremely variable (Gao *et al.*, 1994; Tornaletti and Pfeifer, 1994) and slow repair rates provided the best correlation with the endpoint of mutational "hotspots" (Tornaletti and Pfeifer, 1994).

5. ACKNOWLEDGMENTS

The authors would like to thank Dr. Stephen Lloyd for the supply of T_4 endonuclease V, and Dr. E. Drobetsky for a critical evaluation of the manuscript. The authors were supported by NSERC-Pharmacia Biotech Industrial Research Council Award. G. Kotturi was also supported by a Science Council of British Columbia G.R.E.A.T. scholarship in collaboration with AXYS Analytical Services Inc.

CHAPTER IV. UVB-INDUCED MUTATIONAL SPECTRA IN THE *LACI* GENE FROM TRANSGENIC MOUSE SKIN.

Abstract

The UVB (295-320 nm) component of sunlight is recognized as a significant contributor to photoaging and skin cancer. We investigated UVB-induced mutagenesis *in vivo* using a *lacI* transgenic mouse mutation assay. Shaved C57BL/6 Big Blue® female mice were exposed to UVB light [1.8 J/(cm²*day) at 3.3 W/m²] for 5 consecutive days to a total dose of 9.0 J/cm². After correction for possible clonal expansion events, the mutation frequency of the treated and untreated animals was $80 \pm 20 \times 10^{-5}$ (n=8) and $7.5 \pm 1.1 \times 10^{-5}$ (n=8), respectively. The predominant class of mutations from both untreated (27/51) and treated (53/75) skin was GC → AT transitions. However, the sequence context of these transitions differed significantly between the UVB-exposed and control groups. The majority of the GC → AT transitions recovered from control animals were found at RpCpG sites (21/27; where R=G,A) which implicated deamination of 5-methylcytosine as an intermediate. GC → AT transitions from the UVB-irradiated skin were recovered predominantly at YpCpH or RpCpY sites (37/53; where H=A,T,C and Y=C,T). The frequency of GC→AT transitions at RpCpG sites (where R=G,A) was almost identical in the control ($3.3 \pm 0.8 \times 10^{-5}$) and UVB-irradiated groups ($5.3 \pm 1.2 \times 10^{-5}$; p=0.94). Thus, a clear delineation between mutations attributed to endogenous processes and UVB exposure was possible based on sequence specificity. Another indicative result of UVB irradiation was the recovery of tandem CC → TT transitions (3/75) which were exclusively recovered from UVB-treated skin. We suggest the Big Blue® mouse is a useful model to test sunscreens and topical agents for their ability to reduce UVB-induced mutagenesis.

To be submitted to Carcinogenesis.

1. INTRODUCTION

Exposure of the skin to sunlight leads to photoaging and skin cancer. Molecular epidemiology studies have clearly established this correlation. The predominant mutations in the p53 tumour suppressor gene in human non-melanoma skin tumours (Brash *et al.*, 1991; Ziegler *et al.*, 1993) are C → T or CC → TT transitions at such sites

(Daya-Grosjean *et al.*, 1995). These changes are consistent with DNA damage occurring at dipyrimidine sites after the direct absorption of UVB photons (Sage, 1993). With gradual depletion of the ozone layer, the contribution of highly genotoxic UVB light to disease incidence can be expected to increase (Slaper *et al.*, 1996). This emphasizes the requirement for a short term *in vivo* model to study the effects of sunlight and UV blocking agents. Mice may provide a useful biological system since p53 alterations in mouse skin appear to be an early event in the progression to cancer (Berg *et al.*, 1996). Frijhoff *et al.* (1997) investigated the mutagenic effects of UVB light using the F1 progeny of hairless SKH1 and *λlacZ*-transgenic mice strain 40.6. After 0.1 J/cm^2 of UVB light, an approximate 10-fold increase in mutant frequency above background was observed.

Another transgenic mouse model which has been extensively used to study in vivo mutagenesis carries the *lacI* gene as a mutational target in a λ shuttle vector (Kohler *et al.*, 1991). The lambda-*lacI* transgenic model was particularly useful because there exists both a large database of *lacI* mutations recovered from transgenic rodents (de Boer, 1995) and a large historical database of UV-induced effects using the *lacI* gene as a target in *E. coli* (Schaaper *et al.*, 1987; Schaaper and Glickman, 1982; Koehler *et al.*, 1991; Mitchell *et al.*, 1992; Sage *et al.*, 1992).

To determine whether the genetic changes observed in lambda-*lacI* transgenic mice are similar to those in human cancers, we irradiated the shaved skin of C57BL/6 Big Blue® female mice with UVB light. *LacI*$^-$ mutants were recovered from the genomic skin

DNA and the mutant frequency was determined. The mutant *lacI* genes were sequenced to establish the nature of the DNA sequence alterations. A significant increase in mutant frequency (MF) was observed over background levels. The mutational spectra were consistent with UVB mutagenesis as observed in other systems and with molecular alterations found in the p53 gene from human non-melanoma skin cancer.

2. MATERIALS AND METHODS

2.1. Exposure to UVB light

An area of approximately 3 cm by 5 cm on the backs of adult C57Bl/6 Big Blue® female mice (Stratagene, La Jolla, CA, USA; 9-12 weeks old) was shaved before the first exposure. Eight mice per exposure were placed in wire cages and exposed to UVB light at a dose rate of 3.3 W/m² for 92 min/day which resulted in a daily dose of 1.8 J/cm². The mice were treated for five consecutive days for a total dose of 9.0 J/cm². The UVB light was generated by a solar simulator (Oriel #6271 bulb with Schott GG19 and UG5 filters; Schott, Mainz, Germany) as shown in Figure 8. Concomitant UVA exposure through these filters was 0.27 J/cm²/day which probably did not effect the mutagenic response because of the relatively inefficient DNA absorption at UVA wavelengths.

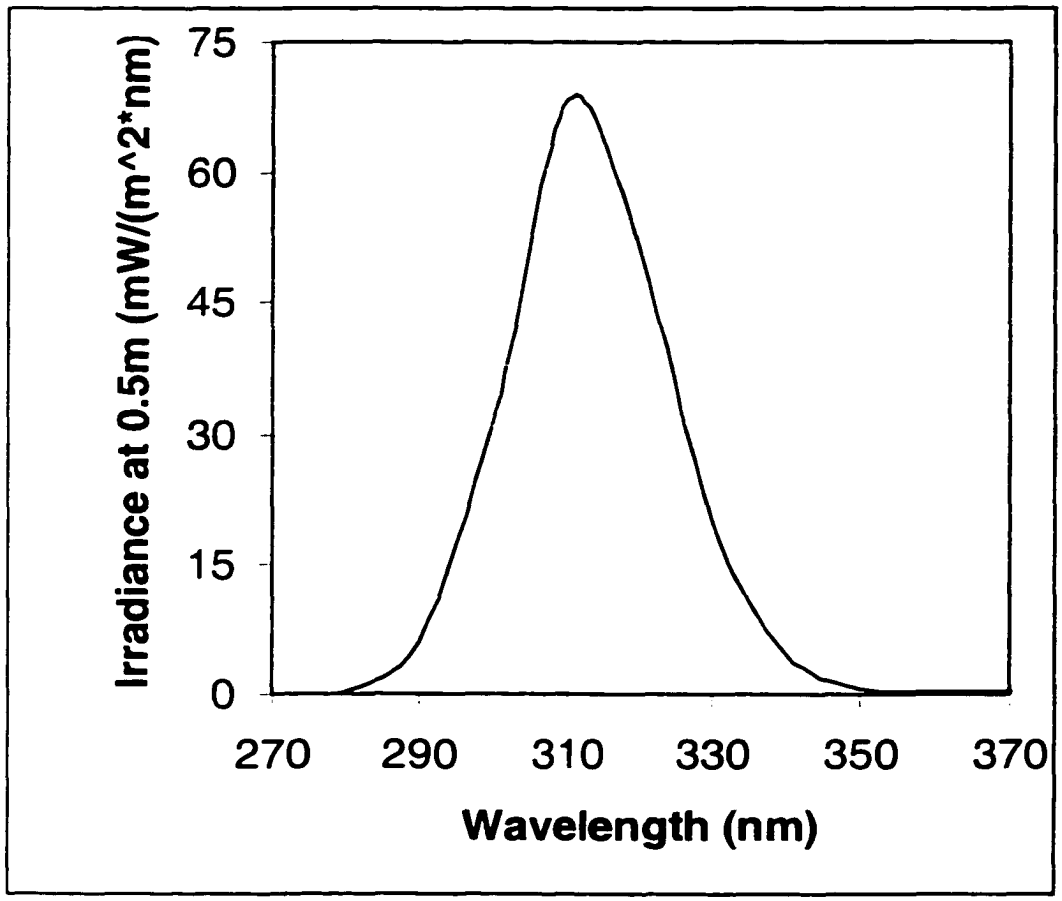

Figure 8. Irradiance at 0.5m using the illumination system of Oriel bulb #6271 filtered by Schott filters UG5 and GG19.

2.2. Mutant Frequencies

Skin samples (approximately 2 cm^2) from the backs of untreated or UV-exposed mice were recovered 14 days after the last dose to determine the MF in the *lacI* transgene. The extraction of DNA and recovery of *lacI* mutants was conducted as described [Big Blue® Mutagenesis Assay Manual (Stratagene), Kohler *et al.*, (1990)]. Briefly, skin tissue was minced with a razor blade and incubated at 50 °C for 3 h in 3 mL of dounce buffer [12.3 mM Na_2HPO_4, 140 mM NaCl, 2.7 mM KCl, 10 mM EDTA (ph=8.0), RNAce-IT 20 μL/ mL (Stratagene)] with 3 mL of proteinase K solution [2mg/mL proteinase K, 10% w/v SDS, 100 mM EDTA (ph=7.5)]. Genomic DNA was extracted by gently inverting the tube several times with a 50:50 phenol/chloroform mixture. The DNA was spooled after an ethanol precipitation and resuspended in TE buffer. The λ*lacI* transgene insert of the genomic DNA was packaged into λ phage particles with Transpack (Stratagene), transfected into the *lacI* deficient *E. coli* strain SCS-8, and plated in the presence of 1.5 mg/mL 5-bromo-4-chloro-3-indoyl-β-D-galactopyranosidase (X-gal) to a target plaque density of 8000 plaques per 25cm x 25 cm plate. Total plaque numbers were determined using an automated image analysis system by counting the number of plaques in areas covering ~13% of each plate. Colour controls were included in each plating experiment to monitor the variance of plating conditions. Statistical analyses were

conducted using the Generalized Score Test (Carr and Gorelick, 1994). Putative mutants which appeared as blue plaques were cored and verified by replating.

2.3. Mutational Spectra

LacI mutations were determined by direct sequencing of isolated "blue" mutant plaques as described previously (Erfle *et al.*, 1996). In summary, the *lacI* gene was amplified by PCR from a plaque suspension. Amplified DNA was purified using a Wizard preparative column (Promega, Madison, WI). The DNA sequence of each mutant *lacI* gene was determined by cycle sequencing with fluorescent end-labelled primers with analysis on the Pharmacia ALF™ sequencer (Pharmacia Biotech, Piscataway, NJ, USA) as described elsewhere. Statistical comparisons of mutational spectra were made according to the methods of Adams and Skopek (1987). Comparison of differences in classes of mutations were performed using the 2x2 χ^2 analysis with Statistica Version 5.0 for Windows (Statsoft Inc., Tulsa, OK, USA).

3. RESULTS

3.1. Mutant Frequency at the *lacI* transgene in mouse skin.

The mutant frequency (MF) fourteen days after five consecutive daily exposures of 1.8 J/cm^2 UVB was approximately 10-fold above controls. Mutant frequencies in the treated

(total UVB dose = 9.0 J/cm^2) and control groups were $89 \pm 21 \times 10^{-5}$ and $8.7 \pm 1.1 \times 10^{-5}$, respectively (Table IX). The difference is significant with $p < 0.01$ as determined by the Generalized Score Test (Carr and Gorelick, 1994). Although the mutant frequencies of two out of eight mice (i.e., Animal W2 and W6, in Table IX) were not elevated, the data were included in analysis.

Of the 717 mutants detected from the UVB exposed skin of 8 animals, 83 mutants were plaque purified and characterized at the DNA sequence level. A total of 78 mutants were generated from the control experiment and 59 were further characterized (as shown in Table X). Sequence analysis revealed that multiple identical mutations had been recovered from individual animals suggesting "clonal expansion" due to cellular proliferation. This information is used to apply a correction to the mutant frequency in order to obtain the mutation frequency. The adjustment is conservative since it is not currently possible to determine if these mutants are of clonal origin or arose from independent events. After correction for this 'clonal expansion' the adjusted MF is referred to as the mutation frequency. The mutation frequency for the UVB-exposed and control groups were $80 \pm 20 \times 10^{-5}$ and $7.5 \pm 1.1 \times 10^{-5}$, respectively. This represents 8/83 and 8/59 of the mutants attributed to clonal expansion in the UVB-induced and control groups, respectively.

3.2. Mutagenic Specificity of UVB-induced and spontaneous mutations.

The majority of the mutations recovered in the *lacI* gene both from the untreated mice (56/59) and UVB-treated mice (76/83) were base substitutions. The observed

distribution of base substitutions from UVB-treated mice was significantly different than those recovered from untreated mice ($p<0.05$, Table XI). The two largest classes of independent mutations recovered from untreated mice were GC → AT transitions (27/51)

Table IX. UVB is mutagenic in the skin of *lacI* mice.

Mouse	Treatment	Plaques	Mutants	MF × 10^5
Y1	None	160,991	11	6.8
Y2	None	116,354	14	12.
Y3	None	109,318	12	11.
Y4	None	113,863	10	8.8
Y5	None	101,282	14	14.
Y6	None	100,063	2	2.0
Y7	None	67,595	7	10.
Y8	None	130,339	8	6.1
TOTAL		899,805	78	8.7 ± 1.1*
W1	UVB†	79,578	64	80.
W2	UVB	61,864	8	13.
W3	UVB	80,052	91	114.
W4	UVB	67,333	42	62.
W5	UVB	141,406	190	134.
W6	UVB	123,187	19	15.
W7	UVB	157,405	252	160.
W8	UVB	98,021	51	52.
TOTAL		808,846	717	89 ± 21*,‡

Shaved adult female C57BL/6 *lacI* mice were held, or administered UV from a solar simulator (Oriel #6271 bulb with Schott GG19 and UG5 filters once each day for five days. Skin samples from the backs of mice were recovered 14 days after the last dose to determine MF in *lacI*.

* Avg ± SEM, Generalized Score Test methods.

† The UVB dose was 1.8 J/cm², administered in 92 min. The coincident exposure to UVA was 0.27 J/cm².

‡ Significantly different from controls, $P < 0.01$.

Table X. *lacI* mutations in skin from untreated or UVB-treated transgenic mice.

Base Pair Position*	Mutation†	Sequence Context‡	Mouse
A. Base Substitutions			
Untreated			
-15	G → C	GTA G GGC	Y1
20	G → C	AGG G TGG	Y2
42	C → T	TAA C GTT	Y1
56	G → A	GTC G CAG	Y4 (2)‡
82	G → T	TCA G ACC	Y1,Y2
86	G → T	ACC G TTT	Y5
93	G → A	CCC G CGT	Y7
95	G → T	CGC G TGG	Y2
96	T → C	GCG T GGT	Y7
116	G → A	CAC G TTT	Y8 (2)
129	C → T	AAA C GCG	Y5, Y7
131	C → T	ACG C GGG	Y5
140	G → T	AAA G TGG	Y4
173	C → T	ATT C CCA	Y4
178	C → A	CAA C CGC	Y3
180	G → A	ACC G CGT	Y5 (4)
186	C → T	TGG C ACA	Y2
191	C → T	CAA C AAC	Y1
250	C → G	GCA C GCG	Y5
269	G → A	GTC G CGG	Y3
270	C → T	TCG C GGC	Y2
273	C → A	CGG C GAT	Y1, Y3 (2)
284	C → T	TCT C GCG	Y5
284	C → G	TCT C GCG	Y8
308	G → A	AGC G TGG	Y7
329	C → T	GAA C GAA	Y3 (2), Y7

Base Pair Position*	Mutation†	Sequence Context‡	Mouse
A. Base Substitutions cont'd			
341	G → T	GTC G AAG	Y1
375	C → T	TCG C GCA	Y1, Y2, Y7
381	G → A	AAC G CGT	Y1, Y2
518	G → T	CAT G AAG	Y4
561	G → T	TGG G TCA	Y2
701	G → C	TCC G GTT	Y8 (2)
753	T → A	CGA T GCT	Y5
777	C → T	TGG C GCT	Y1, Y2
785	G → C	GCC G CAA	Y1
792	G → T	TGC G CGC	Y4
803	G → A	ACC G AGT	Y5
842	G → T	GTG G GAT	Y8
920	C → T	GGG C AAA	Y4
984	T → A	TGT T GCC	Y5
UVB-Treated			
31	G → A	TGT G AAA	W3, W7¥
41	A → C	GTA A CGT	W1¥
56	G → A	GTC G CAG	W1§
90	C → T	TTT C CCG	W1 (2), W3, W7¥
92	C → T	TCC C GCG	W1, W4§,¥
93	G → A	CCC G CGT	W2§,¥
113	C → G	AGC C ACG	W4
120	C → T	TTT C TGC	W1 (2), W5, W7 (2), W8¥
137	A → T	GAA A AAG	W1¥
140	G → A	AAA G TGG	W2, W3, W7¥.a
141	T → C	AAG T GGA	W6a
150	C → A	CGG C GAT	W5
153	T → A	CGA T GGC	W2

Base Pair Position*	Mutation†	Sequence Context[d]	Mouse
A. Base Substitutions cont'd			
162	T → C	AG<u>C</u> T G<u>A</u>A	W4
173	C → T	<u>A</u>TT <u>C</u> CC<u>A</u>	W1, W2, W5 (2), W7 (2), W8 (2)§,¥
173	C → G	<u>A</u>TT <u>C</u> CC<u>A</u>	W2¶,a
179	C → T	<u>A</u>AC <u>C</u> GC<u>G</u>	W4§,¥
180	G → A	AC<u>C</u> G CG<u>T</u>	W6§,¥
185	G → T	<u>G</u>TG <u>G</u> CA<u>C</u>	W5¶
270	C → T	TC<u>G</u> C G<u>G</u>C	W4§
282	C → T	AA<u>T</u> C T<u>C</u>G	W6¥
284	C → T	<u>T</u>CT <u>C</u> GC<u>G</u>	W1 (2), W2, W4, W8§,a
293	C → T	<u>G</u>AT <u>C</u> AA<u>C</u>	W3, W4, W7¥
330	G → A	AA<u>C</u> G A<u>A</u>G	W3, W5
369	T → C	AT<u>C</u> T T<u>C</u>T	W3¶
399	T → A	TC<u>A</u> T T<u>A</u>A	W5
470	C → T	<u>T</u>TT <u>C</u> TT<u>G</u>	W8¥
653	C → T	<u>A</u>AT <u>C</u> AA<u>A</u>	W3, W7¥
659	C → T	<u>A</u>TT <u>C</u> AG<u>C</u>	W2¥
687	G → A	AC<u>T</u> G G<u>A</u>G	W8¥
688	G → A	C<u>T</u>G G <u>A</u>GT	W8¥
701	G → C	T<u>C</u>C G <u>G</u>TT	W3§,¥
702	G → A	<u>C</u>CG <u>G</u> TT<u>T</u>	W5
707	C → T	<u>T</u>TT <u>C</u> AA<u>C</u>	W4, W5 (2)¥
756	T → G	TG<u>C</u> T G<u>G</u>T	W7
774	T → A	AG<u>A</u> T G<u>G</u>C	W8
791	C → T	<u>A</u>TG <u>C</u> GC<u>G</u>	W6¥
803	G → A	<u>A</u>CC <u>G</u> AG<u>T</u>	W4§
842	G → A	<u>G</u>TG <u>G</u> GA<u>T</u>	W8¥,a

Base Pair Position*	Mutation†	Sequence Context[d]	Mouse
A. Base Substitutions cont'd			
891	C → T	CCA C CAT	W3¥
908	C → T	TTT C GCC	W5
918	G → A	TGG G GCA	W4, W6
927	G → A	CCA G CGT	W4
977	C → T	AAT C AGC	W7, W8¥
1006	A → T	AAG A AAA	W8
B. Frameshift, Deletion and Tandem Substitution Mutations			
Untreated			
146-147	-GC	GAA**GC**GGCG	Y8
199-201	-G	CTGGC**GG**GC	Y2
891-892	CC → AA	CCA CC ATC	Y3
UVB-Treated			
91-92	CC→TT	TTC CC GCG	W8¥
234-235	CC→TT	CCT CC AGT	W6
470-471	CT→TA	TTT CT TGA	W1
524, 526	G→A/T→A	GACGGTACG	W2
638, 640	T→A/ -T	AAA T ATCTC	W5
707	-C	TTTCAACAA	W3
841-842	GG→AA	AGT GG GAT	W6

* Numbering of the *lacI* gene according to Farabaugh (1978).

† The mutation in the coding strand is reported.

d The mutated base(s) is (are) the center base(s); the first base of each codon is underlined. Bases in boldface include those possibly deleted or inserted. The deleted or substituted bases are stricken. The arrow indicates a possible site of base insertion.

‡ Number of occurrences, when more than one, per mouse.

§ The same mutation has been recovered in an untreated mouse.

¥ The same mutation has been recovered in a mouse treated with UVA (see Chapter V).

¶ A different mutation at the same site has been recovered in a mouse treated with UVA.

[a] A different mutation at the same site has been recovered in an untreated mouse.

[b] The same mutation has been recovered in a mouse treated with UVB.

[c] A different mutation at the same site has been recovered in a mouse treated with UVB.

and GC → TA transversions (12/51). Most of the GC → AT transitions in untreated mice 21/27 were located at RpCpG sites (where R= G,A; Table XII) which potentially reflected deamination of 5-methylcytosine. Only 1/27 GC → AT transitions at YpCpH or RpCpY sites (where H=A,T,C and Y=C,T) was recovered in the spontaneous spectrum. As will be discussed, this sequence context of YpCpH or RpCpY was indicative of UV exposure. GC → AT transitions also dominated the UVB-induced mutation spectra. However, the sequence context of these mutations differed substantially from controls. GC → AT transitions at YpCpH (31) or RpCpY (6) sites (37/53) was quite characteristic of UV-induced mutagenesis (Drobetsky and Glickman, 1990). The induced GC → AT transitions exhibited a high degree of sequence specificity with 27/31 occurring at TpCpH sites. While only 4/31 GC → AT transitions were recovered at CpCpH sites. The difference was not biased by the number of available site because 22 TpCpH and 23 CpCpH sites have had GC → AT transitions recovered in the *lacI* gene (de Boer and Glickman, 1998). With 5/53 UVB-induced GC → AT transitions at RpCpG sites, the class-specific mutation frequency of GC → AT transitions at RpCpG sites was very similar in the control ($21 / 51 * 7.5 \times 10^{-5} = 3.1 \pm 0.8 \times 10^{-5}$) and exposed ($5 / 75 * 80 \times 10^{-5} = 5.3 \pm 1.2 \times 10^{-5}$; p=0.94) groups.

Three tandem CC → TT mutations were recovered from the UVB-treated mice whereas none were recovered from the untreated mice. Other classes of mutations recovered at elevated frequencies in UVB-treated mice are AT → GC transitions and AT → TA and AT → CG transversions (Table XI).

Table XI. Summary of *lacI* mutations in untreated, UVB-treated or full spectrum-treated mouse skin.

	Mutation frequency × 10^5 (number of occurrences*)			
Mutation class	**Untreated**		**UVB-treated**	
Transitions:				
G:C → A:T	4.0	(27*)	57†	(53)
A:T → G:C	0.15	(1)	3.2†	(3)
Transversions:				
A:T → T:A	0.3	(2)	5.3†	(5)
A:T → C:G	<0.15	(0)	2.1	(2)
G:C → T:A	1.8	(12)	2.1	(2)
G:C → C:G	0.9	(6)	3.2	(3)
Others:				
Frameshifts	0.3	(2)	1.1	(1)
Tandem Base Substitutions	0.15	(1)	4.3†	(4)
Complex	<0.15	(0)	2.1	(2)
Total Mutation Frequency ×10^5	7.5‡		80	
Total Mutant Frequency ×10^5	8.7		89	
Total no. of mutations after clonal corrections		51		75
Total no. of mutations identified		59		83
Total no. of mutants recovered		78		717
Total plaques per group		899,805		808,846

* number of occurrences, corrected for possible clonal expansions.

† Significantly different than background mutation frequency ($P < 0.05$), after multiplicity adjustment, as determined by the methods of Carr and Gorelick (1996).

‡ The sum of class-specific mutation frequencies does not equal the overall mutation frequency exactly due to rounding errors.

Table XII. Sequence Specificity of GC → AT Transitions.

Mutation class	Sequence context†	Mutation Frequency x 10^5 (number of occurrences*) Untreated	UVB-treated
G:C → A:T		4.0 (27)*	57 (53)
	RpCpG	*(21)*	*(5)*
	YpCpG	*(2)*	*(11)‡*
	YpCpH (H=A,T,C)	*(1)*	*(31)‡*
	RpCpY	*(0)*	*(6)‡*
	Other	*(3)*	*(0)*
TOTAL		**7.5 (51)**	**80 (75)**

* number of occurrences, corrected for possible clonal expansion

† The sequence context for all GC →AT mutations is expressed in terms of cytosine (C in bolded underlined font) as the mutated base. This assumes that the relevant mutation in each case was C → T. Y = pyrimidine; R = purine; H = possible nucleotides are specified parenthetically.

‡Significantly different than background mutation frequency ($P < 0.01$), after multiplicity adjustment, as determined by the methods of Carr and Gorelick (1996).

Animals W2 and W6 in the exposed group had a MF comparable to the unexposed animals (Table IX). Despite the lack of mutation induction, both of these animals did show a shift in mutational spectra consistent with their UVB exposure. Specifically, for animal W2, 5 out of 8 recovered mutations were GC → AT transitions. Three were either at YpCpH or RpCpY sites, 1 was at a YpCpG site and the last GC → AT transition was at a RpCpG site. Four of seven mutants recovered from animal W6 were GC → AT transitions. Two were recovered at YpCpH sites and two at RpCpG sites. In addition, from animal W6, two of the seven mutations were tandem CC → TT transition which was very characteristic of UV-induced mutagenesis.

4. DISCUSSION AND CONCLUSIONS

We exposed C57BL/6 Big Blue® female mice to a total of 9.0 J/cm^2 of UVB light. This treatment resulted in a 10-fold increase in mutation frequency from $7.5 \pm 1.1 \times 10^{-5}$ to $80 \pm 21 \times 10^{-5}$. In the UVB-exposed group, we observed a large animal-to-animal variability in the MF. This was primarily due to two animals, which failed to produce an in increase in MF following exposure to UVB. Sequence analysis of the recovered mutants indicated that the mutaitons from the UVB-irradiated mice reflected the treatment, although animals W2 and W6 had potentially limited exposure. Why the increase in MF was so limited in these two animals was unknown. Whether it reflected individual sensitivity or a reduced exposure was uncertain. The fact that such ranges existed of course was very

suggestive of different exposures. The UVB-irradiated animals were able to move and possibly avoided direct irradiation to varying degrees.

The mutational spectra of the independent mutations shifted to that consistent with mutagenesis of UVB light (Sage *et al.*, 1996). While GC → AT transitions dominated the point mutations recovered from both the untreated (27/51) and treated (53/75) animals, the sequence specificity of these transitions was significantly different ($p<0.01$). The majority of the GC → AT transitions in the background spectra were located at RpCpG sites (21/27) which are thought to result from spontaneous deamination of 5-methylcytosine. In accordance with UV-induced mutagenesis the sequence context of the GC → AT transitions from the exposed animals shifted from RpCpG to YpCpH and RpCpY sites (37/53; Table XII). The class-specific mutation frequency attributed to GC → AT transitions at RpCpG sites in the exposed animals ($5.3 \pm 1.2 \times 10^{-5}$) was the same as that of the unexposed animals ($3.3 \pm 0.8 \times 10^{-5}$; $p=0.94$). Induced and background mutations could, therefore, largely be delineated by sequence context and further corroborated the easy demarcation of UVB-induced and endogenous events. Thus the majority (56%) of the induced mutations may be directly attributed to UV-induced GC → AT transitions at YpCpH and RpCpY sites.

The majority of the GC → AT transitions at YpCpH sites were recovered at TpCpH sites (27/31) and not CpCpH sites (4/31). The recovery of mutations was not biased by the number of available sites since a total of 22 TpCpH sites and 23 CpCpH sites have had GC → AT transitions recovered in the *lacI* gene (de Boer and Glickman, 1998). Thus, there

appeared to be a strong bias of the 5' nucleotide with respect to GC → AT transitions at 5'-YpC sites. With the biased recovery of GC → AT transitions at TpCpH sites, it potentially implicated the 64PyPy as a possible premutagenic lesion. While both 64 PyPy and CPDs form at dipyrimidine sites, 64PyPys are formed most frequently at TpC sites (Mitchell *et al.*, 1992). Also, replication of a site-specific UV lesion in SOS-induced *E. coli* resulted in a weak mutagenic response from the *cis-syn* CPD at a TpC site (Horsfall *et al.*, 1997). The 64PyPy and, in particular, its Dewar isomer are very mutagenic (Horsfall and Lawrence, 1994).

64PyPys were probably not the only premutagenic lesion at TpC sites since 8 GC →AT transitions were observed at TpCpG sites. 8 GC →AT transitions recovered at TpCpG sites suggested an influence of spontanous deamination in mutation fixation. 64PyPys form at lower frequencies at dipyrimidines containing methylated cytosines (Brash and Haseltine, 1982; Pfeifer *et al.*, 1991). All CpG sites in the *lacI* gene of the transgenic mouse are assumed to be methylated (Wyborski *et al.*, 1996). In these particular cases, it suggested a CPD may be the premutagenic lesion. Since the rate of photoproduct repair varies significantly with nucleotide position (Tornaletti and Pfeifer, 1993), it seemed likely that both 64PyPys and CPDs possibly played a role in UVB mutagenesis in the skin of the lambda-lacI transgenic mouse.

Another study of *in vivo* UVB-induced mutagenesis was reported by Frijhoff *et al.* (1997). A MF of $38 \pm 8.0 \times 10^{-5}$ in a transgenic mouse with the bacterial *lacZ* gene following an irradiation of 0.1 J/cm^2 of UVB light. This represented an approximate 10-

fold induction in MF above background levels ($3.5 \pm 1.5 \times 10^{-5}$). In comparison, our study also achieved a 10-fold induction but after 9.0 J/cm^2 of UVB. The many differences between the two experimental systems made it difficult to directly compare the biological responses. Two major differences were the genetic background of the mice and the irradiation sources. First, the transgenic lacZ mice were hairless and the altered skin structure may have been more sensitive to light. Second, the UVB exposures were different. The light source used in our study was an Oriel lamp with Schott cutoff filters GG19 and UG5 and a dose rate of 3.3 W/m^2. The hairless mice were irradiated with an unfiltered Philips FS40 sun lamp at a UVB fluence of 1.3 W/m^2 (Frijhoff *et al.*, 1997). Small differences in light intensities below 300 nm would impact the biological response significantly because light < 300 nm is highly cytotoxic and mutagenic (Tyrell and Pidoux, 1987). Comparative biological dosimetry would be necessary to compare the different exposures.

Even though the MF inductions for a given fluence were different, the UVB-induced mutational spectra were similar for both transgenic systems. The UVB-induced mutations recovered from the hairless mice showed an induction of GC → AT transitions at YpCpH sites since 10/24 (42%) independent mutations were recovered from the exposed skin. This compared with 31/75 (41%) from the lambda-lacI transgenic model. A further similarity was the recovery of CC → TT transitions which occurred at the same percentage of UVB-induced mutational spectra in the skin of hairless SKH1 *lacZ* (4%) and shaved C57Bl/6 *lacI* (4%) transgenic mice.

UVB irradiation of cells in culture also produced similar results to those observed with the *lacI* transgenic mouse assay. The cell culture system which has been extensively used to study the mutagenic effects of the three classes of UV light (i.e., UVA, UVB and UVC) detects mutants at the *adenine phosphoribosyltransferase* (*aprt*) locus of Chinese hamster ovary (CHO) cells (Drobetsky *et al.*, 1987; Drobetsky *et al.*, 1994; Drobetsky *et al.*, 1995; Sage *et al.*, 1996). A ≈25-fold increase in mutation frequency over background levels of aprt$^-$ mutants was observed after 0.01 J/cm^2 of UVB light (Drobetsky *et al.*, 1995). CHO cells were irradiated at a dose rate of 1 W/m^2 with Spectroline model XX25B lamps. Wavelengths below 290 nm were filtered by Schott filter WG305. The induced spectra contained a predominance of GC → AT transitions at YpCpH or RpCpY sites (45/74; 61%) and was comparable to our results (38/75; 51%). Tandem CC → TT transitions also contributed similarly to both UVB-induced spectra [5% (4/74) and 4% (3/75), respectively].

Comparisons of our UVB-induced mutation data with studies using UVC light must be made with an understanding of the differences and similarities between UVB and UVC light. The CHO system, described above, was also used to investigate the mutagenic effects of UVC light (Drobetsky *et al.*, 1987). While UVC light is considerably more cytotoxic and mutagenic than UVB light based on the total energy of irradiation, the mutational spectra are not significantly different. The recovery of the two key UV-induced mutational classes, the GC → AT transitions and tandem CC → TT transitions, was very similar for both the UVB and UVC exposures. GC → AT transitions composed 66% (49/74) and 57% (33/59)

and tandem CC → TT transitions represented 5% (4/74) and 5% (3/59) of the UVB and UVC-induced mutational spectra, respectively. Interestingly, only 1/74 of the GC → AT transitions recovered from the UVB exposure was found at a CpG site.

Perhaps the most important comparison that can be made was that to mutations found in the p53 tumour suppressor gene recovered in human non-melanoma skin tumours from both normal and xerodoma pigmentosum (XP) patients (Brash *et al.*, 1991). The UV portion of sunlight was implicated because of the predominance (80%) of mutations at dipyrimidine sites. The pattern of single base substitutions found in the p53 gene isolated from non-XP patients revealed 68-74% GC → AT transitions at dipyrimidine sites (Dumaz *et al.*, 1994; Stary *et al.*, 1997). This fingerprint appeared to clearly implicate the UVB portion of the sunlight spectrum. The tandem CC → TT transitions was even a more significant fingerprint for UV-induced carcinogenesis because they occurred at 14%-20% in skin tumours compared to 0.8% in internal malignancies. In our study and others approximately 5% of the recovered mutations were tandem CC → TT transitions. Although certain oxidative species induced these tandem transitions (Reid and Loeb, 1993), UV-induced tandem transitions have been widely reported.

In summary, the UVB-induced spectra in the skin of C57Bl/6 *lacI* transgenic female mice were consistent with other UVB mutation studies. This suggested that the *lacI* transgenic mouse assay provided a useful model to further investigate the effects of UVB light. The spectrum of p53 mutants from non-melanoma skin cancers strongly suggested a role for UVB light, however the increased yield of tandem CC → TT transitions was also

consistent with a role for other mutagenic sources such as oxidative damage (Reid and Loeb, 1993). Insights from the biological impact of UV light potentially implicated 64PyPys at TpCpH sites and CPDs at TpCpG sites as premutagenic lesions.

ACKNOWLEDGEMENTS

The authors would like to acknowledge the use of the Procter & Gamble solar simulator.

CHAPTER V. UVA-INDUCED MUTATIONAL SPECTRA IN THE *LACI* GENE FROM TRANSGENIC MOUSE SKIN.

G. Kotturi[1], B.W. Glickman[2], J.G. de Boer[2] and N.J. Gorelick[3]

[1] Stratagene, 11011 N. Torrey Pines Rd., La Jolla, CA, USA 92037

[2] Centre for Environmental Health, Department of Biology, University of Victoria, P.O. Box 3020 STN CSC, Victoria, B.C., Canada V8W 3N5.

[3] Procter & Gamble, Ivorydale Technical Center, 5299 Spring Grove Ave., Cinncinati, Ohio, USA 45217-1087

To be submitted to Proc. Natl. Acad. Sci. USA

Abstract

There is now compelling evidence to suggest that chronic irradiation with UVA (320-400 nm) is a significant component of the etiologies of photoaging and skin cancer. To identify acute markers of UVA damage, we investigated UVA-induced mutagenesis *in vivo* by using a *lacI* transgenic mouse mutation assay. The backs of adult female C57BL/6 Big Blue® mice were shaved and exposed daily to UVA for 5 consecutive days. UVA was generated by a solar simulator (Oriel) fitted with filters to permit the transmission of UVA. An initial experiment using mice sacrificed twelve days after the last exposure, revealed a significantly increased mutant frequency in the UVA-treated (800 J/cm^2) group of (Avg ± SEM, n=7) 17 ± 3.4 x 10^{-5} compared with 6.1 ± 0.5 x 10^{-5} in the concurrent untreated controls. Subsequently, 4 groups of animals were treated with a total of 0, 230, 450 and 900 J/cm^2 in five consecutive equal daily doses. In the dose-response experiment, the mutant frequency increased in a non-linear manner. The attenuated dose response and increased number of clonal events in the exposed group suggested that UVA light induced a high degree of cell death which was followed by cell repopulation. DNA sequence analysis of mutant *lacI* genes demonstrates that UVA treatment produced a different mutational spectra compared to control. The predominant classes of recovered mutations from untreated skin were GC → AT transitions at CpG sites (17/61) and GC → TA transversions (21/61). In contrast, in the UVA-treated group, GC → AT transitions at non-CpG sites predominated (49/118 mutations) and four unique tandem base substitutions (all CC → TT) were recovered. In addition, increased frequencies of GC → CG and AT → TA substitutions were observed. The UVA-induced mutational spectra were consistent with UVA-induced DNA damage which included dipyrimidine lesions and reactive oxygen species.

1. INTRODUCTION

The UVB component (290-320 nm) of sunlight has been considered a greater risk factor than UVA (320-400 nm) because of its higher relative direct absorption by DNA compared to UVA. The essential role of UVB in the induction of non-melanoma skin cancer was suggested by the recovery of CC → TT mutations in the *p53* gene as characteristic of far-UV mutagenesis (Brash *et al.*, 1991; Dumaz *et al.*, 1993; Ziegler *et al.*, 1993; Ziegler *et al.*, 1994; Daya-Grosjean *et al.*, 1995). Hence, solar light and, by association, the UVB portion, has been accepted as the main causative agent. However, in a cell culture study, CC → TT mutations were recovered following UVA exposure (Drobetsky *et al.*, 1995) and UVA was shown to be tumorigenic in rodents (de Laat *et al.*, 1997). Furthermore, with the advent of long wave (340-400nm) UVA tanning beds, human exposure to the UVA portion of the spectrum has become increasingly prevalent. Estimation of human exposure to UVA in daylight is complicated by the changing spectrum of light throughout the day. At midday, 40% of the action spectrum of solar light, as defined by cytotoxicity of human primary cell lines, can be attributed to the UVB component (Tyrrell and Pidoux, 1987). However, at lower solar zeniths, UVA light contributed as much as 80% of the action spectrum (Tyrrell and Pidoux, 1987). In addition, the relationship between melanoma induction and sunlight exposure has not been clearly determined. Specific risk factors such as migration to a sunny climate during youth, appeared to be important (Lee, 1989) and UVA may indeed play a role (Setlow *et al.*, 1993). Although recently, it was proposed melanoma was not caused by sunlight but rather increased skin temperature (Christophers, 1998).

UVA and UVB light have different skin transmission characteristics and cellular effects. UVA light penetrates with a greater efficiency through to the basal skin layer than UVB as indicated by direct measurements (Bruls *et al.*, 1984). Twenty-four hours after UVB exposure *p53* induction was observed throughout the viable layer while UVA-induced expression was primarily limited to the basal layer (Campbell *et al.*, 1993). The dose of UVA to the cells above the basal layer may have been too great to permit an

increase in p53 levels, or possibly this was a cell-type specific response. *p53* induction was correlated with the ability of UVA but not UVB to effectively induce immediate apoptosis (Godar and Lucas, 1995). Alternatively, the pathway of immediate apoptosis may be mediated by oxygen radicals which were associated primarily with UVA light (Tyrrell, 1996).

Studies of the DNA-damaging and mutagenic effects of UVB and UVA have demonstrated some differences. UVB light effectively induced pyrimidine dimers such as cyclobutane pyrimidine dimers (CPDs) and pyrimidine-pyrimidone 6-4 photoproducts (64PyPys) in purified DNA (Cleaver *et al.*, 1991). The characteristic mutations thought to arise from the pyrimidine dimers were single and tandem GC → AT transitions at dipyrimidine sites. While induction of CPDs and 64PyPys has been shown to occur in hairless mice exposed to UVA light (Kinley *et al.*, 1995; Ley and Fourtanier, 1997), more attention has been placed recently on the ability of UVA to generate reactive oxygen species (ROS; Wlaschek *et al.*, 1997; Warner and Wei, 1997; Zhang *et al.*, 1997). Evidence suggested that cytotoxicity and mutagenicity of UVA light was primarily mediated by singlet oxygen in cultured cells (Tyrrell and Pidoux, 1989; Basu-Modak and Tyrrell, 1993; Tebbe *et al.*, 1997), although hydrogen peroxide and superoxide radicals have also been detected (Albro *et al.*, 1997; Shindo and Hashimoto, 1997) and shown to be mutagenic (Knowles and Eisenstark, 1989).

UVA-induced mutagenesis appears to be the combined effect of pyrimidine dimers leading to GC → AT transitions and modified purine bases leading to transversions at AT basepairs (Drobetsky *et al.*, 1995; Robert *et al.*, 1996). The predominant base substitution recovered after exposure to UVA light in the *lacZ'* gene stably introduced into a human embryonic kidney cell line was the GC → AT transition (27%; 12/45). The UVA-induced contribution of this point mutation was significantly less than either UVC (69%) or UVB (82%) induced mutagenesis after UV-treatments of similar survival levels (Robert *et al.*, 1996). A similar trend was detected using the *adenine phosphoribosyltransferase* (*aprt*) locus of Chinese hamster ovary (CHO) cells.

The recovery of GC → AT transitions was 57%, 66% and 22% for UVC, UVB and UVA, respectively (Drobetsky *et al.*, 1995). The most profound shift in the UVA-induced mutation spectrum was a high recovery of AT → CG transversions (45%) in the UVA-exposed cells (Drobetsky *et al.*, 1995). The predominance of this mutation and its relatively rare recovery in controls or mutagenic treatments led to the suggestion that it may be a fingerprint for UVA mutagenesis. However, Robert *et al.* (1996) reported 41% of the mutations occurred at AT basepairs after UVA treatment but recovered no AT → CG transversion. The differences may have been a result of the two biological systems. They also differed in light source, dose rate and total dose. A dose rate of 75 W/m^2 and dose of 500 kJ/ m^2 was consistent for the entire data set reported by Drobetsky *et al.* (1995). While the dose rate of 150 W/m^2 was constant for each total dose but the UVA-induced spectrum was composed of a compilation of mutations from recovered from all the doses from 200 to 800 kJ/m^2 (Robert *et al.*, 1996).

In this study, we have used a transgenic mouse system to identify mutational events induced in skin after exposure to UVA light. The transgene contained approximately 40 tandem copies of a bacteriophage lambda with the *E. coli lacI* gene as the mutational reporter (Short *et al.*, 1990). We reported the mutant frequency, mutation frequency and mutational spectra following 5 consecutive daily exposures to UVA light and for concurrent untreated controls. The mutant frequency dose response from a parallel experiment was also reported. In the initial experiment, female mice were either exposed to 800 J/cm^2 of UVA light (n=7) or left untreated (n=7). UVA-treatment (800 J/cm^2) produced a significant elevation of the mutant frequency (17×10^{-5}) compared to background (6.1×10^{-5}). The mutational spectra showed specific differences in the types of mutations after irradiation. In particular, GC → AT transitions at dipyrimidine sites, GC → CG transversions and AT → TA transversions were significantly elevated above the expected background frequency. A significant increase in the number of clonal events was observed over background. A second experiment in which mice (n=8) were exposed

to total fluences of 0, 230, 450 and 900 J/cm^2/day of UVA light, resulted in a mutant frequency increase from 8.7 to 19.3 x 10^{-5}, respectively. We analyzed the results and proposed mechanisms to account for the observations.

2. MATERIAL AND METHODS

2.1. Exposures

An area covering approximately 3 cm by 5 cm on the backs of adult female C57Bl/6 Big Blue® mice (9-12 weeks old) (Stratagene, La Jolla, CA, USA) was shaved before the first UVA exposure. Mice were placed in wire cages during the duration of the UV exposures. In the first experiment, UVA (123 J/cm²/day in 4 hr/day for 2 days + 185 J/cm²/day in 6 hr/day for 3 days = 800 J/cm²) was administered to mice (n=7) from a solar simulator (Oriel #6271 bulb with Schott UG-11 and WG335 filters; Schott Yonkers, NY, USA) as shown in Figure 9. Less than 1% UVB (radiation (primarily 318-320 nm) passes through these filters, which contributes less than 1.5% of the total erythemal effectiveness. The UVA exposure is equivalent to human exposure from ~15 - 24 hr in the North American summer sun. In a second experiment, female mice (n=8) were exposed to the same light system for 0, 57, 114 and 227 min / day for five days for UVA doses of 0, 45, 90, and 180 J/cm² /day. This resulted in total UVA doses of 0, 230, 450, and 900 J/cm², respectively.

2.2. Mutant Frequencies

In the first experiment, skin samples (approximately 2 cm²) from the backs of untreated or UV-exposed mice were recovered 12 days after the last dose to determine the mutant frequency (MF) in the *lacI* transgene. Tissues were frozen immediately in dry ice. The extraction of DNA and recovery of *lacI* mutants was conducted as previously described (Big Blue® Mutagenesis Assay Manual, Stratagene). Briefly, tissues were thawed in 5 mL of dounce buffer [12 mM Na_2HPO_4, 140 mM NaCl, 2.7mM KCl,

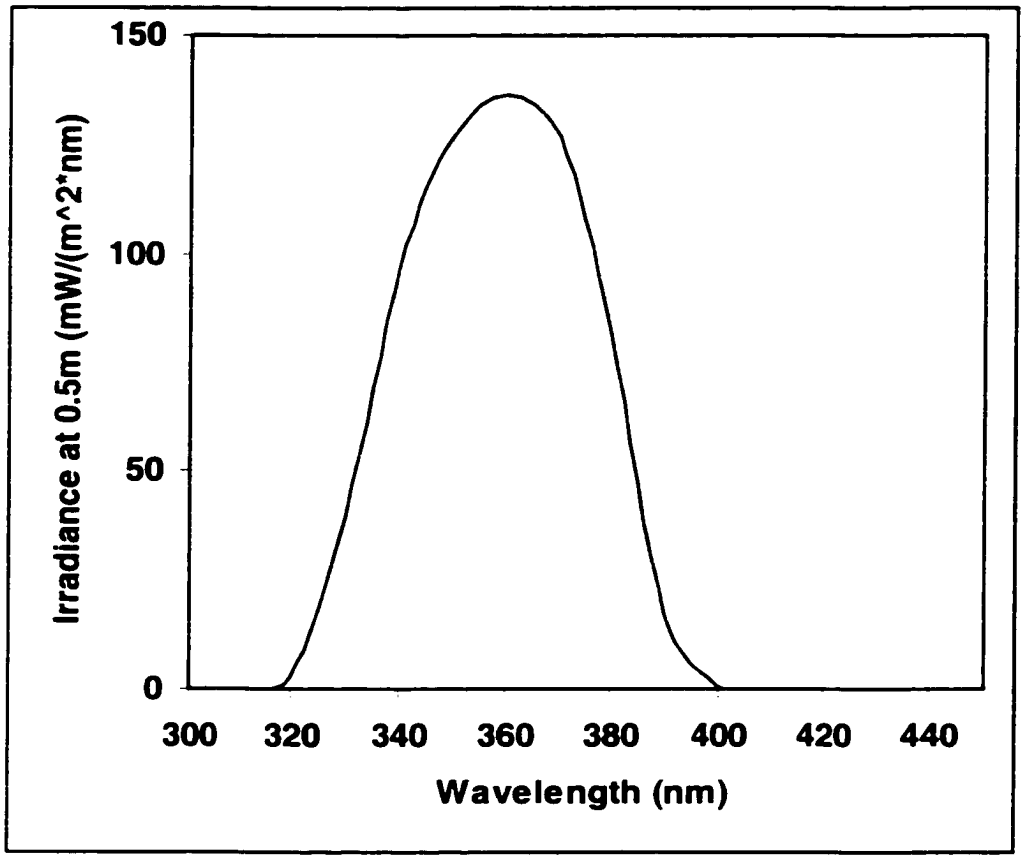

Figure 9. Irradiance at 0.5m using the illumination system of Oriel bulb #6271 and Schott filters UG11 and WG335.

1.5 mM KH_2PO_4, 10 mM EDTA, 20 µL/mL RNace-It™ cocktail (Stratagene), pH=8.0] and placed, with the buffer in a 7 mL Wheaton glass homogenizer (Wheaton, USA). The tissues were dounced until disaggregrated. The mixture is transferred into a 50 mL tube with 3 mL of Proteinase K solution [20 mg/mL Proteinase K, 2% (w/v) SDS, 100 mM EDTA, pH=7.5] and incubated for approximately 3 h at 50°C. The DNA was extracted by 2 consecutive phenol:chloroform extractions and precipitated with ethanol. DNA was resuspended into TE buffer (10 mM Tris-HCl, 1mM EDTA, pH=7.5). Packaging of the lambda vector was performed by mixing 8 µL of DNA with the packaging extract (Transpack, Stratagene). The packaged phage were plated on 625 cm^2 plates with 250 mL bottom NZY agar (Stratagene) and 45 mL top NZY agarose (Stratagene). Plates were poured with a plaque density of 8000 plaques/plate. Total plaque numbers were determined using a Macintosh-based automated image analysis system where the number of plaques in an area covering ~13% of each plate were determined. Statistical analyses were conducted using the Generalized Score Test (Carr and Gorelick, 1994).

2.3. Mutational Spectra

LacI mutations were determined by direct sequencing of the *lacI* gene in isolated "blue" mutant plaques, as described in Erfle *et al.* (1996). In summary, the *lacI* gene was amplified by PCR from a plaque suspension. Amplified DNA was purified using a Wizard preparative column (Promega, Madison, WI, USA). The DNA sequence of each mutant *lacI* gene was determined by cycle sequencing with fluorescent end-labelled primers with analysis on the Pharmacia ALF™ sequencer (Pharmacia Biotech,

Piscataway, NJ, USA). Statistical comparisons of mutational spectra were made according to the methods of Carr and Gorelick (1996).

2.4. Clonal Expansion

Clonal expansion events are defined as mutations which arise more than once in a single tissue from a single animal. It is assumed that one independent mutation was considered a 'founder' mutation which gave rise to the clonal events. The ratio of independent / total (independent + clonal) mutations corrects the mutant frequency to the mutation frequency. Differences in possible clonal expansion events were analyzed by a 2x2 table using a two-tailed Fisher's exact test (FE; SAS Version 6.12, SAS Institute, Inc., Cary, North Carolina, USA). Typically this involved comparing independent versus possible clonal expansion events for two treated or untreated mutational spectra. The untreated spectra of several experiments (unpublished data; Gorelick *et al.*, 1995) were pooled. Jackpot analysis was performed and the Fisher's exact test was repeated. The jackpot analysis involved removing any one animal which appeared to have a particularly high number of clonal events.

3. RESULTS

3.1. Mutant Frequencies

LacI gene mutations were screened after the packaging and plating of genomic DNA which originated in untreated and UVA-irradiated skin of C57/BL6 transgenic mice. In an initial experiment, seven mice were exposed to a total UVA exposure of 800 J/cm^2 while seven animals served as untreated controls. The mutant frequency (MF) in each individual animal is shown in Table XIII. The background MF was $6.1 \pm 0.5 \times 10^{-5}$ (average ± standard error). After UVA irradiation, the MF increased to $17 \pm 3.4 \times 10^{-5}$, which is significantly different from controls ($p<0.05$; Gorelick *et al.*, 1996).

A second experiment was designed to determine the mutant frequency dose response for UVA irradiation in the *lacI* transgene. Female mice were irradiated in groups of eight with 0, 230, 450 or 900 J/cm^2. While the MF increased with dose (see Table XIV), the response was not linear. We believe the increase in background MF was due to a change in media composition that increased the darkness of blue plaques. *LacI* mutant plaques, which normally would have appeared white or clear, were detected as extremely light blue plaques.

3.2. Mutation Frequencies

The recovered mutants were characterized by DNA sequence analysis (Table XV). *LacI* DNA sequences were determined for sixty-nine of the seventy-nine mutants recovered from untreated mice. The remaining eight mutations did not reveal DNA sequence changes in the *lacI* coding region. When the same mutation was recovered more than once from a single mouse, all but one occurrence of the mutation were considered part of the clonal expansion and eliminated from the mutational spectrum. Thus, sixty-one of the sixty-nine mutations from the control group were considered independent. The background mutation frequency was calculated by multiplying the background mutant frequency by the ratio of the number of independent mutations to total number of mutations to give a mutation frequency of [$(6.1 \times 10^{-5}) \times (61/69) =$] $5.4 \pm 0.5 \times 10^{-5}$. One hundred and seventy two mutants were recovered from the UVA-irradiated mice. Using the criteria for possible clonal expansions described above, 118 independent mutations were identified from a total of 156 characterized mutants. The mutation frequency of the UVA-exposed group was calculated as [$(17 \times 10^{-5}) \times (118/156) =$] $13 \pm 3 \times 10^{-5}$.

3.3. Clonal Expansions

As shown in Table XVI the ratios of possible clonal events to independent mutations were 8/61 and 38/118 for the control and treated groups, respectively. This difference was marginally significant (FE; p=0.046). A combined database of *lacI*

Table XIII. UVA is mutagenic in skin from *lacI* transgenic mice.

Mouse	Treatment	Plaques	Mutants	MF × 10^5
N1	None	257,510	11	4.3
N2	None	146,034	9	6.2
N4	None	242,787	17	7.0
N5	None	178,269	11	6.2
N6	None	172,283	10	5.8
N8	None	144,253	12	8.3
N9	None	127,703	9	7.0
TOTAL		1,168,839	79	6.1 ± 0.5*
Q1	UVA	248,300	65	26.
Q2	UVA	87,267	8	9.2
Q4	UVA	126,178	28	22.
Q5	UVA	139,925	30	21.
Q6	UVA	95,918	14	15.
Q7	UVA	104,691	8	7.6
Q8	UVA	242,436	19	7.8
TOTAL		1,044,715	172	17 ± 3*,†

Shaved adult female C57BL/6 *lacI* mice were held ("None") or administered UVA (123 J/cm^2 in 4 hr/day for 2 days + 185 J/cm^2 in 6 hr/day for 3 days) from a solar simulator (Oriel #6271 bulb with Schott UG11 and WG335 filters) ("UVA"). Skin samples from the backs of mice were recovered 12 days after the last dose to determine MF in *lacI*.

* Avg ± SEM, based on Generalized Score Test methods (Carr and Gorelick, 1994).

† Significantly different than untreated controls, $p<0.01$ ($p = 0.0189$?), by Generalized Score Test methods.

Table XIV. UVA mutagenicity is dose-dependent in skin of *lacI* mice.

Treatment (J/cm^2)	Plaques	Mutants	MF × 10^5*
None	899,805	78	8.7 ± 1.1
230†	978,287	142	14.5 ± 2¶
450‡	836,893	140	16.7 ± 2¶
900§	907,917	175	19.3 ± 2¶

Shaved adult female C57BL/6 *lacI* mice were held ("None"), or administered UVA from a solar simulator (Oriel #6271 bulb with Schott UG11 and WG335 filters) once each day for five days. Skin samples from the backs of mice were recovered 14 days after the last dose to determine MF in *lacI*.

* Avg ± SEM, n=8

† Dose administered in 57 min each day for five consecutive days.

‡ Dose administered in 114 min each day for five consecutive days.

§ Dose administered in 227 min each day for five consecutive days.

¶ Significantly different from controls, $p<0.01$, by Generalized Score Test methods.

Table XV. *lacI* mutations in skin from UVA-treated (800J/cm^2) or untreated transgenic mice.

Base Pair Position*	Mutation†	Sequence Context¶	Mouse
A. Base Substitutions			
Untreated			
42	C → T	TA<u>A</u> C G<u>T</u>T	N1,N6,N8
53	G → T	<u>G</u>AT <u>G</u> TC<u>G</u>	N2
56	G → A	<u>G</u>TC <u>G</u> CA<u>G</u>	N1, N8
57	C → A	TC<u>G</u> C A<u>G</u>A	N2
78	A → C	CT<u>T</u> A T<u>C</u>A	N1
78	A → G	CT<u>T</u> A T<u>C</u>A	N1
82	G → T	T<u>C</u>A G <u>A</u>CC	N4
84	C → A	AG<u>A</u> C C<u>G</u>T	N5
86	G → T	<u>A</u>CC <u>G</u> TT<u>T</u>	N5, N6
89	T → C	<u>G</u>TT <u>T</u> CC<u>C</u>	N9
92	C → T	<u>T</u>CC <u>C</u> GC<u>G</u>	N6
92	C → A	<u>T</u>CC <u>C</u> GC<u>G</u>	N8
93	G → A	CC<u>C</u> G C<u>G</u>T	N5 (2)‡
95	G → T	<u>C</u>GC <u>G</u> TG<u>G</u>	N6, N9
103	C → G	G<u>A</u>A C <u>C</u>AG	N4
103	C → A	G<u>A</u>A C <u>C</u>AG	N2
129	C → A	AA<u>A</u> C G<u>C</u>G	N2, N4
134	G → T	<u>C</u>GG <u>G</u> AA<u>A</u>	N8
140	G → T	<u>A</u>AA <u>G</u> TG<u>G</u>	N5, N9
141	T → G	AA<u>G</u> T G<u>G</u>A	N4
171	T → C	AC<u>A</u> T T<u>C</u>C	N1
179	C → T	<u>A</u>AC <u>C</u> GC<u>G</u>	N4
180	G → A	AC<u>C</u> G C<u>G</u>T	N5
189	A → C	CA<u>C</u> A A<u>C</u>A	N5

Base Pair Position*	Mutation†	Sequence Context¶	Mouse
A. Base Substitutions cont'd			
197	G → C	CTG G CGG	N2
198	C → T	TGG C GGG	N9
210	C → A	AGT C GTT	N4
258	C → A	CGT C GCA	N6
270	C → T	TCG C GGC	N2, N4 (3), N6, N9 (2)
287	G → C	CGC G CCG	N8
308	G → A	AGC G TGG	N4
369	T → G	TCA T TAA	N5, N9
381	G → A	AAC G CGT	N6
518	G → T	CAT G AAG	N8
528	C → G	GTA C GCG	N1
542	G → T	GTG G AGC	N6
588	G → A	CGG G CCC	N5
680	G → C	GAA G GCG	N5
714	C → A	AAA C CAT	N4 (3)
769	T → G	CGA T CAG	N1
785	G → C	GCC G CAA	N5
792	G → A	TGC G CGC	N1
803	G → T	ACC G AGT	N4
871	T → A	ATG T TAT	N1
887	A → C	TTA A CCA	N2
UVA-Treated			
-15	G → A	GTA G GGC	Q2
31	G → A	TGT G AAA	Q1 (6), Q5 (5), Q7
33	A → C	TGA A ACC	Q1
41	A → C	GTA A CGT	Q8
42	C → T	TAA C GTT	Q4 (2), Q8§
66	C → G	ATG C CGG	Q6 (2)

Base Pair Position*	Mutation†	Sequence Context¶	Mouse
A. Base Substitutions cont'd			
72	T → C	GTG T CTC	Q7
75	C → T	TCT C TTA	Q1 (4)
80	C → T	TAT C AGA	Q4, Q5, Q8
84	C → T	AGA C CGT	Q1¥
86	G → T	ACC G TTT	Q2, Q4, Q6§
90	C → T	TTT C CCG	Q1, Q2, Q5 (2)
92	C → T	TCC C GCG	Q1, Q2§,¥
103	C → G	GAA C CAG	Q4§,¥
107	G → C	CAG G CCA	Q1
116	G → C	CAC G TTT	Q6 (6)
116	G → T	CAC G TTT	Q7
119	T → A	GTT T CTG	Q1
120	C → T	TTT C TGC	Q1 (3), Q4 (2), Q5
120	C → A	TTT C TGC	Q1
137	A → T	GAA A AAG	Q4
140	G → A	AAA G TGG	Q1, Q5¥
146	G → A	GAA G CGG	Q1
173	C → T	ATT C CCA	Q1(3), Q5(2), Q8(2)
179	C → T	AAC C GCG	Q4, Q5§ (3)
179	C → G	AAC C GCG	Q4¥
180	G → A	ACC G CGT	Q2§
185	G → A	GTG G CAC	Q1
186	C → T	TGG C ACA	Q8
191	C → G	CAA C AAC	Q1
198	C → T	TGG C GGG	Q4§
222	G → A	TTG G CGT	Q8
234	C → T	CCT C CAG	Q1 (2)
237	G → T	CCA G TCT	Q4
246	T → C	CCC T GCA	Q8
282	C → T	AAT C TCG	Q1, Q4

Base Pair Position*	Mutation†	Sequence Context¶	Mouse
A. Base Substitutions cont'd			
287	G → C	CGC G CCG	Q8§
293	C → T	GAT C AAC	Q1, Q5
350	A → T	TGT A AAG	Q1
369	T → G	ATC T TCT	Q1, Q6§
470	C → T	TTT C TTG	Q1, Q5
528	C → G	GTA C GCG	Q2§
530	C → T	ACG C GAC	Q4, Q7
531	G → C	CGC G ACT	Q5
549	T → C	ATC T GGT	Q5
582	T → C	TGT T AGC	Q1, Q4
594	T → A	CAT T AAG	Q4
630	G → A	GCT G GCA	Q5
653	C → T	AAT C AAA	Q4
659	C → T	ATT C AGC	Q1 (4), Q4
683	G → A	GGC G ACT	Q1
687	G → A	ACT G GAG	Q1
688	G → A	CTG G AGT	Q1 (2)
701	G → C	TCC G GTT	Q1
707	C → T	TTT C AAC	Q1, Q5 (2), Q8
765	A → T	CCA A CGA	Q5
770	C → T	GAT C AGA	Q5
791	C → T	ATG C GCG	Q1
792	G → C	TGC G CGC	Q1¥
834	C → T	TCT C GGT	Q1
842	G → A	GTG G GAT	Q5, Q7
843	G → A	TGG G ATA	Q1
847	C → A	ATA C GAC	Q8
865	C → A	CAG C TCA	Q7

Base Pair Position*	Mutation†	Sequence Context¶	Mouse
A. Base Substitutions cont'd			
882	C → T	CG<u>C</u> C G<u>T</u>T	Q1, Q7
891	C → T	CC<u>A</u> C C<u>A</u>T	Q1
899	C → T	<u>A</u>AA <u>C</u> AG<u>G</u>	Q4
917	G → C	G<u>C</u>T G <u>G</u>GG	Q8
928	C → G	C<u>A</u>G C <u>G</u>TG	Q4
928	C → A	C<u>A</u>G C <u>G</u>TG	Q4, Q6
953	C → T	<u>T</u>CT <u>C</u> AG<u>G</u>	Q1
977	C → T	<u>A</u>AT <u>C</u> AG<u>C</u>	Q1, Q4
1001	A → T	<u>G</u>TG <u>A</u> AA<u>A</u>	Q4
1004	A → T	<u>A</u>AA <u>A</u> GA<u>A</u>	Q7
1007	A → T	<u>A</u>GA <u>A</u> AA<u>A</u>	Q1 (2)
B. Frameshift, Deletion and Tandem Substitution Mutations			
Untreated			
330	INS GAACG**AAGCGGCGTCGAAGCCTGTA**AAGC		N4
368	-C?	CACAAT<u>C</u>TTCTC	N6
620-632	+CTGG	CTGGCTGGCTGG	N8 (2), N9 (2)
1006-1010	-A	AAAAG**AAAAA**CC	N4
UVA-Treated			
-11/-8	T → A/T→G	GCA ~~T~~GA ~~T~~AG	Q5
7-388	DEL GAAGA~~GAGTCAA...GTCAGTG~~GGC		Q4
64	-TGCCGG	G<u>T</u>A~~T<u>G</u>C<u>C</u>G<u>G</u>~~T<u>G</u>T	Q8 (3)
91-92	CC → TT	T<u>T</u>C C<u>C</u> GC<u>G</u>	Q1, Q8
561/563	G → T/C→T	<u>T</u>TG<u>G</u>~~G~~T<u>C</u>AC	Q5
587-588	GG → AA	<u>G</u>CG <u>G</u>G C<u>C</u>C	Q1
620-632	+CTGG	CTGGCTGGCTGG	Q4§
620-632	-CTGG	CTGGCTGGCTGG	Q6¥
630-631	GG → AA	GC<u>T</u> GG <u>C</u>AT	Q1¥

Base Pair Position*	Mutation†	Sequence Context¶	Mouse
A. Base Substitutions cont'd			
678	-A	CGGGAAGGC	Q1
782-857	DEL	CTGGGC...CCGAAG	Q2
904-7	-T	CAGGATTTTCGC	Q4
1006-1010	+A	AAAAGAAAAACC	Q1¥

* Numbering of the *lacI* gene according to Farabaugh (1978).

† The mutation in the coding strand is reported.

¶ The mutated base(s) is (are) the center base(s); the first base of each codon is underlined. Bases in boldface include those possibly deleted or inserted. The deleted or substituted bases are stricken.

÷ Number of occurrences, when more than one, per mouse.

§ The same mutation has been recovered in an untreated mouse.

¥ A different mutation at the same site has been recovered in an untreated mouse.

Table XVI. Summary of possible clonal expansion effects in untreated and UVA-treated skin.

Treatment	Independent Mutations	Founder Mutations*	Possible Clonal Expansions	Total # of mutations per spectrum
Untreated	61	6	8	69
Combined Untreated†	184	14	19	203
UVA- treated	118	19	38‡	156

* The founder mutations are included in the independent mutations.

† The combined spectra was obtained by combining statistically similar spectra from other untreated female mouse skin (Gorelick *et al.*, 1995 and unpublished data).

‡ Significantly different than background mutation frequency ($P < 0.001$), as determined by the two-tailed Fisher's Exact test.

mutations recovered from the skin of BigBlue® transgenic animals has a total of 203 spontaneous skin mutations (unpublished data; Gorelick *et al.*, 1995). This combined spectra has a total of 19 clonal events. By using this larger data set, the number of clonal events in the UVA-induced spectra was significantly different than the combined spontaneous spectra when compared to the total number of independent mutations (FE; $p<0.001$). A jackpot analysis was performed removing animal Q1 with the highest number of clonal events (18) and a statistically higher portion of clonal events in the UVA-induced spectra was still observed compared to the combined untreated spectra (FE; $p<0.02$).

By assuming that one of mutations within a clonal event was the 'founder' mutation, a comparison of the number of founder to resultant clonal mutations was performed. These founder mutations were considered independent mutations and counted thusly. The number of founder mutations was 6, 14 and 19 for the control, combined control and treated groups, respectively. The founder mutants in the UVA-irradiated spectra did not rise to proportionally higher number of clonal events compared to either background spectra (FE; $p>0.2$).

The clonal events in the UVA-induced spectra were predominantly GC → AT transitions at non-CpG sites (26/38). These transitions were identified as specific to the UVA-irradiation as discussed later. The clonal GC → AT transitions were distributed among 12 founder mutations at 8 unique DNA sequence positions.

3.4. Mutational Spectra

The majority of the mutations recovered from untreated and UVA-treated mice were base substitutions, (see Table XVII and Table XVIII). In the control group, a high proportion of the mutations (17/61 mutations) were GC → AT transitions at CpG (see Table XVIII). Another dominant class of base substitutions was GC → TA transversions (21 out of 61). These classes of mutations are usually predominant in spontaneous *lacI* spectra recovered from various tissues including mouse skin (de Boer *et al.*, 1996; de

Boer *et al.*, 1996; de Boer *et al.*, 1997). Significant differences from the background were detected in the spectrum from UVA-treated mice. Using trend analysis (Carr and Gorelick, 1996), inductions of the following mutational classes were observed: 1) GC → AT transitions ($p< 0.001$); 2) GC → CG transversions ($p=0.03$); and 3) AT → TA transversions ($p=0.05$).

A comparison of the sequence specificity of GC → AT transitions (Table XVIII) in each treatment group indicated a considerable shift in sequence context with treatment. from mostly RpCpG sites in untreated mice (15/18 GC → AT transitions) to predominantly YpCpH sites (where R=purine, Y=pyrimidine and H=A,T,C) in the UVA-treated mice (40/64 GC → AT transitions). CpG sites were important since ≈ 50% of mutations from untreated animals were recovered at CpG sites. This represents the endogenous processes within the target organ. For GC → TA transversions 10/21 and 7/10 mutations from the control and treated groups were recovered at CpG sites, respectively. GC → CG transversions mutations were recovered at CpG sites in both the control (3 of 6) and treated (8 out of 13) samples, respectively. An unique sequence specificity was determined for the AT → TA transversions, as all 7 of these transversions in the treated group and the single AT → TA transversion in the untreated group were located at TT dinucleotide sequences.

4. DISCUSSION

4.1. UVA light is mutagenic in the skin of mice

The mutation frequency increased 2.4 fold over background after irradiation with a total of 800 J/cm^2 over 5 days. UVA irradiation was also reported to increase mutation frequency in cell culture studies with human embryonic kidney cells and CHO cells (Drobetsky *et al.*, 1995; Robert *et al.*, 1996). When a stably-integrated shuttle vector was used as a mutational target in human embryonic kidney cells, a fluence of 60 J/cm^2 resulted in a 5-fold increase in mutation frequency (Robert *et al.*, 1996). A similar 3 to

Table XVII. Summary of *lacI* mutations in untreated and UVA-treated skin by mutation class.

Mutation class	Mutation Frequency x 10^5 (number of occurrences*) Untreated		UVA-treated	
Transitions:				
G:C → A:T	1.6	(18)	7.1†	(64)
A:T → G:C	0.3	(3)	0.6	(5)
Transversions:				
A:T → T:A	0.1	(1)	0.9	(8)
A:T → C:G	0.6	(7)	0.4	(4)
G:C → T:A	1.9	(21)	1.1	(10)
G:C → C:G	0.5	(6)	1.4	(13)
Others:				
Frameshifts	0.2	(2)	0.3	(3)
Deletions/Insertions	0.3	(3)	0.6	(5)
Tandem Substitutions	<0.1	(0)	0.4	(4)
Complex	<0.1	(0)	0.2	(2)
Total Mutation Frequency x10^5	5.4‡		13.	
Total Mutant Frequency x10^5	6.1		17.	
Total no. of mutations after clonal corrections			61	118
Total no. of mutations identified		69		156
Total no. of mutants recovered		79		172
Total plaques per group		1,168,839		1,044,715

* number of occurrences, corrected for possible clonal expansions.

† Significantly different than background mutation frequency ($P < 0.001$), after multiplicity adjustment, as determined by the methods of Carr and Gorelick (1996).

‡ The sum of class-specific mutation frequencies does not equal the overall mutation frequency exactly due to rounding errors.

Table XVIII. Sequence specificity of GC → AT transitions in UVA-treated mouse skin.

Mutation class	Sequence context†	Mutation frequency x 10^5 (number of occurrences*) Untreated		UVA-treated	
G:C → A:T		1.6	(18)	7.1	(64)
	RpCpG		*(15)*		*(7)*
	YpCpG		*(2)*		*(8)*‡
	YpCpH (H=A,T,C)		*(0)*		*(40)*‡
	RpCpY		*(1)*		*(7)*‡
	Other		*(0)*		*(2)*
TOTAL		5.4	(61)	13	(118)

* number of occurrences, corrected for possible clonal expansion

† The sequence context for all GC → AT mutations is expressed in terms of cytosine as the mutated base. This assumes that the relevant mutation in each case was C → T. Y = pyrimidine; R = purine; H = possible nucleotides are specified parenthetically.

‡ Significantly different than background mutation frequency ($P < 0.05$) as determined by the methods of Carr and Gorelick (1996) without multiplicity adjustment.

5 fold increase in mutation frequency after a 50 J/cm^2 exposure was observed at the endogenous *aprt* gene in CHO cells (Drobetsky *et al.*, 1995). The CHO cells had a 100% survival after 50 J/cm^2 (Drobetsky *et al.*, 1995), whereas only 8% of the human kidney cells survived after 60 J/cm^2 (Robert *et al.*, 1996). The total irradiation in the two cell culture studies was 13 to 16-fold lower compared to the 50 J/cm^2. The decreased sensitivity of the mouse skin can be partially explained by incident energy received by the replicating cells. The UVA light (365nm) transmission was reduced by ≈ 20 or 50% after it reached the top or bottom viable layer of human skin, respectively (Bruls *et al.*, 1984). The effective dose to replicating cells was still ≈ 2 to 8-fold lower in the cell culture studies which implied incident UVA may not explain the observed mutagenic response. Comparative dosimetry would be necessary to directly measure the biological effect of the different light sources.

The concomitant exposure to UVB (290-320 nm) may have contributed to the observed mutant frequency from the UVA-treated animals. However, in our experiments, the UVB exposure was < 0.5% of incident energy and comprised of only 318-320 nm light. For light below 302 nm, DNA absorption was closely linked to mutagenicity and the association was generally attributed to the formation of CPDs and 64PyPys. CPDs were detected at very low rates in exposed DNA after irradiation of light > 305nm (Shennan *et al.*, 1996). UV light > 320 nm induced no appreciable levels of CPDs above background (Shennan *et al.*, 1996). Light above 302 nm has a logarithmic decrease in mutagenicity and cytotoxicity with increasing wavelength (reviewed in Coohill *et al.*, 1987). Thus, light of wavelengths 318-320 nm probably has a similar biological outcome as the classically defined UVA (320-400 nm) spectrum. Based on the total incident energy of the UVB light and the similarity of the biological effect of the specific wavelength range to that of UVA, the impact of the contaminant UVB exposure on the frequency of mutations was likely to be relatively small.

4.2. Dose response in the *lacI* transgene following UVA irradiation

The mutations that occur in the *lacI* transgene are thought to be selectively neutral and to accumulate additively (Tao and Heddle, 1994; Heddle *et al.*, 1995). Thus an increased dose of a mutagenic exposure should increase the MF in a linear manner given biological limits such as lethality. We expected to observe a linear increase in MF with increased dose as observed using a similar protocol with UVB (unpublished data). The results, shown in Table XIV, indicate a more complex dose response for the UVA-induced MF. The small and consistent confidence intervals (Table XIII and Table XIV) of the UVA-induced MFs suggested interanimal variability or physical manipulations of irradiation were likely not important. With experimental variability excluded, various biological responses were investigated to explain the non-linear dose response curve.

The attenuated dose response at higher levels of UVA exposure may have been a result of cell death (Godar and Lucas, 1995) or the induction of protective mechanisms (Vile and Tyrrell, 1993). Biological effects of UVA light appeared to be mainly mediated through cellular chromophores (Runger *et al.*, 1995) producing singlet oxygen (Basu-Modak and Tyrrell, 1993), although other ROS (Albro *et al.*, 1997; Shindo and Hashimoto, 1997) and CPDs (Ley and Fourtanier, 1997) have been detected after UVA irradiation. A cascade effect of singlet oxygen scavengers appeared to lead to the production of peroxides (Albro *et al.*, 1997). In addition, hydrogen peroxide and superoxide radicals were produced by a single UVA irradiation (12 J/cm^2) of human skin fibroblasts as evidenced by the significant reduction of catalase and superoxide dismutase activity (Shindo and Hashimoto, 1997).

One pathway or protective mechanism against ROS appeared to be mediated through the sequestering of iron from endogenous heme sources into ferritin (Vile and Tyrrell, 1993). With the iron contained in the ferritin, it was unavailable to participate in the generation of singlet oxygen (Vile and Tyrrell, 1995). Different cell types within skin have various levels of ferritin (Applegate and Frenk, 1995). Epidermal keratinocytes have a higher constitutive level of ferritin compared to lower dermal fibroblasts. While the

ferritin levels in keratinocytes were not inducible, at low UVA fluences (20-40 J/cm^2) ferritin levels increase 25% in fibroblasts (Applegate and Frenk, 1995). At a higher UVA doses ferritin levels decreased in both fibroblasts and keratinocytes, although the levels in keratinocytes did not decrease until a UVA fluence of (125 J/cm^2). This suggested at higher UVA doses, the protective nature of ferritin was reduced which in our study, presumably would have lead to increased DNA damage and increased MF at higher UVA fluences.

Other protective mechanisms such as catalase and superoxide dismutase in fibroblasts which were decreased after low UVA irradiation (6, or 12 J/cm^2) took 1-3 days to recover to original levels (Shindo and Hashimoto, 1997). Thus, in our experiment with 5 daily irradiations, the animals during the later of the 5 days of exposure may have had decreased catalase and superoxide dismutase activities. The decreased protective capacity of ferritin, catalase and superoxide dismutase would presumably have increased DNA damage. It would be expected that at higher doses, it would result in a correspondingly increased UVA-induced MF unless the level of DNA damage was sufficient to induce cell death, or apoptosis.

Maintenance of the cellular redox states is important for the integrity of the cell and an imbalance due to oxidative stress can lead to apoptosis (Clutton, 1997; Trosko and Inoue, 1997). UVA light effectively induced apoptosis in cultured murine lymphoma cells (Godar and Lucas, 1995). UVA can produce a nearly immediate apoptosis (<4h) in contrast to the delayed apoptosis which was observed after the equivalent erythemal doses of either UVB or UVC light (Godar and Lucas, 1995). With skin cells committed to immediate apoptosis following UVA-treatment and the subsequent daily exposures of UVA light, cell turnover in UVA-exposed skin may have been enhanced compared to controls. The dose response, as measured in terms of mutant frequency, was consistent with the model that, above a threshold of UVA light, mouse skin cells retained sufficient damage and proceeded into apoptosis. This was consistent with the cell replacement model as UVA-irradiated skin cells showed enhanced cellular proliferation as evidenced by the increased number of clonal events in the UVA-induced mutational spectra

(38/118) compared to the combined background spectra (19/184; $p<0.001$; unpublished data; Gorelick *et al.*, 1995). A further confirmation that the increased clonal events arose as a result of the UVA irradiation was the predominant clonal events were GC → AT transitions at YpCpH sites (26/38).

4.3. UVA-Induced Mutation Spectra

The most significant shift in mutational spectra in the control compared to the UVA-exposed group was the change in sequence context of the GC → AT transitions ($p<0.05$). The sequence context changed from RpCpG to sites in the untreated spectrum to YpCpH sites in the treated spectrum ($p<0.05$). The frequent detection of GC → AT transitions at RpCpG sites among mutations from untreated mice was consistent with proposed mechanisms of mutation involving the deamination of 5-methylcytosine (de Boer *et al.*, 1997). GC → AT transitions at YpCpH sites were consistent with the mutagenic effects of CPDs or 64PyPys. Reports of CPD formation, after UVA irradiation, were not consistent. Some studies have indicated CPDs, in which CPDs were determined by T_4 endonuclease sensitive sites (T_4 ES sites), were not present after UVA irradiation (Drobetsky *et al.*, 1995; Shennan *et al.*, 1996). While others have measured CPDs in mouse skin after UVA irradiation (Ley and Fourtanier, 1997). The wavelength cutoff of the lighting system is crucial because an UV irradiation of 5 J/cm^2 (> 305 nm) generated detectable quantities of T_4 ES sites (Shennan *et al.*, 1996). Using this same system, no CPDs were detected with UV light > 320 nm. DNA damage from oxidative stress may have also contributed to the GC →AT transitions at YpCpH sites since oxidative damage induced tandem CC → TT transitions (Reid and Loeb, 1993). Tandem CC → TT transitions were recovered at a frequency of 3.3% (4/118) in our study which was similar to the frequency after UVA exposure of CHO cells (3/53; Drobetsky *et al.*, 1995).

Additional evidence for the occurrence of oxidative DNA damage was the induction of GC → CG transversions. GC → CG transversions were reported to be induced by singlet oxygen (de Oliveira RC *et al.*, 1992). The sequence specificity of the

GC → CG transversions in the reported results very closely matched the background spectra with a high proportion of these transversions recovered at CpG sites. This similarity in the mutational spectra may have reflected an increase of an endogenous mutagenic process such as oxidative damage.

Since singlet oxygen is the main ROS generated by UVA and singlet oxygen modified only guanine *in vitro* (Ravanat and Cadet, 1995), the induction of mutations at AT basepairs in our results implies other mutagenic species were present. In the UVA-induced spectra, the marginal induction of AT → TA transversions may have been the result of the superoxide radical since AT → TA transversions were recovered after treatment with superoxide anion (Knowles and Eisenstark, 1989). Interestingly, the AT → TA transversions had a unique target sequence of TT dimers (8/8). The same sequence context was noted for AT → TA transversions (4/4) at the *lacZ'* gene in human embryonic cells after UVA treatment (Robert *et al.*, 1996). While no AT → TA transversions were recovered at the *aprt* gene in CHO cells after UVA irradiation, the relatively rare AT → CG transversion occurred primarily at dithymidine sites (17/20; (Drobetsky *et al.*, 1995). In the CHO cell study (Drobetsky *et al.*, 1995), Drobetsky et al. cite a personal communication which stated that by using an identical light source and filters, no detectable T_4 ES sites were found by a plasmid relaxation assay. This suggested that CPDs and certain monomeric adenine adducts were likely not the premutagenic lesions, since T_4 endonuclease V also released 4,6-diamino-4-hydroxy-5-formamidopyrimidine (FapyAde) (Dizdaroglu *et al.*, 1996) which, if either were present, would probably have been detected.

The predominance of GC → AT transitions at YpCpH sites, in this study, was somewhat unexpected given the mutational spectra after UVA irradiation in cell culture. Both cell culture studies of UVA mutagenesis mentioned above, reported a UVA-specific increase in the fraction of base substitutions at A:T basepairs compared to exposures of UVB or UVC light. Mutations at A:T basepairs accounted for 41% (9/22) of the recovered mutations in the plasmid-based lacZ' gene (Robert *et al.*, 1996) and 58%

(26/45) in the endogenous *aprt* gene (Drobetsky *et al.*, 1995). The decreased prevalence of mutations at A:T basepairs in this study may have reflected the differences in the light sources and/or the *in vivo* effect of UVA light in mouse skin.

5. CONCLUSIONS

An increased mutation frequency was detected in the skin of UVA-treated mice compared to control mice. UVA mutation induction was non-linear and attenuated at higher fluences. It was hypothesized that cell death mediated by oxidative damage, possibly from immediate apoptosis may have accounted for the observed mutagenic response. The increase in GC → CG and AT → TA transversions compared to controls was consistent with a role for oxidative damage. The high number of clonal events and the prevalence of GC → AT transitions at YpCpH sites in the UVA-induced mutational spectra supported the hypothesis that UVA induces skin cells to undergo immediate apoptosis. Thus, the apoptotic cells would likely have been replaced through clonal expansion during the mutation fixation period. The predominance of GC → AT transitions at YpCpH sites in the mutational spectra implicated dipyrimidine lesions, such as CPDs, as the premutagenic lesions. This may have reflected the particular UVA source or maybe a unique response to UVA light in the C57Bl/6 mouse skin. The complex nature of these results indicated the importance of further study of UVA-induced mutagenesis in general and, in particular, as it related to skin carcinogenesis.

ACKNOWLEDGEMENTS

The authors would like to acknowledge the use of the Procter & Gamble solar simulator.

CHAPTER VI. BENZO(a)PYRENE-INDUCED DOSE RESPONSE OF THE MUTANT FREQUENCY, MUTATIONAL FREQUENCY AND MUTATIONAL SPECTRA IN THE *LACI* TRANSGENE OF BIG BLUE® C57BL/6 MALE MOUSE LIVER.

G. (Paul) Kotturi[1,2], H. Yang[2], J.G. de Boer[2], K. Sojonky[2], D. Walsh[2], J. Kangas[2], J. Holcroft[2] and B.W. Glickman[2]

[1] Stratagene, 11011 N. Torrey Pines Rd., La Jolla, CA, USA 92037

[2] Centre for Environmental Health, Department of Biology, University of Victoria, P.O. Box 3020 STN CSC, Victoria, B.C., Canada V8W 3N5.

To be submitted to Environmental Mutagenesis

Abstract

The dose response of mutation recovered in the *lacI* transgene of Big Blue® C57BL/6 male mouse liver to benzo(*a*)pyrene [B(*a*)P] was analyzed as measured by mutant frequency, mutational frequency and mutational spectra. Groups of male mice (n=5) 8-9 weeks of age received a single intraperitoneally dose of corn-oil laden B(a)P to various levels. Two weeks after the injection, the animals were sacrificed and the mutant frequencies of the following doses 0, 62.5, 125, 250 and 500 mg/kg were 5.7, 12, 18, 22, 57 x 10^{-5}, respectively. After characterizing a subset of the mutations from each dose by DNA sequencing, the mutant frequencies were corrected by the 'conservative' estimate for clonal expansion to give the mutational frequencies of 4.8, 11, 16, 20, 53 x 10^{-5}. One animal with a jackpot mutation was identified and the clonal events were removed from consideration. Clonal expansion did not significantly change as a function of B(a)P dose and was calculated to be an average of 9.9%. The results of a trend analysis indicated that the mutation frequency of all mutation classes at G:C basepairs, including +1/-1 frameshifts, were increased following B(a)P exposure. CpG sites were mutated preferentially by B(a)P ($p<0.004$).

1. INTRODUCTION

Benzo(a)pyrene B(a)P is a potent pro-mutagen and a pro-carcinogen (Mane *et al.*, 1990). Because of its presence in diesel exhaust, cigarette smoke and burnt meat, human exposures are of concern. Activation results in benzo(a)pyrene dihydrodiol epoxides (BPDE) that alkylate nucleic acids and produces predominantly (95% of the adducts) a

covalent bond to the exocyclic N^2 amino group of guanine (Sayer *et al.*, 1991). Adducts to the N^6 position of adenine are also formed, but to a lesser degree than the exocyclic N^2-adducts (Sayer *et al.*, 1991; Cheng *et al.*, 1989; Harvey, 1979). Other minor adducts form at N^7 amino group of guanine (King *et al.*, 1979), deoxycytosine bases (Meehan *et al.*, 1977) and those which are present due to alkylation of denatured DNA (Sayer *et al.*, 1991).

Consistent with the importance of GC sites as targets for adduct formation by BPDE was the observation that GC→TA transversions were the hallmark of B[*a*]P-induced mutation. This transversion represented about 60% of the induced base substitutions (Andersson *et al.*, 1992; Bernelot-Moens *et al.*, 1990; Chen *et al.*, 1990; Mazur and Glickman, 1988; Rodriguez and Loechler, 1993b; Yang *et al.*, 1987). However, the complete mutational spectrum was quite complex. Following B[*a*]P treatment mutations such as GC→AT transitions, GC→CG transversions and frameshifts also were induced (Mazur and Glickman, 1988; Rodriguez and Loechler, 1993a; Zhu *et al.*, 1994). Base substitutions recovered in the *lacI* gene of *E. coli* (Bernelot-Moens *et al.*, 1990) following BPDE treatment were predominantly GC→TA transversions. However, 50% of the mutations recovered were -1 bp frameshifts which occurred mostly in runs of guanines. BPDE also induced frameshift mutations in runs of guanine in the human *adenosine phosphoribosyltransferase* (*aprt*) gene (Zhu *et al.*, 1994) and in the *E. coli lacI* gene in a transgenic mouse model by Kohler *et al.* (1991).

Only a few studies have reported the *in vivo* B(a)P-induced mutagenic effects (Kohler *et al.*, 1991; Skopek et al., 1996; Shane et al., 1997). Kohler et al. (1991) performed a proof of concept experiment that demonstrated B(a)P-induced mutations were recovered from the *lacI* reporter gene contained within a shuttle vector. Skopek et al. (1996) used B(a)P-induced mutagenesis to compare the induced mutant frequency (MF) in the *lacI* transgene to that in the endogenous *hypoxanthine-guanine phosphoribosyltransferase* (*hprt*) gene. After a treatment of either 50 or 150 mg/kg B(a)P, the average induction of mutation / 100 mg/kg B(a)P over background was 5.9-fold at the *lacI* loci as opposed to 3.5-fold at the *hprt* loci. The greater increase in MF at the *lacI* loci may have been a result of the increased DNA damage at methlyated CpGs (Denissenko *et al.*, 1997). The CpGs in the *lacI* transgene are presumably highly methylated and CpG sites are considerably more prevalent in the *lacI* gene than the *hprt* gene. Using B(a)P-induced mutagenesis, Shane and colleagues (1997) investigated the effect of cell proliferation by determining the MF before and after a partially hepatectomized liver. Interestingly, the MF did not differ significantly as a result of the partial hepatectomy, presumably, because the liver was not allowed sufficient time to regenerate before sacrifice. Thus, the liver cells were not allowed time to divide and potentially fix B(a)P-induced adducts into mutations. The total B(a)P dose received by the transgenic mice was 3 daily intraperitoneal (i.p.) injections of 40 mg/kg B(a)P. The mutational spectra revealed the influence of B(a)P-induced mutagenesis as the predominant mutation was the GC→ TA transversion (Shane, personal communication).

We were interested in performing a B(a)P dose response experiment to determine the effect of B(a)P dose on MF, mutational frequency (MnF) and the mutational spectra. By analyzing the mutagenic response in the liver, we were also able to compare the results of previous studies and evaluate the reproducibility of the assay. We performed a single i.p. injection of either vehicle alone, or corn-oil laden B(a)P at 62.5, 125, 250, 500 mg/kg into *lacI* transgenic male C57Bl/6 mice. Two weeks after the treatment, the animals were sacrificed and mutations in the *lacI* transgene isolated from liver genomic DNA were measured. A linear dose response was observed. Large mutational spectra (75-125 mutations / exposure) were generated and molecular analysis revealed that mutations involving GC basepairs were increased. Mutations at AT basepairs were not induced by B(a)P treatment.

2. MATERIAL AND METHODS

2.1. Chemicals

Benzo(a)pyrene (purity > 99%) (Sigma-Aldrich, St. Louis, MI, USA) was dissolved in corn-oil (Sigma). Solutions of ≥ 250 mg/kg B(a)P required sonication to maintain homogeneity (Sonicator® XL, Heat Systems Inc., Farmingdale, NY, USA).

2.2. Treatment of mice

A single intraperatoneal (i.p.) injection of B(a)P-laden corn oil was given to 8-9 week old C57BL/6 Big Blue ® transgenic male mice (Stratagene, La Jolla, CA, USA). Mice, five per group, were dosed with either 0, 62.5, 125, 250, 500 mg/kg B(a)P. The

volume was standardized to approximately 200 uL, irrespective of dose. The animals were housed individually for two weeks and were sacrificed by cervical dislocation. Brain, heart, lungs, liver, gall bladder, spleen, kidneys, testes and femurs were removed, frozen in liquid nitrogen and stored at -80°C for future use.

2.3. Liver DNA isolation

A piece of frozen liver approximating 50-100 mg was sliced off, added to 5 mL of ice cold CLS solution (10 mM Tris HCl pH=8.3; 140 mM NaCl; 3 mM KCl; 0.35M sucrose; 1mM EDTA; 1% Triton X-100) and dounced in a Wheaton 7 mL tissue homogenizer. The tissue was filtered using 100 micron nylon mesh filter (Falcon, Becton Dickenson Labware, Franklin Lakes, NJ, USA), into a sterile 50 mL tube. The filtered solution was centrifuged at 1000g for 10 min at 4°C, decanted and the nuclei pellet was washed with another 5 mL of ice-cold CLS solution. After decanting the supernatant, five hundred μL of phosphate buffered saline (12.3 Na_2HPO_4, 1.4 mMKH_2PO_4, 13.7 mM NaCl, 2.7 mM KCl, 10 mM EDTA pH=8.0) was added to the 50 mL tube. The pellet was transferred into a 1.5 mL eppendorf tube and an equal volume of proteinase K solution [2 mg/mL proteinase K (Gibco-BRL, Gaithersburg, MD, USA), 2% SDS, 100 mM EDTA] was added to the pellet and incubated for 1-2 h at 50°C. The resulting solution was transferred to a 0.45 μm pore size type HA filter (25 mm diameter; Millipore, Bedford, MA, USA) with a wide bore pipette tip. The filter was placed on sterile glass rods in a sterile petri dish. Sufficient TE buffer was gently poured into the petri dish to just wet the bottom of the filter. The buffer was exchanged daily for up to 4 days or until the DNA

solution appeared homogeneous. Dialyzing DNA samples were shielded from the light and DNA was stored at 4 ^{o}C for future work.

2.4. Screening for *lacI*$^{-}$ mutants

Mutant frequencies in the *lacI* transgene were determined by the standard procedures in the Big Blue® manual (Stratagene, La Jolla, CA, USA). To minimize the variation of the mutant frequency below the animal-to-animal level, a blocking approach was used in which one animal from each dose was screened in parallel (Piegorsch *et al.*, 1994). A brief explanation of the screening protocol is as follows. Eight µL of genomic DNA was added to Transpack® packaging reaction (Stratagene) and incubated at 30^{o}C to *in vitro* package phage particles. Packaging reactions were titered in triplicate using culture of SCS-8 *E. coli* (Stratagene) resuspended in 10 mM $MgSO_4$ to an OD_{600} of 0.5. The number of plaque forming units (pfu) was calculated after a series of dilutions of the phage particles was incubated overnight on NZY media (Stratagene). Based on the titers, the dilution was prepared to produce a plaque density of 10 x 10^3 pfu/ (25 cm x 25 cm plate). Approximately 200 mL of NZY bottom agar was added to the 25 x 25 cm plates and once solidified the excess moisture was wiped from the lids. The large plates were incubated overnight with only the bottom agar to identify any contamination. The predetermined aliquot of phage was added to 2.0 mL of SCS-8 cells which were prepared as for the titrations and incubated at 37^{o}C for 15 min. Thirty-five mL of molten agarose [50^{o}C; NZY top agarose with 1.5 mg/mL of 5-bromo-4-chloro-3-indoyl-β-D-

galactopyranoside (X-gal); Biosynth AG, Staad, Switzerland] was added to the bacterial cell / phage mixture and dispersed evenly over the surface of the 25 x 25 cm plates. The lids of the plates were wiped again to avoid 'rivers' forming from condensation after the top agarose was solidified and incubated overnight. Plates were screened for *lacI* plaques the following day. A control (SCS-8 alone) and all four-colour standards (CM0-3; Stratagene) were plated in parallel to ensure the standard colour selection conditions were maintained. The total number of pfu was estimated by counting the phage plaques in five 2.5 x 2.5 cm squares from at least 3 of the 25 x 25 cm plates. Each plating experiment involved 40 plates for the control group and 30 plates for each of the control groups. The plating experiments were repeated once per for each animal in a treatment group. The mutant frequency (MF) was calculated by dividing the number of full blue plaques by the estimate of the total number of pfu. Mutants were picked and placed in 0.5 mL SM buffer (100 mM NaCl, 8 mM $MgSO_4$, 50 mM Tris-HCl pH=7.5, 0.01% gelatin) and 50 µL of chloroform. Plaques were purified using Big Blue® media supplemented with X-gal (1.5 mg/mL) for further characterization by DNA sequencing. Sectored plaques were excluded from the calculation of mutant frequency (Stuart *et al.*, 1996).

2.5. DNA characterization of *lacI*$^-$ mutants

Ten uL of a mutant phage solution was added to a 200 µL reaction vessel containing 90 uL amplification solution for final concentrations of forward and reverse primers at 0.2 pmol/µL (5'-AGCGTCGATTTTTGTGATGCT-3', 5'-GCGTATTACGCCAGCTGG-3', respectively; Dalton Chemicals, North York, Ontario,

Canada), dNTPs at 200 μM (Amersham Pharmacia Biotech, Piscataway, NJ, USA), buffer at 15 mM Tris/HCl pH 8.8, 60 mM KCl, 1.5 mM $MgCl_2$ and Taq enzyme at 0.1 U/μL. After a 4 min initial heating at 94°C, the samples were subjected to 30 cycles of 95°C for 36 seconds, 59°C for 36 seconds and 72°C for 90 seconds using a Perkin Elmer 9600 thermocycler. The resulting PCR product is purified using Wizard PCR kits (Promega, Madison, WI, USA) with the vacuum manifold and resuspended in 50 uL of TE buffer. Approximately 5.5 μL of the purified DNA was added to a standard Sequitherm II Long-read DNA sequencing reaction (Epicentre Technologies, Madison, WI, USA) with both forward IRD700-labelled (5'-CTGTGGATAACCGTATTACCGC-3'; Licor Biotech, Lincoln, NB, USA) and reverse IRD800 labelled (5'-TCCGCTCACAATTCCACACAAC-3') primers (2 pmol each). DNA sequencing reactions are loaded onto a 4% Long Ranger™ polyacrylamide gel (FMC, Rockland, ME, USA) with a well to read distance of 66 cm. Electrophoresis was performed by using a Licor 4200 DNA sequencer (Licor) using default conditions. DNA sequence was determined by the DNA sequence analysis software (Licor) and the DNA sequence from the *lacI*$^-$ mutants was aligned against the wild type sequence in Seqman II sequence assembler (DNAStar, Madison, WI, USA).

2.6. Statistical Analysis

Trends in mutant frequencies, mutant frequencies and class-specific mutation frequencies were analyzed using the COCHARM program described in Carr and Gorelick (1995). An analysis of variance was used as alternative method to determine trends in the

mutant frequencies (Statistica Ver. 5.0, Statsoft Inc., Tulsa, OK, USA). Pairwise comparison using 2x2 tables used either the two-tailed Fisher's Exact test or χ^2 analysis with Yates correction as determined by Statistica (Statsoft). Mutational spectra were compared using a Monte Carlo estimation of Fisher's exact test (Adams and Skopek, 1987). When a statistically significant difference was observed between two mutational spectra, contingency χ^2 analyses were performed using the SAS program (SAS Version 6.12., SAS Institute, Inc., Cary, North Carolina, USA) to quantify the class-specific differences.

3. RESULTS

3.1. B(a)P-induced mutant and mutation frequencies in the liver of C557Bl/6 Big Blue® male mice.

A single i.p. injection of B(a)P-laden corn oil even at the highest dose of 500 mg/kg did not produce any obvious toxic effects during the mutation fixation time. Two weeks after the injection the mice were sacrificed and upon dissection one of the mice which received 500 mg/kg appeared to have slight necrosis of the liver. The liver DNA from one animal per exposure group was analyzed in parallel from each dose to minimize packaging to packaging variation. Animals that were plated together have the same number in the first digit of the animal code (e.g., animals 1-x were plated together) as shown in Table XIX. The generalized Cochran-Armitage (GCA) test was primarily used to analzye the results because of the small numbers of animals per dose group (Carr and

Gorelick, 1995). Thus extrabinomial variability at the animal level was considered. Significant increases in the mutant frequencies over background were observed for each of the doses and there was a significant overall trend in increase in mutant frequency ($p<0.005$; see Table XIX). An analysis of variance using the individual animal MF was performed as an alternate method to determine if similar results to the GCA test were obtained. The results, presented in Table XX, indicated the mean value of the MF were significantly different from each other with the exception of the MF from the next lower or higher dose. However, the means of the 250 and 500 mg/kg B(a)P treatment groups were different from each other. Sectored plaques were observed at frequencies of $1.9 \pm 2.0 \times 10^{-5}$ and $2.9 \pm 2.0 \times 10^{-5}$, $3.2 \pm 1.7 \times 10^{-5}$, $4.5 \pm 5.3 \times 10^{-5}$, and $7.3 \pm 6.2 \times 10^{-5}$ (average ± standard deviation) for the control and treated groups, respectively.

A subset of the mutants from each dose was further characterized at the DNA sequence level to determine the nature of B(a)P-induced mutations. A total of 9 and 27 mutations from the untreated and treated groups did not have mutations in the *lacI* gene which represented 7.0 and 7.6% of mutations in the untreated and treated groups, respectively. The numbers of mutations that were characterized as $lacI^-$ mutants were 129, 83, 142, 80, and 78 for the B(a)P doses of 0, 62.5, 125, 250, and 500 mg/kg, respectively. These mutations are listed in Table XXI. This resulted in 110, 75, 128, 73 and 72 independent mutants for the respective doses. A jackpot event of 8 identical mutations was isolated from the liver one of the untreated animal (3-0).

Table XIX. Mutant frequencies (MF) in liver from untreated and B(*a*)P-treated mice.

Mouse	Treatment [mg/ kg B(*a*)P]	*lacI* Mutation Data		
		Plaques	Mutants	MF x 10^5
1-0	none	898,000	38	4.2
2-0	none	423,000	27	6.4
3-0	none	1,290,000	66	5.1
4-0	none	669,000	55	8.2
5-0	none	453,000	22	4.9
		Control		**5.7 ± 1.6**†
1-1	62.5	372,000	37	10.
2-1	62.5	266,000	31	12.
3-1	62.5	409,000	37	9.1
4-1	62.5	482,000	97	20.
5-1	62.5	430,000	39	9.1
		B(*a*)P- 62.5		**12 ± 4.6***
1-2	125	342,000	43	13.
2-2	125	300,000	81	27.
3-2	125	466,000	67	14.
4-2	125	381,000	70	18.
5-2	125	357,000	51	16.
		B(*a*)P- 125		**18 ± 5.7**⇧
1-3	250	238,000	34	14.
2-3	250	290,000	77	27.
3-3	250	494,000	121	24.
4-3	250	625,000	130	21.
5-3	250	335,000	76	23.
		B(*a*)P- 250		**22 ± 4.7**⇧
1-4	500	200,000	133	71.
2-4	500	323,000	164	51.
3-4	500	482,000	182	39.
4-4	500	354,000	224	63.
5-4	500	327,000	209	64.
		B(*a*)P- 500		**57 ± 13**⇧

The overall increase in the mutant frequency was significant ($p < 0.005$; Carr and Gorelick, 1995).

† Avg ± Standard deviation.

* Significantly different than untreated controls, $p<0.05$. (Carr and Gorelick, 1995).

⇧ Significantly different than untreated controls, $p<0.01$. (Carr and Gorelick, 1995).

Table XX. Analysis of variance testing the differences of the means of mutant frequencies from each dose of B(a)P in the liver of the C57Bl/6 Big Blue® mice.

	Dose of B(a)P (mg/kg)				
	0	62.5	125	250	500
Mean Mutant Frequency	5.7	12	18	22	57
Dose of B(a)P (mg/kg)					
0		0.15	0.01	0.001	0.000
62.5	0.15[Ψ]		0.19	0.031	0.000
125	0.01[Φ]	0.19		0.34	0.000
250	0.001	0.031	0.34		0.000
500	0.000	0.000	0.000	0.000	

[Ψ]The probabilities listed in the table were calculated by the least significant differences test (Statistica Ver 5.0 for Windows) to determine whether the means were significantly different from one another.

[Φ]Underlined values indicate a significant difference ($p<0.05$).

3.2. Clonal expansion of B(a)P-induced mutagenesis

With the jackpot removed, the estimates of clonal expansion for the B(a)P doses of 0, 62.5, 125, 250, and 500 mg/kg was 9.1, 9.6, 9.9, 8.8, and 7.7%, respectively. The mutant frequencies corrected by the original estimates of clonal expansion became mutation frequencies of 4.8 ± 1.5, 11 ± 4.1, 16 ± 3.7, 20 ± 4.3, and 53 ± 10 x 10^{-5} (average ± standard deviation) for the respective B(a)P doses of 0, 62.5, 125, 250, and 500 mg/kg. By subtracting the B(a)P-induced MnF from the average background MnF, a linear dose response for B(a)P-induced mutagenesis in the liver of C57Bl/6 male mice was 9.0 ± 4.5 x 10^{-5} MnF / [100 mg/kg B(a)P].

3.3. Class-specific mutation frequencies

In addition to be classified by position, the independent mutations were categorized by the type of mutagenic event, as shown in Table XXII. Base substitutions represented ≈80% of the independent mutations. The class-specific MnF involved multiplying the percentage of mutations from a particular class (e.g., GC → AT transitions in the control group occurred at 41/110 or 37% of the total mutations) by the total MnF (4.8x 10^{-5}) which resulted in a class-specific MnF of 1.8x 10^{-5}. The class-specific MnFs are presented in Table XXII. Trends in class-specific MnFs were determined by the methods outlined in Carr and Gorelick (1995). The effective size which is the number of wild type plaques corrected by the ratio of the sample size of

Table XXI. *LacI* mutations in the liver from untreated and B(a)P-treated C57Bl/6 male mice.

Base Pair Position*	Mutation†	Sequence Context¶	Mouse
A. Base Substitutions			
Untreated			
-34	G → A	AAT G GTG	2-0
42	C → T	TAA C GTT	1-0, 2-0, 3-0 (2)‡
49	C → A	ATA C GAT	1-0 (2), 4-0
56	G → A	GTC G CAG	2-0 (4), 3-0
57	C → A	TCG C AGA	5-0
82	G → T	TCA G ACC	4-0
83	A → G	CAG A CCG	3-0, 5-0 (2)
84	C → A	AGA C CGT	1-0
86	G → T	ACC G TTT	1-0, 4-0
87	T → A	CCG T TT	C 1-0
87	T → C	CCG T TT	C 2-0
89	T → C	GTT T CCC	4-0
90	C → A	TTT C CCG	1-0
92	C → G	TCC C GCG	1-0
92	C → T	TCC C GCG	1-0
93	G → A	CCC G CGT	3-0 (2)
95	G → A	CGC G TGG	1-0
95	G → T	CGC G TGG	2-0
104	C → G	AA C CAGG	3-0
116	G → A	CAC G TTT	4-0
117	T → G	ACG T TTC	2-0 (2)
120	C → T	TTT C TGC	4-0
129	C → A	AAA C GCG	4-0
131	C → T	ACG C GGG	4-0
132	G → T	CGC G GGA	5-0
168	A → G	ATT A CAT	5-0 (2)
174	C → A	ATT C CCA	5-0
179	C → A	AAC C GCG	4-0
179	C → T	AAC C GCG	1-0

Base Pair Position*	Mutation†	Sequence Context¶	Mouse
A. Base Substitutions cont'd			
180	G → A	ACC G CGT	2-0, 5-0
185	G → A	GTG G CAC	2-0
190	A → T	ACAA CAA	4-0
197	G → A	CTG G CGG	2-0
198	C → T	TGG C GGG	1-0, 2-0 (2), 3-0, 4-0
240	T → C	GTC T GGC	4-0
243	C → T	TGG C CCT	5-0
250	C → A	GCA C GCG	2-0
269	G → A	GTC G CGG	5-0
270	C → T	TCG C GGC	2-0
273	C → A	CGG C GAT	4-0
273	C → G	CGG C GAT	1-0
276	T → A	CGA T TAA	2-0
329	C → T	GAA C GAA	1-0, 3-0
341	G → T	GTC G AAG	2-0
364	C → A	GCA C AAT	4-0
369	T → C	TCA T TAA	1-0
369	T → G	TCA T TAA	1-0, 2-0
374	G → T	CTC G CGC	3-0 (2)
377	C → T	GCG C AAC	1-0 (2)
380	C → A	CAA C GCG	4-0
381	G → A	AAC G CGT	4-0
465	T → A	CGT T ATT	4-0 (2)
485	C → T	GAC C AGA	2-0
537	G → A	TGG G CGT	5-0
569	C → T	CAG C AAA	5-0
629	T → C	GGC T GGC	5-0
631	G → A	CTG G CAT	1-0, 5-0
659	C → T	ATT C AGC	1-0 (2)
677	G → T	CGG G AAG	1-0
731	G → T	AAT G AGG	4-0

Base Pair Position*	Mutation†	Sequence Context¶	Mouse
A. Base Substitutions cont'd			
744	C → G	TTC C CAC	3-0
756	T → C	TGC T GGT	4-0
777	C → A	TGG C GCT	4-0
791	C → T	ATG C GCG	2-0, 4-0
843	G → A	TGG G ATA	2-0, 3-0
873	A → C	GTT A TAT	3-0
882	C → T	CGC C GTT	1-0
928	C → A	CAG C GTG	5-0
944	C → T	CTG C AAC	1-0
1001	A → T	GTG A AAA	Q4
B(a)P-treated			
-15	G → A	GTA G GGC	3-2
-12	A → C	GGC A TGA	5-2
31	G → T	TGT G AAA	3-4
42	C → A	TAA C GTT	5-4
42	C → T	TAA C GTT	4-2
44	T → G	ACG T TAT	1-1
47	T → C	TTA T ACG	1-1 (2)
49	C → A	ATA C GAT	5-2
53	G → T	GAT G TCG	3-4
54	T → C	ATG T CGC	2-2
56	G → A	GTC G CAG	1-2 (3), 1-3, 2-2 (3), 3-4, 4-4, 5-2, 5-4(2)
56	G → C	GTC G CAG	2-1, 2-2
66	C → A	ATG C CGG	1-2, 3-3
66	C → G	ATG C CGG	1-3
69	G → T	CCG G TGT	1-2, 1-3, 3-2
71	G → T	GGT G TCT	5-4
72	T → A	GTG T CTC	3-2
78	A → T	CTT A TCA	5-2

Base Pair Position*	Mutation†	Sequence Context¶	Mouse
A. Base Substitutions cont'd			
80	C → T	TAT C AGA	3-1, 3-4
82	G → T	TCA G ACC	3-4, 5-1
83	A → G	CAG A CCG	3-1
84	C → A	AGA C CGT	1-4
84	C → G	AGA C CGT	4-2 (2)
86	G → A	ACC G TTT	2-2, 4-2, 4-3
86	G → C	ACC G TTT	4-1
86	G → T	ACC G TTT	3-1, 3-2, 5-1
87	T → A	CCG T TTC	5-2
87	T → G	CCG T TTC	1-2
89	T → C	GTT T CCC	4-1
90	C → A	TTT C CCG	4-1
90	C → G	TTT C CCG	4-2
90	C → T	TTT C CCG	4-3
92	C → A	TCC C GCG	2-1, 2-2 (2), 3-2, 5-2, 5-3
92	C → G	TCC C GCG	1-2
93	G → A	CCC G CGT	2-1 (2), 2-3, 5-3
93	G → C	CCC G CGT	1-2, 1-4, 2-1, 4-2, 5-2 (2), 5-4
93	G → T	CCC G CGT	1-2, 1-3, 2-2, 2-3, 2-4, 3-4, 4-1, 5-1, 5-2 (3), 5-4 (3)
94	C → T	CCG C GTG	3-2
95	G → A	CGC G TGG	3-2, 4-1, 4-3 (2), 4-4 (3), 5-2
95	G → T	CGC G TGG	1-4, 5-2 , 5-3
99	T → A	TGG T GAA	2-3 (3)
101	A → G	GTG A ACC	5-1
103	C → A	GAA C CAG	4-1
113	C → G	AGC C ACG	2-2
116	G → C	CAC G TTT	5-2
116	G → T	CAC G TTT	1-2, 5-1
117	T → C	ACG T TTC	2-2
122	G → T	TCT G CGA	5-4

Base Pair Position*	Mutation†	Sequence Context¶	Mouse
A. Base Substitutions cont'd			
129	C → T	AAA C GCG	5-2
130	G → T	AAC G CGG	5-3
131	C → G	ACG C GGG	2-2, 3-4, 4-2, 5-2, 5-3, 5-4 (2)
131	C → T	ACG C GGG	1-2
132	G → C	CGC G GGA	5-3
132	G → T	CGC G GGA	5-3
134	G → T	CGG G AAA	2-2
143	G → T	GTG G AAG	3-3
150	C → A	CGG C GAT	2-2, 5-3
158	G → T	GCG G AGC	2-4
167	T → C	AAT T ACA	1-1
168	A → G	ATT A CAT	4-1
173	C → T	ATT C CCA	5-1 (2)
174	C → A	TTC C CAA	4-2
174	C → T	TTC C CAA	5-2
176	A → G	CCC A ACC	2-2
178	C → A	CAA C CGC	1-4, 4-2
179	C → A	AAC C GCG	1-4
179	C → T	AAC C GCG	1-1, 5-1
180	G → A	ACC G CGT	5-1, 5-3
180	G → C	ACC G CGT	1-2
180	G → T	ACC G CGT	3-4, 4-2
183	T → A	GCG T GGC	1-2, 1-3
186	C → A	TGG C ACA	3-2
191	C → G	CAA C AAC	5-1
191	C → T	CAA C AAC	3-1
198	C → A	TGG C GGG	3-2 (2), 5-4
198	C → T	TGG C GGG	4-1, 4-2
200	G → T	GCG G GCA	2-2, 5-3
201	G → T	CGG G CAA	2-1
206	C → T	AAA C AGT	5-2

Base Pair Position*	Mutation†	Sequence Context¶	Mouse
A. Base Substitutions cont'd			
210	C → A	AGT C GTT	1-2
221	G → T	ATT G GCG	1-4, 2-1
222	G → A	TTG G CGT	5-2, 5-3
222	G → T	TTG G CGT	1-1, 3-3, 3-4, 4-2, 4-3, 5-3
225	T → A	GCG T TGC	4-3
228	C → A	TTG C CAC	5-4
250	C → A	GCA C GCG	3-2, 4-1, 4-4
250	C → G	GCA C GCG	5-4
258	C → A	CGT C GCA	2-1, 2-2, 2-4
260	C → G	TCG C AAA	2-2, 5-3
269	G → A	GTC G CGG	5-2, 5-4
270	C → A	TCG C GGC	1-1, 4-1, 5-3
270	C → T	TCG C GGC	1-3, 3-1(2)
273	C → A	CGG C GAT	1-2, 4-2
285	G → C	CTC G CGC	3-3, 4-3, 5-2
288	C → A	GCG C CGA	3-1
293	C → A	GAT C AAC	2-3
303	C → A	GTG C CAG	2-2
308	G → A	AGC G TGG	4-2, 4-3
318	C → A	TGT C GAT	4-4
329	C → T	GAA C GAA	2-1, 2-2, 3-2(2), 5-1, 5-4
357	C → A	CGG C GGT	2-2, 3-2, 4-3
369	T → G	TCA T TAA	2-2, 3-1
374	G → T	CTC G CGC	4-3
376	G → C	CGC G CAA	5-2
377	C → T	GCG C AAC	3-2, 4-3
380	C → A	CAA C GCG	3-1, 4-2
381	G → A	AAC G CGT	1-2, 2-2, 3-1, 3-2 (3), 5-1 (5), 5-2, 5-4
381	G → C	AAC G CGT	4-1
381	G → T	AAC G CGT	3-2, 5-4

Base Pair Position*	Mutation†	Sequence Context¶	Mouse
A. Base Substitutions cont'd			
383	G → T	CGC G TCA	1-2, 5-4
437	G → T	GTG G AAG	3-3
485	C → A	GAC C AGA	5-3
525	G → A	ACG G TAC	4-4
525	G → T	ACG G TAC	4-2
528	C → A	GTA C GCG	3-2, 3-4
530	C → T	ACG C GAC	5-1
542	G → T	GTG G AGC	4-2, 4-4
561	G → T	TGG G TCA	5-2
566	C → T	CAC C AGC	1-2
576	C → A	TCG C GCT	1-4, 3-3
582	T → A	TGT T AGC	1-1
588	G → A	CGG G CCC	2-2
606	C → A	TCT C GGC	4-2
618	G → C	TGC G TCT	4-2
627	G → T	CTG G CTG	5-2
671	G → T	GCG G AAC	1-2
677	G → T	CGG G AAG	4-4
707	C → T	TTT C AAC	5-1
744	C → G	TTC C CAC	1-3
770	C → T	GAT C AGA	3-1
780	T → A	CGC T GGC	4-2
782	G → T	CTG G GCG	1-4, 4-4
786	C → A	CCG C AAT	5-3
791	C → A	ATG C GCG	1-4, 5-3, 5-4
791	C → T	ATG C GCG	1-2 (2)
792	G → C	TGC G CGC	1-2
803	G → A	ACC G AGT	4-2
803	G → T	ACC G AGT	2-2, 5-1
834	C → A	TCT C GGT	1-4, 2-3 (2)
842	G → T	GTG G GAT	2-2

Base Pair Position*	Mutation†	Sequence Context¶	Mouse
A. Base Substitutions cont'd			
843	G → T	TGG G ATA	4-2
847	C → A	ATA C GAC	3-4, 5-2
857	G → T	ACC G AAG	2-1, 4-4
867	C → A	GCT C ATG	1-2, 2-1, 3-2, 5-4
874	T → G	TTA T ATC	4-4
882	C → T	CGC C GTT	1-3
885	T → A	CGT T AAC	5-3
917	G → A	GCT G GGG	5-3
917	G → C	GCT G GGG	2-3, 4-1, 4-4
918	G → A	TGG G GCA	5-4
928	C → A	CAG C GTG	2-2(2), 3-4, 4-3, 5-2(2), 5-4(2)
939	T → A	GCT T GCT	5-3
953	C → T	TCT C AGG	3-1
959	C → T	GGC C AGG	2-4
977	C → T	AAT C AGC	1-1
989	G → T	CCC T TCT	4-1
1004	A → T	AAA A GAA	5-1 (2)
1005	G → A	AAA G AAA	2-1
B. Frameshifts			
Untreated			
132	-G	CGC ~~G~~ GGA	1-0
135	-A	GGG A AAA	2-0
335	-G	AGC ~~G~~ GCG	2-0
350	-A	TGT ~~A~~ AAG	5-0
666	-T	CGA T AGC	5-0
702	+T	CCGG↑TTTT	2-0
733	-G	ATGA~~G~~GGC	2-0
733	+G	ATGA↑GGGC	4-0
857	-G	ACC ~~G~~ AAG	1-0
1001	-A	GTG A AAA	3-0
1006	-A	AAG A AAA	4-0

Base Pair Position*	Mutation†	Sequence Context¶	Mouse
B. Frameshifts cont'd			
B(a)P Treated			
66	-C	ATG ∈ CGG	5-2
70	+T	CGG ↑T GTC	1-2 (2)
83	+A	CAG ↑A CCG	2-4
84	-C	AGA ∈ CGT	3-2
90	-C	TTT ∈ CCG	1-4
132	+G	CGC ↑G GGA	3-2, 5-2
132	-G	CGC ∈ GGA	3-4
135	+A	GGG ↑A AAA	1-3 (2)
176	+A	CCC ↑A ACC	3-2
176	-A	CCC ∈ ACC	3-2
180	-G	ACC ∈ CGT	4-2
196	-G	ACT ∈ GCG	3-3
199	-G	GGC ∈ GGC	4-2
228	-C	TTG ∈ CAC	5-2
230	+A	GCC ↑A CCT	2-4
250	+C	GCA ↑C GCG	1-3
250	-C	GCA ↑C GCG	3-4
270	-C	TCG ∈ GGC	5-3, 5-4
313	-G	GGT ∈ GTG	3-2
355	-G	AGC G GCG	4-4, 5-1
389	-G	AGT G GGC	1-1 (2)
418	-C	TGA C CAG	1-3, 3-2
470	-C	TTT C TTG	5-3
484	-C	TGA C CAG	1-3(2), 5-4
507	+T	TTA ↑T TTT	5-3
598	-T	AAG ∓ TCT	1-1
666	-A	CCG ∈ TAG	1-2
675	+T	ACG ↑G GAA	3-3
746	+A	CCC ↑A CTG	2-1
836	-G	CTC ∈ GTA	1-2

Base Pair Position*	Mutation†	Sequence Context¶	Mouse
B. Frameshifts cont'd			
877	+C	TAT ↑C CCG	4-1
881	-C	CCG ~~C~~ CGT	4-2, 4-3
955	+G	TCA ↑G GGC	3-1
1006	-A	AAG ~~A~~ AAA	5-1
C. Deletions and Insertions			
Untreated			
592	DELETION	CCCA~~TTAA~~GTT	5-0
620-632	-CTGG	CTGGCTGGCTGG	5-0
B(a)P Treated			
-7/-8	DELETION	GCATGA~~TA~~GGCGC	3-2
179	DELETION	AAC~~CG~~CGTG	2-4
249	DELETION(249-279)	GC~~AC~~...~~AA~~AT	5-3
380	DELETION	CAA~~CG~~CG	5-2 (2)
395	DELETION(395-630)	CTG~~AT~~...~~TG~~GCAT	1-3
620-632	-CTGG	CTGGCTGGCTGG	4-1, 5-1
620-632	+CTGG	CTGGCTGGCTGG	5-1
D. Double Mutations			
Untreated			
-15/-14	GG → TT	GTA GG GC	5-0
65/66	GC → AA	AT GC CGG	1-0
92/93	CG → GA	TCC CG CG	4-0
886/887	AA → TT	TT AA CCA	1-0
1010/1011	AC → TT	AA AC CAC	3-0 (10)
B(a)P Treated			
146/148	G→A, G→C	GAA GCG G	2-4
153/154	T→A, G→T	CGA TG GC	5-4

Base Pair Position*	Mutation†	Sequence Context¶	Mouse
D. Double Mutations cont'd			
155/157	G→T, G→T	ATG GCG GA	3-3
221/222	G→T, G→T	ATT GG CG	2-3
534/535	T→C, G→A	GAC TG G GCGT	1-1
536/537	G→T, G→T	TG GG CGT	2-3
541/542	G→A, G→T	GT GG AGC	5-2
693/694	C→A, C→T	GTG CC ATG	2-3
699/700	C→A, C→A	TGT CC GG	3-4
785/786	G→T, C→A	GCC GC AA	3-1
847/848	C→A, G→T	ATA CG AC	3-3
1000/1001	G→A, A→T	GT GA AAA	3-2
E. Complex Mutations			
Untreated			
90/509	C→A, T→C	2 base substitutions	5-0
173/208	C→T, G→T	2 base substitutions	4-0
B(a)P Treated			
49-51	CGA→ATT	ATA CGA TGTC	3-3
180-182	GCG→ A	ACC GCG TGGC	3-3
357-358	CG → A	CGG CG GT	1-4
376-378	GCA → T	GC GCA AC	5-3
781-7853	GGG→TTT	CT GGG CG	4-1
784/928	C→A, C→A	2 base substitutions	5-4
896/899	+A, C→A	ATC ↑AAA C AGG	1-2

* Numbering of the *lacI* gene according to Farabaugh (1978).

† The mutation in the coding strand is reported.

¶ The mutated base(s) is (are) the center base(s); the first base of each codon is underlined. Bases in boldface include those possibly deleted or inserted. The deleted or substituted bases are stricken. The arrow indicates a possible site of base insertion.

÷ Number of occurrences, when more than one, per mouse.

independent mutations to the total number of detected mutations, was determined for each animal. The results which incorporated every treatment group indicated all mutation classes at G:C basepairs (i.e., GC → AT, GC → TA and GC → CG) significantly increased in frequency above background. The overall trends were more significant for GC → TA and GC → CG transversions ($p < 0.005$), than the increase in GC → AT transitions ($p<0.02$). The increases in MnF due to B(a)P were detected at CpG sites for GC → TA ($p<0.005$) and GC → CG ($p<0.02$) transversions and GC → AT transitions ($p<0.05$). Frameshifts were also significantly increased above background ($p<0.001$) largely reflecting the contribution of +/-1 frameshift events involving G:C basepairs (29/43). Class-specific MnF which did not increase significantly above background, were base substitutions at A:T basepairs ($p<0.54$) and all other types of mutations (deletions/insertions, complex changes and double mutants; $p<0.15$).

4. DISCUSSION

4.1. B(a)P-induced Mutant Frequency

We have analyzed the dose response of an environmentally important chemical, B(a)P, on the liver of C57Bl/6 Big Blue® male mice. A total of 25 mice (5/dose) were treated to B(a)P levels of 0, 62.5, 125, 250 and 500 mg/kg with a single i.p. dose. Two weeks after the i.p. injection, the mice were sacrificed and the *lacI*$^-$ mutations were assessed. Two methods were used to determine if the MF from each dose was statistically different from

Table XXII. Summary of relevant *lacI* mutations by class as a portion of the total mutation frequency.

		MUTATION FREQUENCY (X 10^5) BY EXPOSURE			
MUTATION	**CNTRL**	**B(*a*)P-62.5**	**B(*a*)P-125**	**B(*a*)P-250**	**B(*a*)P-500**
Transitions:					
GC → AT	1.8 (41)[a]	3.1 (21)	3.5 (29)	3.9 (14)	8.0 (11)
at CpG sites	1.1 (26)[b]	1.9 (13)	2.7 (22)	2.5 (9)	5.2 (7)
AT → GC	0.4 (9)	1.0 (7)	0.4 (3)	0.0 (0)	0.0 (0)
Transversions:					
GC → TA	1.1 (25)	3.1 (21)	5.9 (49)	6.9 (25)	29. (39)
at CpG sites	0.7 (17)	2.1 (14)	3.5 (29)	3.9 (14)	15. (21)
GC → CG	0.2 (5)	0.9 (6)	2.4 (20)	2.5 (9)	5.2 (7)
at CpG sites	0.08 (2)	0.6 (4)	1.9 (16)	1.4 (5)	4.5 (6)
AT → TA	0.2 (5)	0.3 (2)	0.6 (5)	1.4 (5)	0.0 (0)
AT → CG	0.2 (5)	0.4 (3)	0.2 (2)	0.0 (0)	0.7 (1)
Other mutations:					
+1/-1 Frameshifts	0.5 (11)	1.3 (9)	1.8 (15)	3.0 (11)	5.8 (8)
Deletions/Insertions	0.08 (2)	0.4 (3)	0.2 (2)	0.6 (2)	0.7 (1)
Complex changes	0.0 (0)	0.2 (1)	0.1 (1)	0.6 (2)	0.7 (1)
Double mutants	0.3 (7)	0.3 (2)	0.2 (2)	1.4 (5)	2.9 (4)
Mutation Frequency	**4.8 (110)[c]**	**11. (75)**	**16. (128)**	**20. (73)**	**53. (72)**

[a] The mutation frequency attributed to the class of mutation calculated by the percentage of mutations in the class multiplied by the total mutation frequency [e.g., From the percentage of GC → AT mutations in the control group at 37% (41/110) and the total mutation frequency of 4.8×10^{-5}, the mutation frequency of GC → AT transitions is $0.37 * 4.8 \times 10^{-5} = 1.8 \times 10^{-5}$].

[b] The tabulated values are reported as the mutation frequency for the class of mutation recovered at CpG sites.

[c] Number of independent occurrences.

one another. The first method was an analysis of variance (ANOVA) using the criteria of the least significant difference test. As indicated in Table XX, the MF of each dose was significantly different from one another with the exception of the nearest dose. Thus, the MF of the control and 62.5 mg/kg B(a)P treated groups were not significantly different from one another. However, by applying the Generalized Cochran-Armitage (GCA) method (Carr and Gorelick, 1995), the MFs of these groups were statistically different (see Table XIX). The ability to detect a significant difference between these two treatments was consistent with other studies which determined the necessary experimental design to detect a doubling in MF (Callahan and Short, 1995). This indicated, as one might expect, the Generalized Cochran-Armitage test might be better suited to detect differences in MF.

Once a selection of the mutants was sequenced (see Table XXI), other methods to analyze the mutagenic outcome of treatments used the mutational spectra as the basis for comparison. Mutations were divided into classes such as the specific transitions and transversions (see Table XXII) and the classes were compared. A method to compare these classes based on the Monte-Carlo estimation of the Fisher's Exact test has been described by Adams and Skopek (1987). Table XXIII presents the comparison of different spectra. As in the ANOVA, no statistical difference between the control and 62.5 mg/kg B(a)P-treated groups difference was detected.

A more detailed analysis was performed comparing the untreated and 125 mg/kg B(a)P-treated group because of the large size of the mutational spectra (>100 / group).

These mutational spectra were significantly different (Table XXIII). Further analysis shown in Table XXIV, by using a contingency χ^2 analysis, revealed the relative contributions of the various mutation classes to the total χ^2 value. The larger the χ^2 value for a particular class, the greater the class contributed to the overall difference. The contingency χ^2 analysis identified GC → AT transitions, AT → GC transitions, GC → TA transversions and GC → CG transversions as contributing the greatest to the differences in mutational spectra.

Using the Generalized Cochran-Armitage (GCA) method (Carr and Gorelick, 1995) a 125 mg/kg B(a)P treatment significantly increased the MnF over the untreated group. At the level of comparung MnF, the results of the GCA method and estimation of the Fisher's Exact test agreed with each other. However when the GCA method was expanded to identify mutation frequency class-specific differences, the results were not entirely consistent with those obtained from the contingency χ^2 analysis. From the contingency χ^2 analysis, the relative contribution of the AT → GC transitions to the total χ^2 value was approximately equal to that of the GC → TA transversions. This indicated there was a relative reduction of AT → GC transitions in the same order of magnitude as the induction of GC → TA transversions. Using the GCA method, the class-specific MnFs of AT → GC transitions from the 125 mg/kg B(a)P and untreated groups were statistically identical (0.4×10^{-5}; see Table XXII). AT → GC transitions were neither induced nor reduced, while in contrast GC → TA transversions increased 5.4 fold. The

effect of B(a)P on frameshift mutagenesis may also have been misinterpreted based on results of the estimation of the Fisher's exact test. Since the expected and observed occurrences of frameshifts were the same in both spectra, presumably one might have concluded there was no effect. A clear induction of frameshifts was observed ($p < 0.001$) with by using the GCA method. The main advantage of the GCA method was the inclusion of the MnF data from each individual animal. Thus the major source of variability, the interanimal variability (Callahan and Short, 1995), was considered.

The comparison of mutational spectra by the Monte Carlo estimation technique may be best applied if both treatment groups have similar MnF because the measured variable is mutation frequency and not isolated events further categorized as mutations. If the overall MFs or MnFs are similar, the use of the Monte Carlo estimation technique would be applicable since frequency could be factored out of the analysis. For example, the mutational spectra from the liver of genetically identical animals treated with 120 mg/kg B(a)P (Shane *et al.*, 1998) and the 125 mg/kg B(a)P treatment group were identical ($p=0.89$). The similarity of the B(a)P-induced mutational spectra indicated that the reesutls of the transgenic rodent mutagenesis assay was comparable between 2 independent experiments.

4.2. Biological Interpretation of B(a)P-Induced Mutagenesis.

The results of the GCA trend analysis identified the induction of mutations at G:C basepairs which are consistent with the biological action of B(a)P. The mutagenic properties of B(a)P arise during its metabolism and excretion. Of the many B(a)P

Table XXIII. Monte-Carlo estimations of the Fisher's Exact test to determine the difference in mutational spectra.

	Dose of B(a)P (mg/kg)				
	0	62.5	125	250	500
Dose of B(a)P (mg/kg)					
0		0.87	0.001	0.0005	<0.00001
62.5	0.87[Ψ]		0.11	0.043	0.006
125	0.001[Φ]	0.11		0.39	0.12
250	0.0005	0.043	0.39		0.098
500	<0.00001	0.006	0.12	0.098	

[Ψ]The probabilities listed in the table were calculated by Monte-Carlo estimation of the Fisher's exact test using the methods presented by Adams and Skopek (1987). The 95% confidence interval of the estimations was approximately 10-20% of the value.

[Φ]Underlined values indicate a significant difference ($p<0.05$).

Table XXIV. Contingency χ^2 analysis of background and B(a)P-induced (125mg/kg) mutational spectra of the liver of C57Bl/6 male mice.

Mutation Class	Spontaneous Background Spectra	B(a)P-induced spectra (125 mg/kg)
	41$^{\Psi}$	29
GC → AT	32$^{\Phi}$	38
	2.3$^{\Omega}$	2.0
	9	3
AT → GC	5.5	6.5
	2.2	1.8
	25	49
GC → TA	34	40
	2.5	2.1
	5	20
GC → CG	12	13
	3.7	3.2
	5	5
AT → TA	4.6	5.4
	0.03	0.03
	5	2
AT → CG	3.2	3.8
	1.0	0.82
	11	15
+/- 1 frameshifts	12	14
	0.09	0.08
	9	5
Other mutations$^{\propto}$	6.5	7.5
	1.0	0.84

$^{\Psi}$Number of observed independent mutations.

$^{\Phi}$ The expected frequency of mutations based on the given distribution of mutations.

$^{\Omega}$The contribution to the χ^2 value from the particular observation.

$^{\propto}$ 'Other mutations' are the sum of complex and double mutations, and insertions/deletions.

metabolites, the diol-epoxides are the mutagenic and tumorigenic compounds. The extent of the biological effect is dependent on the enantiomeric form of the diol-epoxide and the biological system (Stevens *et al.*, 1985). In mammalian systems, the enantiomer which was the predominant mutagenic/carcinogenic stereoisomer is (+)-7*R*,8*S*-dihydroxy-9*S*,10*R*-epoxy-7,8,9,10-tetrahydrobenzo(a)pyrene [(+)-*anti*-BPDE]. The enantiomer, (+)-*anti*-BPDE, predominantly modifies guanine either at the N2 or N7 position. B(a)P adducts and mutations at A:T basepairs have been reported, although to a lower extent than at G:C basepairs. The lack of B(a)P-induced mutations at A:T basepairs suggested that, these mutations did not contribute significantly to the MF.

Over the dose range of 62.5 to 500 mg/kg B(a)P, the dose response of $9.0 \pm 4.5 \times 10^{-5}$ MF / [100 mg/kg B(a)P] in the liver of C57Bl/6 Big Blue® male mice was linear. The value was comparable to other studies measuring the B(a)P-induced MF in Big Blue mice (Skopek *et al.*, 1996; Shane *et al.*, 1997). The dose response after 50 or 150 mg/kg B(a)P in the splenic T-lymphocytes was 6.8 and 5.9×10^{-5} MF / [100 mg/kg B(a)P] (Skopek *et al.*, 1996). In the liver of C57Bl/6 Big Blue® male mice treated with a total of 120 mg/kg B(a)P resulted in an average dose response of 6.3×10^{-5} MF / [100 mg/kg B(a)P] (Shane *et al.*, 1997). However, these results were obtained 3 days or less after the last treatment and a portion of the effect of B(a)P may not have been fixed into mutations. This was reflected by the average sectored plaque MF of 5.8×10^{-5} which corresponded to a dose response of 3.4×10^{-5} MF / [100 mg/kg B(a)P]. Adding the sectored and *in vivo* MF yielded a similar dose response as observed in our study. The biological implications

of a linear dose response was interpreted as the DNA repair pathways were saturated from 62.5 to 500 mg/kg B(a)P.

After 500 mg/kg B(a)P, the greatest increases in class-specific MnF were for GC → TA transversions (26-fold) and GC → CG transversions (7.4-fold). These increases were anticipated by the nature of B(a)P-induced mutagenesis which predominantly induce these transversions (Yang *et al.*, 1987; Mazur and Glickman, 1988). Frameshifts and GC → AT transitions were increased approximately 4 fold in the 500 mg/kg B(a)P treatment group over the untreated group.

An interesting observation was the portion of B(a)P-induced mutations at CpG sites in both the mutational spectra from the B(a)P-induced and untreated groups. In the background mutational spectra, the contribution was approximately 65% of mutations at G:C basepairs. This large percentage has been found in several other studies (Dycaico *et al.*, 1996; de Boer *et al.*, 1996; de Boer *et al.*, 1997) and has been attributed to mutagenic events at 5-methylcytosine such as deamination leading to a GC → AT transition. In general, these transitions decreased their relative contribution to the MF as the percentage of GC → TA transversions increase with increasing B(a)P dose. However, the percentage of GC → TA transversions at CpG sites was higher than expected based on the number of available sites in the *lacI* gene. A total of 81 G:C basepairs at CpG sites have been found mutated which compared to 155 G:C basepairs at sites other than CpG (de Boer and Glickman, 1998). In the cumulative B(a)P-induced spectra a total of 47 G:C basepairs were mutated compared to only 58 G:C basepairs at non-CpG sites. The preferentially

recovery (Fisher's Exact test: $p<0.004$) of GC → TA transversions at CpG sites may have been indicative of higher DNA adduction at 5-methylcytosine (Denissenko *et al.*, 1997)

5. CONCLUSIONS

The treatment of Big Blue male mice with 62.5, 125, 250 and 50 mg/kg B(a)P to resulted in a linear increase of $9.0 \pm 4.5 \times 10^{-5}$ MF / [100 mg/kg B(a)P]. The increase in MF primarily was due to mutagenic events at G:C basepairs since all mutation classes involving G:C basepairs increased with increasing B(a)P treatment. After 500 mg/kg B(a)P treatment, the highest induction GC → TA transversions (26-fold) and GC → CG transversions (7.4-fold) was observed. The GC → TA transversions were predominantly formed at CpG sites which suggested that B(a)P may preferentially adduct at CpG sites.

CHAPTER VII. DISCUSSION AND FUTURE DIRECTIONS

1. GENERAL DISCUSSION

The process in which a treatment with a chemical or physical agent induces a mutation is a complex and multifaceted process. It involves many stages and may include but is not limited to the following: exposure, activation, excretion, DNA damage, DNA repair, and replication. The contribution of each step may vary significantly depending on the biological system and agent. To understand the risk from exposure to potentially mutagenic treatments or exposures, I studied two aspects of the mutagenic process: First, I investigated the role of initial DNA damage distribution and compared it to the distribution of mutations along the same segment of DNA. Second, I analyzed the patterns of mutation induction and mutational spectra.

With respect to determining DNA damage and mutational spectra, the advent of automated DNA sequencing technology allowed detailed and extensive studies to be performed. The studies in this thesis relied extensively on this technology to facilitate the characterization of mutations and semi-automate the process of quantitating DNA damage at the nucleotide level. In this way I could determine the position and quantity of the location of CPDs and 64PyPy along a section of DNA.

The patterns of deposition were analyzed, and post-hoc correlations were determined. Statistical analyses were performed to determine if the 5' or 3' flanking

nucleotide affected the quantity of DNA damage of 64PyPy at 5'-TC-3' and CPD at 5'-TT-3' sites. 64PyPy were predominantly formed at 5'-YTC-3' sites ($p<0.02$; where Y=C,T). The effect of the 3' flanking nucleotide was 64PyPy were formed at lower frequencies at 5'-TCT-3'sites than 5'-TCD-3' sites (where D=A,C; $p<0.03$). No effect of flanking nucleotides was detected for CPDs recovered at 5'-TT-3' sites. When the quantity of 64PyPy or CPD were correlated to frequently mutated sites, high levels of DNA damage appeared to be necessary but not sufficient. There were two UV-induced frequently mutated sites and at these locations, either a large quantity of CPD or 64PyPy damage was recovered.

However, there were considerable numbers of sites that had high quantities of DNA damage, and no UV-induced mutations were recovered at these positions. Mutations have been recovered at or near these other highly damaged sites which implied the mutational assay was able to select for mutations at these positions (Cariello, 1994). Thus, the assay did not overly bias the correlation between DNA damage and mutational spectra. The lack of correlation between the quantity of the DNA damage and the frequency of mutations at a particular nucleotide indicated that DNA damage might not be a good biomarker for mutation risk. This interpretation may be especially true if DNA repair was sequence-specific. The work of Pfeifer and colleagues suggested that DNA repair rates of UV-induced CPDs and B(a)P-induced adducts at adjacent nucleotides may vary by as much as 15 to 20-fold (Tornaletti and Pfeifer, 1994; Wei *et al.*, 1995). Thus,

DNA sequence context affects repair rates to a similar extent it influences initial DNA damage deposition.

UVB light is presumed to be the predominant mutagenic component of sunlight because DNA absorbs UVB light efficiently up to 300 nm. The skin of C57Bl/6 female *lacI* transgenic mice showed a large increase in MnF after a total dose of 9.0 J/cm^2. The 11-fold induction of MnF was predominantly due to the increase in "UV-characteristic C→T and CC→TT transitions occurring at dipyrimidine sites. These mutations were also present in the *p53* gene isolated from nonmelanoma skin cancers (Brash *et al.*, 1991). A higher percentage of CC → TT transitions was recovered in tumors with a mutated *p53* gene (14%) than from the UVB-induced mutational spectrum (5%). This may be related to the difference(s) in exposure, skin or mutation selection. The mouse skin was exposed to 5 daily doses of 1.8 J/cm^2 UVB, whereas human skin is exposed at lower doses over a lifetime. Although DNA repair enzymes are considered conserved genes between species, the human and mouse XPC gene appear to recognize DNA lesions differently (Von Borstel, personal communication). The *p53* gene may preferentially be mutated at these sites or the number of available CC sites may be greater in *p53* than in *lacI*. Even with these different influences, the general pattern of UV-induced mutagenesis in the skin of the mouse and human was similar. This implicated UVB as a contributor to skin carcinogenesis and implied the *lacI* transgenic rodent mutagenesis assay may be used to investigate methods to reduce the influence of UVB light.

A comparison of UVB light exposures to two different transgenic mouse strains yielded significantly different mutational responses. The skin of the hairless backcross of the F1 progeny of hairless SKH1 mice and 40.6 (Muta™-Mouse) mouse was 70-fold more sensitive than the shaved skin of the *lacI* transgenic mouse based on extrapolating a linear response UVB light (Frijhoff *et al.*, 1997). The major unknown between the two studies was the effect of the different light sources. Small differences at the lower end of the spectrum would result in significantly different amounts of DNA damage. Another difference was the different structure of the skin (e.g., thickness, presence of follicles) which were still present in the *lacI* transgenic mouse. Even though the mutation frequency response was different, the mutational UVB-induced spectra showed similar levels of single and tandem GC → AT transitions. The similarity in mutational spectra indicated that there was a common biological mechanism.

In Chapter V, the mutagenic potential of UVA light was determined. UVA light is the predominant form of UV light that reaches the earth's surface. After 5 daily doses were administered (totaling 800 J/cm^2) to the skin of female C57Bl/6 mice, UVA light resulted in a MF of 17 ± 3.4 x 10^{-5}. The UVA-induced MF was a significant increase over the MF observed in the untreated animals (6.1 ± 0.5 x 10^{-5}). The recovery of GC→AT and tandem CC→TT transitions at dipyrimidine sites was surprising, due to the reduced DNA absorption at UVA light wavelengths. A small fraction (<1%) of the filtered light was below the classical UVA/UVB cutoff wavelength of 320 nm. The "UVB" portion of the light was from wavelengths between 318-320 nm, and this light

may have contributed to the induction of CPDs and 64PyPy. It would be extremely difficult to determine its relative contribution without the use of monochromatic light sources or UV filters with an extremely narrow range to specifically allow only light between 318-320 nm.

One of the most surprising results was the lack of AT → CG transversions recovered in the UVA-induced mutational spectrum from the skin of the *lacI* transgenic mouse. This class of mutation was the most predominant mutation recovered in the *aprt* gene in CHO cells after UVA irradiation (Drobetsky *et al.*, 1995). With such a high recovery of AT → CG transversions (45%) from UVA-exposure (Drobetsky *et al.*, 1995) and the relatively rare recovery of this mutation compared to other classes usually reported from mutagenesis experiments, Drobetsky and colleagues (1995) suggested it to be a "UVA-hallmark" mutation. The light source was filtered with no light (< 340 nm) reaching the cells. No CPDs were measured using an *in vitro* assay after extensive irradiation using an identical lamp and filter setup in a laboratory of a colleague (Drobetsky *et al.*, 1995). This implied that the traditional UV-induced DNA lesions were not the premutagenic lesion. The same *aprt* assay had been used for studying the mutagenic effects of UVB and UVC light and AT → CG transversions were not recovered as a result of these exposures. In the current experiments, the lack of AT → CG transversions recovered from the UVA-exposed mouse skin of mice warrants further investigation. Ideally, the lighting system used to expose mouse skin would be identical to that used in the *in vitro* CHO cell study.

Another interesting observation was the dose response curve of the UVA-induced MF as a function of UVA light dose. Rather than a linear response, the higher doses of UVA light resulted in a MF that was lower than expected. The *lacI* transgene was selectively neutral and, thus, all doses were additive given certain biological limits (Cosentino and Heddle 1996). An example of a biological limit would be chemical elimination from the body before the chemical was attached to the DNA or fixed into a mutation. In the case of a physical agent such as UVA light, excretion or elimination before interacting with the target organ (skin) was not a major confounding factor. The UVA light, which reached the skin stem cells, did induce mild erythema. The effect, swelling of the skin, may have reduced the total flux reaching the stem cells because increased hydration of skin reduced flux to the basal layers of skin (Tyrrell, and Pidoux, 1987). A clue as to the origin of the attenuated dose response was the high number of clonal expansion events in the UVA-induced mutational spectrum. The greater-than-expected clonal expansion events were confirmed by statistically comparing them to the number of clonal expansions in spontaneous mutational spectra from several experiments (unpublished data; Gorelick *et al.*, 1995). This suggested that increased clonal expansion events were induced by exposure to UVA light. The mutational spectrum of the clonal expansion events further confirmed that the elevated clonal expansion was a result of UVA light. With 26/38 GC $\rightarrow$ AT transitions at YpCpH sites recovered in the clonal expansion mutational spectra, they represented a similar mutational spectrum to the independent mutants recovered from UVA-exposed samples. Studies have shown that

UVA can induce apoptosis (Godar and Lucas, 1995), and the increased clonal expansion events were suggestive of apoptotic processes followed by repopulation. Confirmation that UVA light exposure induced the effect of increased clonal expansion events may be performed by DNA characterization of UVA-induced mutants from other UVA doses and by directly measuring the cell proliferation from skin. Unfortunately, this research is outside the scope of this thesis.

The novel finding of the potentially increased *in vivo* cell proliferation from UVA light exposure was possible by performing a dose-response experiment and characterizing a large number of mutations at the DNA sequence level. I was interested to determine if the same approach would reveal interesting findings for another chemical. I choose benzo(a)pyrene, B(a)P, since its mutagenic effects have been widely studied. C57Bl/6 male animals were treated with a single i.p. injection which yielded doses of either 0, 62.5, 125, 250 or 500 mg/kg B(a)P. The MF was linear as a dose function with an MF dose response of 9.0×10^{-5} / 100 mg/kg B(a)P. This was similar to other studies which reported values of $6\text{-}8 \times 10^{-5}$ / 100 mg/kg B(a)P (Skopek *et al.*, 1996; Shane *et al.*, 1997). The results of the experiment were extremely interesting when mutational spectra of similar B(a)P doses were compared. Shane and colleagues (personal communication) treated C57Bl/6 animals with 3 daily doses of 40 mg/kg B(a)P, which was very close to the single dose of 125 mg/kg B(a)P. Since the *lacI* transgene is selectively neutral, multiple doses gave an additive effect. Thus 3 doses of 40 mg/kg would equal a single dose of 125 mg/kg. The B(a)P-induced mutational spectra were compared by a Monte

Carlo estimation technique (Adams and Skopek, 1987). The comparison indicated that the two independent experiments resulted in identical mutational spectra ($p<0.90$).

The Monte Carlo estimation was applied to determine if the mutational spectra recovered from the untreated and treated animals were different. A comparison of the 125 mg/kg B(a)P–induced spectra and the background spectra revealed a significant difference. I wanted to compare estimated contributions of various mutation classes (e.g., GC → AT, AT → TA, etc.) to the total difference. I applied a Chi-squared analysis, which calculated the relative contributions of each mutation class to the total difference between spectra. A large value for a mutant class was interpreted as contributing more to the overall difference than a mutant class with a low Chi-square value. As shown in Table XXIV, the mutant classes that contributed most to the difference were, in decreasing order, GC → CG transversions, GC → TA transversions, GC → AT transitions, and AT → GC transitions. These mutant classes either increased or decreased relative to each other.

In subsequent analysis, I used a trend analysis of the class-specific mutation frequency (Carr and Gorelick, 1995). This approach combined the mutational spectra separated by class as shown in Table XXII with the mutation frequency. Using this type of analysis more appropriately identified types or classes of mutations, which were either increasing or decreasing relative to a background mutational spectrum. It was important to note that this method gains statistical power only when applied to the analysis of a dose-response experiment because it analyzed trends in data rather than comparing

occurrences, as with the Monte Carlo estimation. From the results of the trend analysis were B(a)P-induced mutagenesis was specific for mutations that originated at G:C basepairs. The base substitutions, which increased were the GC → TA and GC → CG transversions, the GC → AT transitions, and the +/-1 frameshifts. The increase in frameshift mutagenesis was attributed to the majority of the frameshifts occurring at G:C basepairs. The trend analysis proved to be an excellent analysis tool and its application produced an interpretation that was more in keeping with the accepted literature. Hence, the Big Blue® transgenic rodent mutagenesis assay and analysis tools were a very informative assay to reveal the *in vivo* mutagenic effects of chemical and physical agents. The application of these assays to screen agents for their potential to be human carcinogens is deemed as the assay's ultimate goal. The next two sections reflect on the applicability of transgenic rodent mutagenesis assays for this purpose.

2. MUTATION-BASED TRANSGENIC RODENT MODELS

The *λlacI* -transgenic, Big Blue® transgenic rodents (Kohler *et al.*, 1990; Kohler *et al.*, 1991) can be classified as mutation-based because the assay endpoint is the direct measurement of mutation. This model and the near-equivalent model, the *λlacZ*-transgenic Muta™Mouse mutational assay (Gossen *et al.*, 1989; Myhr, 1991), revolutionized the way *in vivo* mutation is measured. Before these systems were developed, cellular markers, such as the *hprt* gene, were the only methods with which to measure *in vivo* mutation. Systems, such as *hprt* mutagenesis assay, were often limited to

a couple of tissues (Albertini *et al.*, 1982). Now, with a transgene in every nucleated cell of the transgenic rodent, any and all tissues can be tested; consequently, a tremendous amount of information can been generated.

From studies presented in Chapters IV to VI, *in vivo* mutations were readily screened and measured, and the characterization of mutants at the DNA sequence level revealed insight into mutagenic mechanisms. The recovery of tandem CC → TT transitions after UVA skin treatment represented the first *in vivo* case in which these UV-characteristic mutations were detected and characterized. Additionally, I noted an increase in putative cell proliferation, as suggested by an increased proportion of mutants attributed to clonal expansions above background.

Being able to compare UVA-induced spectra against a large spontaneous mutation spectra recovered from the skin of the *lacI* transgenic mouse was key for detecting the apparent increase in cell proliferation. For the study of B(a)P dose-response in the liver of male C57Bl/6 transgenic mice, having a large mutational spectra was also critical for determining the types of mutational events induced by B(a)P. Induction of specific classes of mutations was detected by applying the Generalized Cochran-Armitage test (Carr and Gorelick, 1995).Thus, without access to large mutation databases and their associated analysis tools for comparison I could not have performed the analysis with the same degree of statistical power.

These transgenic-mutation models are being extended to include new targets. An additional mutational target was developed in both the λ*lacI* and λ*lacZ* transgenic rodents

using the target gene λ*cII* (Jakubczak *et al.*, 1996; Swiger *et al.*, 1999). The λ*cII* gene encodes a protein that activates transcriptional promoters in lambda that are essential for lysogenization. In the λ*cII* region mutations that lower the cII protein levels result in lambda's decreased ability to lysogenize. When grown under conditions that favor lysogeny, lambda prophages carrying such mutations (λ*cII*$^-$) survive only by entering the lytic pathway of development, thereby forming plaques. Prophages that are wild-type for the cII region (λ*cII*$^+$) integrate into the host genome and become part of the developing bacterial lawn. There are several benefits to using the λ*cII* gene as a mutational target. First, a selectable system can be used in which only λ*cII*$^-$ prophages grow. The selectable system considerably reduces labor and reagent costs compared to the traditional *lacI* colour plaque-screening assay. Second, the λ*cII* gene is only 300 bp, and the small size facilitates DNA characterization of mutants.

Another model that combines two mutational targets, λspi ("*s*ensitive to *P*2 *i*nterface" region of lambda) and the *E. coli gpt* gene, in one model is 'delta gpt' mouse (Nohmi *et al.*, 1996). The λspi$^-$ phenotype requires a mutation in two regions, the Red and Gam. Two mutations required within 2 kb increases the chances the mutation will be a deletion rather than two base substitutions. Deletions of an average 2 kb in length, were not easily detected by the *lacI* or *lacZ* gene. By using the λspi loci, treatments that induce deletions can be studied. The inclusion of the *gpt* gene provides a 456 bp target for base substitution events similar to the *lacI* or *lacZ* systems. The utility of this model is

currently being tested by the Japanese National Institute for Environmental Health Services.

Transgenic mutational models have seen an increase in popularity as researchers create double transgenic models. This has usually involved crossing the λ*lacI* transgenc model with a knockout model. The double transgenic animals are developed to determine the *in vivo* mutagenic effects of deletion of the knockout gene. Incorporating the genetically neutral transgene from every nucleated cell into a knockout model provides a unique system to study *in vivo* mutagenic effects.

3. TUMOR TRANSGENIC RODENT MODELS

Mutation transgenic models measure mutation and this endpoint, while extremely important, is not paramount from a public health standpoint. The ultimate endpoint of concern from a human perspective is life-threatening cancer. The application of the transgenic mutation models as short-term bioassays to determine the risk of cancer-inducing agents may have practical and scientific merit because mutagenic events usually are a significant part of the progression to cancer. They also offer reduced animal use and decreased time and expense. However, the mutational endpoint is only a part of the formula and has led to the development of tumor transgenic rodent models.

Even extrapolating from a rodent carcinogen to human carcinogen has an associated risk. For example, nongenotoxic carcinogens may not induce mutations and

may not be detected by mutation-based transgenic rodent models. Attempting to predict human carcinogens from a mutation-based model, or even a tumor-based model will carry a risk. One of the best correlations between rodent and human carcinogens appears to be chemicals defined as trans-rodent or trans-species carcinogens. These carcinogens induce tumors in both rats and mice. An even better correlation was determined when the trans-species carcinogens induce tumors in multiple sites in both the rats and mice (Tennant, 1993).

Tumor transgenic rodent lines are genetically initiated in the multistep process of carcinogenesis. They may improve the traditional carcinogen rodent bioassay. These "traditional" studies are the 2-year National Toxicology Program bioassays, which involved large numbers of both rats and mice, and typically take 5 years to complete all the follow-up analysis. The long turnaround time and ever increasing number of chemicals being put into commercial use are key motivators to generating alternative methods of testing. Two models that show promise are the p53 +/- (Donehower *et al.*, 1992) and TG.AC transgenic mice (Leder *et al.*, 1990).

The p53 +/- mice are hemizygous for the p53 allele and are genetically initiated because they have the first germline hit. The loss of one p53 allele increases the probability that a second event will involve the loss of the remaining allele and cause either a loss of tumor suppression or a gain of transforming activity (Hollstein *et al.*, 1991). The p53 +/- mice not only have increased sensitivity to mutagenic carcinogens but the tumors were detected by 6 months rather than the traditional 2 years. At 6 months, the

untreated animals had a low incidence of spontaneous tumors (Harvey *et al.*, 1993a; Harvey *et al.*, 1993b). In the 2-year bioassay, spontaneous tumor incidences were high and reduced the sensitivity of the assay. As an important mechanistic consideration, the tumors in the p53 +/- mice appeared at the same organ sites as did the B6C3F1 mice in the 2-year bioassays (Tennant *et al.*, 1995).

The p53 +/- mice did not appear to be susceptible to tumors induced by nongenotoxic carcinogens, while the TG.AC model seemed to develop tumors in response to this class of carcinogens (Tennant *et al.*, 1995). The TG.AC mice carry a v-Ha-*ras* oncogene fused to the promoter of the zeta-globin gene (Leder *et al.*, 1990). The v-Ha-*ras* transgene contains two point mutations, which confer to the mice a genetically initiated state. These mice develop papillomas as a result of chemical treatment by skin painting or other exposure routes. The incidence of spontaneous papillomas was low. Thus short-term (6 month) use of the TG.AC rodent assay, compared to the 2-year bioassay, may offer greater practical utility.

A strategy for the use of both the p53 +/- and TG.AC transgenic mice was proposed by Tennant *et al.* (1995) and is presented in Figure 10. The process involves the early identification of a chemical as being a bacterial mutagen or having a structure that is likely mutagenic. This class contains the greatest quantity of chemicals. A positive induction of tumors in the p53 +/- model would initiate an NTP study while a negative result would initiate a TG.AC study. A positive result from a p53 +/- and TG.AC study would recommend an NTP bioassay to be carried out. A negative result would

recommend that the chemical is "generally recognized as safe", respectively. A negative bacterial mutagen or structural alert would require a study be made using the TG.AC model. A positive result in the TG.AC study would mean that a NTP bioassay was recommended while a negative result would indicate a "safe" chemical. This approach was supported by the initial studies (Eastin, 1998a; Eastin *et al.*, 1998b) using the strategy described in Figure 10. Additional information as to the toxicity of mutagenic chemicals may be assessed by using a double-transgenic p53 +/- / λ*lacI* model. The tumor endpoint can be measured and, if additional toxicity data is required, the mutant frequency can be determined in either the *lacI* or *cII* gene. The database from the λ*lacI* rodents provides an excellent resource (de Boer and Glickman, 1998). Mutation data from the double transgenic p53 +/- / λ*lacI* model can be compared to the existing database (containing over 100 chemicals and > 10,000 mutations in the *lacI* gene). Therefore inferences as to the *in vivo* chemical mechanisms may be possible.

The future use of transgenic rodents in bioassays will be based on the initial information obtained from using the ground-breaking models, such as λ*lacI* rodents. However, the knowledge base of mouse genetics is rapidly increasing, and new and better alternatives will be developed. As the field of genomics passes from an information-gathering stage to an information-processing stage, the gap in understanding

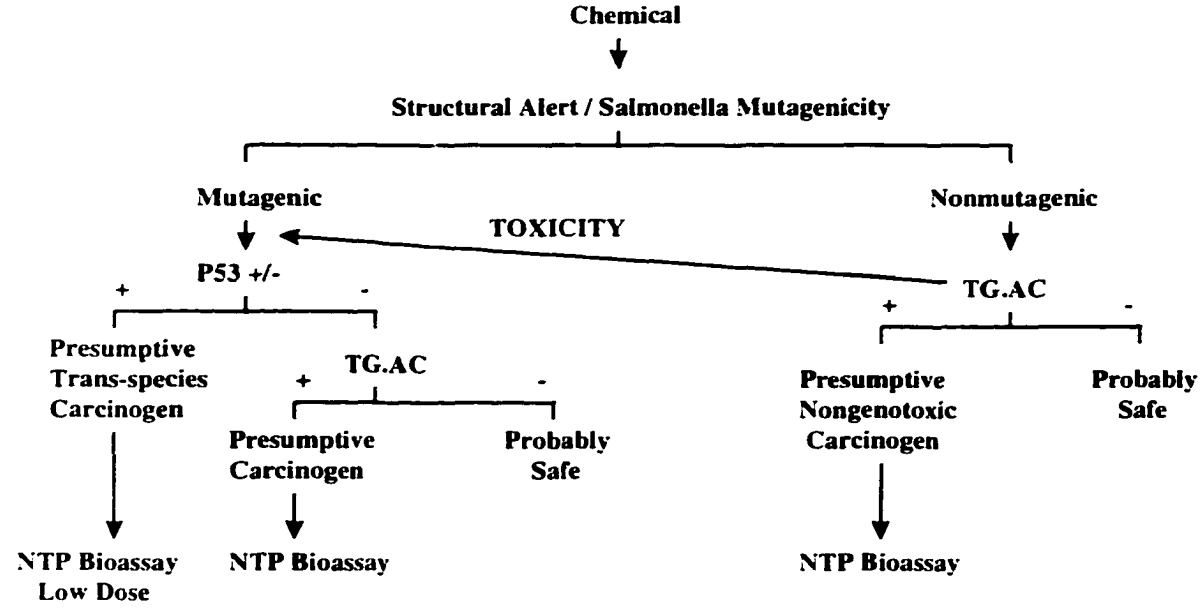

Figure 10. Strategy for the use of the p53 +/- and TG.AC mouse lines for short-term bioassays to identify carcinogens (adopted from Tennant et al., 1995).

why a chemical is a rodent carcinogen and not a human carcinogen will decrease. As transgenic techniques become more and more accessible to researchers, the future use of transgenic rodents in short-term bioassays will be exciting!

VIII. Bibliography

Adams, W.T. and T.R. Skopek (1987) Statistical test for the comparison of samples from mutational spectra. *J Mol Biol* **194**:391-396.

Albertini, R.J., K.L. Castle and W.R. Borcherding (1982) T-cell cloning to detect the mutant 6-thioguanine-resistant lymphocytes present in human peripheral blood. *Proc Natl Acad Sci USA* **79**:6617-6621.

Albro, P.W., P. Bilski, J.T. Corbett, J.L. Schroeder and C.F. Chignell (1997) Photochemical reactions and phototoxicity of sterols: novel self- perpetuating mechanisms for lipid photooxidation. *Photochem Photobiol* **66**:316-325.

Ames, B.N., J. McCann and E. Yamasaki (1975) Methods for detecting carcinogens and mutagens with *Salmonella*/mammalian-microsome mutagenicity test. *Mutat Res* **31**:347-364.

Ansorge, W., B. Sproat, J. Stegemann, C. Schwager, and M. Zenke (1987) Automated DNA sequencing: ultrasensitive detection of fluorescent bands during electrophoresis. *Nucleic Acids Res* **15**:4593-4602.

Armstrong, J.D., and B.A. Kunz (1990) Site and strand specificity of UV-B mutagenesis in the SUP4-o gene of yeast. *Proc Natl Acad Sci USA* **87**:9005-9009.

Armstrong, J.D., and B.A. Kunz (1992) Photoreactivation implicates cyclobutane dimers as the major promutagenic UVB lesions in yeast. *Mutat Res* **268**:83-94.

Baker, J.W. and G.E. Allen (1982) The Study of biology, Addison-Wesley Publishing Company Inc. Menlo Park, CA.

Banerjee, S.K., A. Borden, R.B. Christensen, J.E. LeClerc, and C.W. Lawrence (1990) SOS-dependent replication past a single trans-syn T-T cyclobutane dimer gives a different mutation spectrum and increased error rate compared with replication past this lesion in uninduced cells. *J Bacteriol* **172**:2105-2112.

Banerjee, S.K., R.B. Christensen, C.W. Lawrence, and J.E. LeClerc (1988) Frequency and spectrum of mutations produced by a single cis-syn thymine-thymine cyclobutane dimer in a single-stranded vector. *Proc Natl Acad Sci USA* **85**:8141-8145.

Barnhart, K.M., and G.T. Bowden (1985) Cisplatin as an initiating agent in two-stage mouse skin carcinogenesis. *Cancer Letters* **29**:101-105.

Basu-Modak, S., and R.M. Tyrrell (1993) Singlet oxygen: a primary effector in the ultraviolet A/near-visible light induction of the human heme oxygenase gene. *Cancer Res* **53**:4505-4510.

Beland, F.A., and F.F. Ladlubar (1985) Formation and persistence of arylamine DNA adducts *in vivo*. *Environ Health Perspect* **62:**19-30.

Belguise-Valladier, P, and R.P.P. Fuchs (1991) Strong sequence-dependent polymorphism in adduct-induced DNA structure analysis of single N-2-acetylaminofluorene residues bound within the NarI mutation hot spot. *Biochemistry* **30**:10091-10100.

Berg, R.J., H.J. van Kranen, H.G. Rebel, A. de Vries, W.A. van Vloten, C.F. van Kreijl, J.C. van der Leun and F.R. de Gruijl (1996) Early p53 alterations in mouse skin carcinogenesis by UVB radiation: immunohistochemical detection of mutant p53 protein in clusters of preneoplastic epidermal cells. *Proc Natl Acad Sci USA* **93**:274-278.

Bemelot-Moens, C., B.W. Glickman, and A.J.E Gordon (1990) Induction of specific frameshift and base substitution events by benzo[a]pyrene diol epoxide in excision-repair-deficient *Escherichia coli*. *Carcinogenesis* **11**:781-785.

Bizub, D., A.W. Wood, and A.M. Skala (1986) Mutagenesis of the Ha-ras oncogene in mouse skin tumors induced by polycyclic aromatic hydrocarbons. *Proc Natl Acad Sci USA* **83**:6048-6052.

Boerrigter, M.E.T.I, M.E.T. Dolle, J.H. Maartus, J.A. Gossen and J. Vijg (1995) Plasmid-based transgenic mouse model for studying in vivo mutations. *Nature* **377**:657-659.

Boerrigter, M.E.T.I, and J. Vijg (1997) Sources of variability in mutant frequency determinations in different organs of lacZ plasmid-based transgenic mice: experimental features and statistical analysis. *Environ Mol Mutagen* **29**:221-229.

Boorstein, R.J., T.P. Hilbert, R.P. Cunningham and G.W. Tebor (1990) Formation and stability of repairable pyrimidine photohydrates in DNA. *Biochemistry* **29**:10455-10460.

Brash, D., S. Seetharam, K.H. Kraemer, M.M. Seidman, and A. Bredberg (1987) Photoproduct frequency is not the major determinant of UV base substitution hot spots or cold spots in human cells. *Proc Natl Acad Sci USA* **84**:3782-3786.

Brash, D.E., and W.A. Haseltine (1982) UV-induced mutation hotspots occur at DNA damage hotspots. *Nature* **298**:189-192.

Brash, D.E., J.A. Rudolph, J.A. Simon, A. Lin, G.J. McKenna, H.P. Baden, A.J. Halperin and J. Ponten (1991) A role for sunlight in skin cancer: UV-induced p53 mutations in squamous cell carcinoma, *Proc Natl Acad Sci USA* **88**:10124-10128.

Brash, D.E., S. Seetharam, K.H. Kraemer, M.M. Seidman and A. Bredberg (1987) Photoproduct frequency is not the major determinant of UV base substitution hot spots or cold spots in human cells, *Proc Natl Acad Sci USA* **84**:3782-3786.

Brouwer, J., J. van der Putte, A.M.J. Fichtinger-Schepman, and J. van Reedijk (1981) Base pair substitution hotspots in GAG and GCG nucleotide sequences in *Escherichia coli* K-12 induced by cis-diamminedichloroplatinum(II). *Proc Natl Acad Sci USA* **78:**7010-7014.

Bruls, W.A., H. Slaper, J.C. van der Leun, and L. Berrens (1984) Transmission of human epidermis and stratum corneum as a function of thickness in the ultraviolet and visible wavelengths. *Photochem Photobiol* **40**:485-494.

Buening, M.D., PG. Wislocki, W. Levin, H. Yagi, D.R. Thakker, H. Akagi, M. Koreeda, D.M. Jerina, and A.H. Conney (1978) Tumorigenecity of the optical enantiomers of the diastereomeric benzo[a]pyrene-7,8-diol-9,10-epoxides in newborn mice: exceptional activity of (+)-7-beta,8-alpha-dihydroxy-9-alpha,10-aplha-epoxy-7,8,9,10-tetrahydrobenzo[a] pyrene. *Proc Natl Acad Sci USA* **75**:5358-5361.

Burnhouf, D., P. Koehl, and R.P.P. Fuchs (1989) Single adduct mutagenesis: strong effect of the position of a single acetylaminofluorene adduct within a mutation hot spot. *Proc Natl Acad Sci USA* **86**:4147-4151.

Callahan, J.D. and J.M. Short (1995) Transgenic *lacI* mutagenicity assay: statistical determination of sample size. *Mutat Res* **327**:201-208.

Calsou, P., P. Frit, and B. Salles (1992) Repair synthesis by human cell extracts in cisplatin-damaged DNA is preferentially determined by minor adducts. *Nucleic Acids Res* **20**:6363-6368.

Campbell, C., A.G. Quinn, B. Angus, P.M. Farr, and J.L. Rees (1993) Wavelength specific patterns of p53 induction in human skin following exposure to UV radiation. *Cancer Res* **53**:2697-2699.

Cariello, N.F., J.A. Swenberg, and T.R. Skopek (1992) *In vitro* mutational specificity of cisplatin in the human *hypoxanthine guanine phosphoribosyltransferase* gene. *Cancer Res* **52**:2866-2873.

Cariello, N.F. (1994) Database and software for the analysis of mutations at the human *hprt* gene. *Nucleic Acids Res* **22**:3547-3548.

Cariello, N.F. and T.R. Skopek (1993) Analysis of mutations occurring at the human *hprt* locus. *J Mol Biol* **231**:41-57.

Cariello, N.F., T.R. Craft, H. Vrieling, A.A. van Zeeland, T. Adams and T.R. Skopek (1992) Human *HPRT* Mutant Database: Software for Data Entry and Retrieval. *Environ Mol Mutagen* **20**:81-83.

Carothers, A.M., G. Urlaub, D. Grunberger, and L.A.Chasin (1988) Mapping and characterization of mutations induced by benzo[a]pyrene diol epoxide at *dihydrofolate reductase* locus in CHO cells. *Somat Cell Mol Genet* **14**:169-183.

Carr, G.J. and N.J. Gorelick (1994) Statistical tests of significance in transgenic mutation assays: considerations on the experimental unit. *Environ Mol Mutagen* **24**:276-282.

Carr, G.J. and N.J. Gorelick (1995) Statistical design and analysis of mutation studies in transgenic mice. *Environ Mol Mutagen* **25**:246-255.

Carr, G.J. and N.J. Gorelick (1996) Mutational spectra in transgenic animal research: data analysis and study design based upon the mutant or mutation frequency. *Environ Mol Mutagen* **28**:405-413

Chen, R.H., V.M. Maher, and J.J. Mccormick (1990) Effect of excision repair by diploid human fibroblasts on the kinds and locations of mutations induced by (racemic)-7-beta,8-alpha-dihydroxy-9-alpha,10-alpha-epoxy-7,8,9,10-tetrahydrobe nzo(a)pyrene in the coding region of the HPRT gene. *Proc Natl Acad Sci USA* **87**:8350-8354.

Chen, D.Y., H. P Swerdlow, H.R. Harke, J.Z. Zhang, and N.J. Dovichi (1991) Low-cost, high-sensitivity laser-induced fluorescence detection for DNA sequencing by capillary gel electrophoresis. *J Chromatogr* **559**:237-246.

Cheng, S.C., B.D. Hilton, J.M. Roman, and A. Dipple (1989) DNA adducts from carcinogenic and noncarcinogenic enantiomers of benzo[a]pyrene dihydrodiol epoxide. *Chem Res Toxicol* **2**:334-340.

Cleaver, J.E., J. Jen, W.C. Charles, and D.L. Mitchell (1991) Cyclobutane dimers and (6-4)-photoproducts in human cells are mended with the same patch sizes. *Photochem Photobiol* **54**:393-402.

Comess, K. M., J.N. Burstyn, J.M. Essigmann, and S.J. Lippard (1992) Replication inhibition and translesion synthesis on templates containing site-specifically placed cis-diamminedichloroplatinum(II) DNA adducts. *Biochemistry* **31**:3975-3990.

Coohill, T.P., M.J. Peak, and J.G. Peak (1987) The effects of the ultraviolet wavelengths of radiation present in sunlight on human cells *in vitro*. *Photochem Photobiol* **46**:1043-1050.

Cosentino, L., and J.A. Heddle (1996) A test for neutrality of mutations of the *lacZ* transgene. *Environ Mol Mutagen* **28**:313-316.

Coulondre, C., and J.H. Miller (1977) Genetic studies of the lac repressor. IV. Mutagenic specificity in the *lacI* gene of *Escherichia coli*. *J Mol Biol* **117**:577-606.

Christophers, A.J. (1998) Melanoma is not caused by sunlight. *Mutat Res* **422**:113-117.

Curry, J. (1993) The consequences of *in vivo* T-lymphocyte clonal expansion on mutation frequency as determined by the *hprt* clonal assay in an individual. York University.

Daya-Grosjean, L., N. Dumaz, and A. Sarasin (1995) The specificity of p53 mutation spectra in sunlight induced human cancers. *J Photochem Photobiol B* **28**:115-124.

de Boer, J.G., and B.W. Glickman (1989) Sequence specificity of mutation induced by the anti-tumor drug cisplatin in the CHO *aprt* gene. *Carcinogenesis* **10**:1363-1367.

de Boer, J.G., and B.W. Glickman (1992) Mutations recovered in the Chinese hamster *aprt* gene after exposure to carboplatin: a comparison with cisplatin. *Carcinogenesis* **13**:15-17.

de Boer, J.G. (1995) Software package for the management of sequencing projects using lacI transgenic animals. *Environ Mol Mutagen* **25**:256-262.

de Boer, J.G. and B.W. Glickman (1998) The *lacI* gene as a target for mutation in transgenic rodents and *Escherichia coli*. *Genetics* **148**:1441-1451.

de Boer, J.G., H. Erfle, D. Walsh, J. Holcroft, G.S. Provost, B.J. Rogers, K.R. Tindall, and B.W. Glickman (1997) Spectrum of spontaneous mutations in liver tissue of *lacI* transgenic mice. *Environ Mol Mutagen* **30**:273-286.

de Boer, J.G., H. Erfle, J. Holcroft, D. Walsh, M. Dycaico, S. Provost, J. Short, and B.W. Glickman (1996) Spontaneous mutants recovered from liver and germ cell tissue of low copy number *lacI* transgenic rats. *Mutat Res* **352**:73-78.

de Boer, J.G., J.C. Mirsalis, G.S. Provost, K.R. Tindall and B.W. Glickman (1996) Spectrum of mutations in kidney, stomach, and liver from *lacI* transgenic mice recovered after treatment with tris(2,3- dibromopropyl)phosphate. *Environ Mol Mutagen* **28**:418-423.

de Laat, A., J.C. van der Leun, and F.R. de Gruijl (1997) Carcinogenesis induced by UVA (365-nm) radiation: the dose-time dependence of tumor formation in hairless mice. *Carcinogenesis* **18**:1013-1020.

de Oliveira RC, D.T. Ribeiro, R.G. Nigro, P. di Mascio, and C.F. Menck (1992) Singlet oxygen induced mutation spectrum in mammalian cells. *Nucleic Acids Res* **20**:4319-4323.

Denissenko, M.F., J.X. Chen, M.S. Tang, and G.P. Pfeifer (1997) Cytosine methylation determines hot spots of DNA damage in the human *P53* gene. *Proc Natl Acad Sci USA* **94**:3893-3898.

Dizdaroglu, M., T.H. Zastawny, J.R. Carmical, and R.S. Lloyd (1996) A novel DNA N-glycosylase activity of E. coli T4 endonuclease V that excises 4,6-diamino-5-formamidopyrimidine from DNA, a UV-radiation- and hydroxyl radical-induced product of adenine. *Mutat Res* **362**:1-8.

Donehower, L.A., M. Harvey, B.L. Slagle, M.J. McArthur, C.A.J. Montgomery, J.S. Butel, and A. Bradley (1992) Mice deficient for p53 are developmentally normal but susceptible to spontaneous tumours. Nature, 356, 215-221.

Dorado, J., H. Steingrimsdottir, C.F. Arlett, and A.R. Lehmann, (1991) Molecular analysis of ultraviolet-induced mutations in a xeroderma pigmentosum cell line. *J Mol Biol* **217**:217-222.

Drobetsky E.A., A.J. Grosovsky, and B.W. Glickman BW (1987) The specificity of UV-induced mutations at an endogenous locus in mammalian cells. *Proc Natl Acad Sci USA* **84:**9103-9107.

Drobetsky, E. A., and E. Sage (1993) UV-induced G:C to A:T transitions at the *aprt* locus of Chinese hamster ovary cells cluster at frequently damaged 5'-TCC'3' sequences. *Mutat Res* **289**:131-136.

Drobetsky, E.A. and B.W. Glickman, (1990) The specificity of UV-induced mutations at an endogenous locus in mammalians cells, *Proc Natl Acad Sci USA* **84**:9103-9107.

Drobetsky, E.A., E. Moustacchi, B.W. Glickman, and E. Sage (1994) The mutational specificity of simulated sunlight at the aprt locus in rodent cells. *Carcinogenesis* **15**:1577-1583.

Drobetsky, E.A., J. Turcotte, and A. Chateauneuf (1995) A role for ultraviolet A in solar mutagenesis. *Proc Natl Acad Sci USA* **92**:2350-2354.

Drouin, E.E., and E.L. Loechler (1993) AP sites are not significantly involved in mutagenesis by the (+)-anti diol epoxide of benzo[a]pyrene: the complexity of its mutagenic specificity is likely to arise from adduct conformational polymorphism. *Biochemistry* **32**:6555-6562.

Dumaz, N., A. Stary, T. Soussi, L. Daya-Grosjean, and A. Sarasin (1994) Can we predict solar ultraviolet radiation as the causal event inhuman tumours by analysing the mutation spectra of the p53 gene? *Mutat Res* **307**:375-386.

Dumaz, N., C. Drougard, A. Sarasin, and L. Daya-Grosjean (1993) Specific UV-induced mutation spectrum in the p53 gene of skin tumors from DNA-repair-deficient xeroderma pigmentosum patients. *Proc Natl Acad Sci USA* **90**:10529-10533.

Dycaico, M.J., G.R. Stuart, G.M. Tobal, J.G. de Boer, B.W. Glickman and G.S. Provost (1996) Species-specific differences in hepatic mutant frequency and mutational spectrum among lambda/lacI transgenic rats and mice following exposure to aflatoxin B1. *Carcinogenesis* **17**:2347-2356.

Dycaico, M.J., G.S. Provost, P.L. Kretz, S.L. Ransom, J.C. Moores, and J.M. Short (1994) The use of shuttle vectors for mutation analysis in transgenic mice and rats. *Mutat Res* **307**:461-478.

Eastin, W.C. (1998a) The U.S. National Toxicology Program evaluation of transgenic mice as predictive models for identifying carcinogens. *Environ Health Perspect* **106**(Suppl 1):81-84.

Eastin, W.C., J.K. Haseman, J.F. Mahler, and J.R. Bucher (1998b) The National Toxicology Program evaluation of genetically altered mice as predictive models for identifying carcinogens. *Toxicol Pathol* **26**:461-473.

Emmons, S.W. (1974) bacteriophage lambda derivatives carrying two copies of the cohesive end site. *J Mol Biol* **83**:511-514.

Erfle, H.L., D.F. Walsh, J. Holcroft, N. Hague, J.G. de Boer, and B.W. Glickman (1996) An efficient laboratory protocol for the sequencing of large numbers of lacI mutants recovered from Big Blue transgenic animals. *Environ Mol Mutagen* **28**:393-396.

Farabaugh P.J., U. Schmeissner, M. Hoffer, and J.H Miller (1978) Genetic studies of the *lac* repressor VII. On the molecular nature of spontaneous hotspots in the *lacI* gene of *Escherichia coli. J Mol Biol* **126:**847-857.

Fichtinger-Schepman A.M.J., J.L. van der Veer, J.H.J. den Hartog, P.H.M. Lohman, and J. Reedijk (1985) Adducts of the antitumour drug cis-diaminedichloroplatinum(II) with DNA: formation, identification, and quantitation. *Biochemistry* **24**:707-713.

Fiess, M., and A. Campbell (1974) Duplication of the bacteriophage lambda cohesive end site: Genetic studies. *J Mol Biol* **83**:527-533.

Fiess, M., and A. Becker (1983) DNA packaging and cutting in: *Lambda II* (R.W. Hendrix), Cold Spring harbor Laboratory, Cold Spring Harbor, NY, pp. 305-330.

Frijhoff, A.F., H. Rebel, E.J. Mientjes, M.C. Kelders, M.J. Steenwinkel, R.A. Baan, Z.A. van Veeland, and L. Roza (1997) UVB-induced mutagenesis in hairless lambda lacZ-transgenic mice. *Environ Mol Mutagen* **29**:136-142.

Fuchs R.P., N. Schwartz,and M.P. Daune (1981) Hot spots of frameshift mutations induced by the ultimate carcinogen N- acetoxy-N-2-acetylaminofluorene. *Nature* **294**:657-659.

Fung, K.Y., D. Krewski, Y. Zhu, S. Shephard and W.K. Lutz (1997) Statistical analysis of the lacI transgenic mouse mutagenicity assay. *Mutat Res* **374**:21-40.

Gao, S., R. Drouin, and G.P. Golmquist (1994) DNA repair rates mapped along the human *PGK*1 gene at nucleotide resolution. *Science* **263**:1438-1440.

Gasparro, F.P., and J.R. Fresco (1986) Ultraviolet-induced 8,8-adenine dehydrodimers. *Nucleic Acids Res* **14**:4239-4251.

Gibbs, P.E., B.J. Kilbey, S.K. Banerjee, and C.W. Lawrence (1993) The frequency and accuracy of replication past a thymine-thymine cyclobutane dimer are very different in Saccharomyces cerevisiae and Escherichia coli. *J Bacteriol* **175**:2607-2612.

Glickman, B.W., R.M. Schaaper, W.A. Haseltine, R.L. Dunn, and D.E. Brash, (1986). The C-C (6-4) UV photoproduct is mutagenic in Escherichia coli, *Proc Natl Acad Sci USA* **83**:6945-6949.

Godar, D.E., and A.D. Lucas (1995) Spectral dependence of UV-induced immediate and delayed apoptosis: the role of membrane and DNA damage. *Photochem Photobiol* **62**:108-113.

Goodisman, J., and J. C. Dabrowiak (1992) Quantitative aspects of DNase I footprinting, in: *Advances in DNA Sequence Specific Agents* (L.H. Hurley ed.), JAI Press Inc., Greenwich, CT, pp. 25-50.

Gordon, L. K., and W. A. Haseltine (1982) Quantitation of cyclobutane dimer formation in double and single stranded DNA fragments of defined sequence. *Radiation Res* **89**:99-112.

Gorelick, N.J., J.L. Andrews, M. Gu, and B.W. Glickman (1995) Mutational spectra in the *lacI* gene in skin from 7,12- dimethylbenz[a]anthracene-treated and untreated transgenic mice. *Mol Carcinog* **14**:53-62.

Gossen, J.A., W.J. de Leeuw, C.H. Tan, E.C. Zwarthoff, F. Berends, P.H. Lohman, D.L. Knook, and J. Vijg (1989) Efficient rescue of integrated shuttle vectors from transgenic mice: a model for studying mutations *in vivo*. *Proc Natl Acad Sci USA* **86**:7971-7975.

Gupta, P.K., M.S. Lee, and C.M. King (1988) Comparison of mutagenesis induced in single- and double-stranded M13 viral DNA by treatment with N-hydroxy-2-aminofluorene. *Carcinogenesis* **9**:1337-1345.

Hansson, J., R.D.R. Wood, and D. Wood (1989) Repair synthesis by human extracts in DNA damaged by cis- and trans-diaminedichloroplatinum(II). *Nucleic Acids Res* **17**:8073-8091.

Harvey, M., M.J. McArthur, C.A.J. Montgomery, A. Bradley and L.A. Donehower (1993a) Genetic background alters the spectrum of tumors that develop in p53-deficient mice. *FASEB J* **7**:938-943.

Harvey, M., M.J. McArthur, C.A.J. Montgomery, J.S. Butel, A. Bradley, and L.A. Donehower (1993b) Spontaneous and carcinogen-induced tumorigenesis in p53-deficient mice. *Nat Genet* **5**:225-229.

Heddle, J.A., K. Tao, R.R. Swiger, and J.D. Tucker (1995) The transmission rate of the *lacI* transgene from the Big Blue mouse. *Mutat Res* **348**:63-66.

Hoffmann, J.S., U. Hubscher, B. Michot, and G. Villani (1991) Interaction of cis-diamminedichloroplatinum (II) with single-stranded DNA in the presence or absence of *Escherichia coli* single-stranded binding protein. *Biochem Pharmacol* **42**:1393-1398.

Hollstein, M., D. Sidransky, B. Vogelstein, and C.C. Harris (1991) p53 mutations in human cancers. *Science* **253**:49-53.

Hornstra, I.K., and T.P. Yang (1994) High-resolution methylation analysis of the human *hypoxanthine phosphoribosyltransferase* gene 5' region on the active and inactive X chromosomes: correlation with binding sites for transcription factors. *Mol Cell Biol* **14**:1419-1430.

Horsfall, M.J., and C.W. Lawrence (1994) Accuracy of replication past the T-C (6-4) adduct. *J Mol Biol* **235**:465-471.

Horsfall, M.J., A. Borden, and C.W. Lawrence (1997) Mutagenic properties of the T-C cyclobutane dimer. *J Bacteriol* **179**:2835-2839.

Huang, X. C., M.A. Quesada, and R.A. Mathies (1992) DNA sequencing using capillary array electrophoresis. *Anal Chem* **64**:2149-2154.

Ivanov, E.L., S.V. Koval'tsova, and V.G. Korolev (1983) [Molecular nature of direct gene mutations induced by gamma and ultraviolet irradiation in Saccharomyces cerevisiae yeasts]. *Genetika* **19**:1063-1069.

Iwahana, H., K. Yoshimoto, N. Mizusawa, E. Kudo, and M. Itakura (1994) Multiple fluorescence-based PCR-SSCP analysis. *Biotechniques* **16**:296-305.

Jakubczak, J.L., G. Merlino, J.E. French, W.J. Muller, B. Paul, S. Adhya, and S. Garges (1996) Analysis of genetic instability during mammary tumor progression using a novel selection-based assay for *in vivo* mutations in a bacteriophage lambda transgene target. *Proc Natl Acad Sci USA* **93**:9073-9078.

Jones, J.C., W. Zehn, E. Reed, R.J. Parker, A. Sancar, V.A. Bohr (1991) Gene-specific formation and repair of cisplatin intrastrand adducts and interstrand cross-links in Chinese hamster ovary cells. *J Biol Chem* **266**:7101-7107.

Karger, A. E., J.M. Harris, and R.F. Gesteland, (1991) Multiwavelength fluorescence detection for DNA sequencing using capillary electrophoresis. *Nucleic Acids Res* **19**:4955-4962.

Kempf S.R., and S. Ivankovic (1986) Carcinogenic effect of cisplatin (cis-diamminedichloroplatinum(II), CDDP) in BD IX rats. *J Cancer Res Clin Oncol* **111**:133-136.

Keohavong, P., V.L. Liu, and W.G. Thilly (1991) Analysis of point mutations induced by ultraviolet light in human cells. *Mutat Res* **249**:147-159.

Khrapko, K., J.S. Hanekamp, W.G. Thilly, A. Belenkii, F. Foret, and. B.L. Karger (1994) Constant denaturant capillary electrophoresis (CDCE): a high resolution approach to mutational analysis, *Nucleic Acids Res* **22**:364-369.

King, H.W.S., and P. Brookes (1984) The nature of mutation induced by the diol epoxide of benzo[a]pyrene in mammalian cells. *Carcinogenesis* **5**:965-970.

King, H.W.S., M.E. Osborne, and P. Brookes (1979) The in vitro and *in vivo* reaction at the N7-position of guanine of the ultimate carcinogen derived from benzo[a]pyrene. *Chem Biol Interactions* **24**:345-353.

Kinley, J.S., G. Brunborg, J. Moan, and A.R. Young (1995) Detection of UVR-induced DNA damage in mouse epidermis *in vivo* using alkaline elution. *Photochem Photobiol* **61**:149-158.

Kittler, L., and G. Lober (1977) Photochemistry of nucleic acids. *Photochem Photobiol Rev* **2**:39-45.

Knowles, R.J., and A. Eisenstark (1989) Near-ultraviolet mutagenesis in superoxide dismutase-deficient strains of *Escherichia coli. Environ Health Perspect* **102**:88-94.

Koehler, D. R., Awadallah, S. S., and Glickman, B. W., 1991, Sites of preferential induction of cyclobutane pyrimidine dimers in the nontranscribed strand of *lacI* correspond with sites of UV-induced mutation in *Escherichia coli. J Biol Chem* **266**:11766-11773.

Koffel-Schwartz, N., J.M. Verdier, M. Bichara, A.M. Freund, M.P. Daune, and R.P.P. Fuchs (1984) Carcinogen-induced mutation spectrum in wild-type, uvrA and umuC strains of *Escherichia coli. J Mol Biol* **177**:33-51.

Kohler, S.W., G.S. Provost, A. Fieck, P.L. Kretz, W.O. Bullock, J.A. Sorge, D.L. Putman, and J.M. Short (1991) Spectra of spontaneous and mutagen-induced mutations in the *lacI* gene in transgenic mice. *Proc Natl Acad Sci USA* **88**:7958-7962.

Kohler, S.W., G.S. Provost, P.L. Kretz, A. Fieck, J.A. Sorge, and J.M. Short (1990) The use of transgenic mice for short-term, *in vivo* mutagenicity testing. *Genet Anal Tech Appl* **7**:212-218.

Kotturi, G., de Boer J.G., B.F. Koop, and B.W. Glickman (1998) Correlation of UV-induced mutational spectra and the *in vitro* damage distribution at the human *hprt* gene. *Mutat Res* **403**: 237-248.

Kotturi, G., W.C. Kusser, and B.W. Glickman (1996) "DNA damage analysis using an automated DNA sequencer." in: G.P. Pfeifer (Ed.), Technologies for detection of DNA damage and mutations, Ed. G.P. Pfeifer, Plenum Press, New York, pp.185-196.

Kunala, S., and D.E. Brash (1992) Excision repair at individual bases of the *Escherichia coli lacI* gene: Relation to mutation hot spots and transcription coupling activity. *Proc Natl Acad Sci USA* **89**:11031-11035.

Lawrence, C.W., A. Borden, S.K. Banerjee, and J.E. LeClerc (1990) Mutation frequency and spectrum resulting from a single abasic site in a single-stranded vector. *Nucleic Acids Res* **18**:2153-2157.

LeClerc, J.E., A. Borden, and C.W. Lawrence (1991) The thymine-thymine pyrimidine-pyrimidone(6-4) ultraviolet light photoproduct is highly mutagenic and specifically induces 3' thymine-to-cytosine transitions in *Escherichia coli. Proc Natl Acad Sci USA* **88**:9685-9689.

Leder, A., A. Kuo, R.D. Cardiff, E. Sinn, and P. Leder (1990) v-Ha-ras transgene abrogates the initiation step in mouse skin tumorigenesis: effects of phorbol esters and retinoic acid. *Proc Natl Acad Sci USA* **87**:9178-9182.

Lee, J.A. (1989) The relationship between malignant melanoma of skin and exposure to sunlight. *Photochem Photobiol* **50**:493-496.

Leopold, W.R., E.C. Miller, and J.A. Miller (1979) Carcinogenecity of antitumour cis-platinum(II) coordination complexes in mouse and rat. *Cancer Res* **39**:913-918.

Lepre, C.A., and S.J. Lippard (1990) Interaction if platinum antitumour compounds with DNA, in: F. Eckstein and D.M.J. Lilley (Eds.), Nucleic Acids and Molecular Biology, Springer-Verlag, Berlin, pp. 3-9.

Ley, R.D. and A. Fourtanier (1997) Sunscreen protection against ultraviolet radiation-induced pyrimidine dimers in mouse epidermal DNA. *Photochem Photobiol* **65**:1007-1011.

Lichtenauer-Kaligis, E.G.R., J. Thijssen, H. den Dulk, P. van de Putte, M. Giphart-Gassler, and J.G. Tassseron-de Jong (1995) UV-induced mutagenesis in the endogenous *hprt* gene and in *hprt* cDNA genes integrated at different positions of the human genome. *Mutat Res* **326**:131-146.

Lippke, J.A., L.K. Gordon, D.E. Brash, and W.A. Haseltine (1981) Distribution of UV light-induced damage in a defined sequence of human DNA: detection of alkali-sensitive lesions at pyrimidine nucleoside-cytosine sequences. *Proc Natl Acad Sci USA* **78**:3388-3392.

Mackay, W., M. Benasutti, E. Drouin, and E.L. Loechler (1992) Mutagenesis by (dextro)-anti-B(a)P-N-2-Gua, the major adduct of activated benzo(a)pyrene, when studied in an Escherichia coli plasmid using site-directed methods. *Carcinogenesis* **13**:1415-1425.

Mane, S.S., D.M. Purnell, and I.C. Hsu (1990) Genotoxic effects of five polycyclic aromatic hydrocarbons in human and rat mammary epithelial cells. *Environ Mol Mutagen* **15**:78-82.

Mazur, M. and B.W. Glickman (1988) Sequence specificity of mutations induced by benzo[a]pyrene-7,8- diol-9,10-epoxide at endogenous *aprt* gene in CHO cells. *Som Cell Molec Genet* **14**:393-400.

McGregor, W.G., R.H. Chen, L. Lukash, V.M. Maher, and J.J. McCormick (1991) Cell cycle-dependent strand bias for UV-induced mutations in the transcribed strand of excision repair-proficient human fibroblasts but not in repair-deficient cells. *Mol Cell Biol* **11**:1927-1934.

Meehan, T., K. Straub, M. Calvin (1977) Benzo[alpha]pyrene diol epoxide covalently binds to deoxyguanosine and deoxyadenosine in DNA. *Nature* **269**:725-727.

Mellon, I., and P.C. Hanawalt (1989) Induction of the Escherichia coli lactose operon selectively increases repair of its transcribed strand. *Nature* **342**:95-98.

Mellon, I., G. Spivak, and P.C. Hanawalt (1987) Selective removal of transcription-blocking DNA damage from the transcribed strand on the mammalian *DHFR* gene. *Cell* **51**:241-249.

Menichini, P., H. Vrieling, and A.A. Van Zeeland (1991) Strand-specific mutation spectra in repair-proficient and repair-deficient hamster cells. *Mutat Res* **251**:143-156.

Mitchell, D.L., J. Jen and J.E. Cleaver (1992) Sequence specificity of cyclobutane pyrimidine dimers in DNA treated with solar (ultraviolet B) radiation. *Nucleic Acids Res* **20**:225-230.

Morin-Faure, J., and M. Marcollet (1983) Immunocytochemical study of the action of *cis*-dichlorodiamino platinum on the human metaphase chromosome. *Eur J Cell Biol* **30**:316-319.

Murov, S. L. (1973) *Handbook of Photochemistry*, M. Dekker Inc., New York.

Myhr, B.C. (1991) Validation studies with Muta Mouse: a transgenic mouse model for detecting mutations *in vivo*. *Environ Mol Mutagen* **18**:308-315.

Nohmi, T., M. Katoh, H. Suzuki, M. Matsui, M. Yamada, M. Watanabe, M. Suzuki, N. Horiya, O. Ueda, T. Shibuya, H. Ikeda, and T. Sofuni (1996) A new transgenic mouse mutagenesis test system using *Spi-* and 6- thioguanine selections. *Environ Mol Mutagen* **28**:465-470.

O'Neil, J.P., D.B. Couch, R. Machanoff, J.R. SanSebastian, P.A. Brimer, and A.W. Hsie (1977) A quantitative assay of mutation induction at the *hypoxanthine-guanine phosphoribosyl transferase* locus in Chinese hamster ovary cells (CHO/HGPRT system): utilization with a variety of mutagenic agents. *Mutat Res* **45**:103-109.

Park, J.G., and V.E. Chapman (1994) CpG island promoter region methylation patterns of inactive-X-chromosome *hypoxanthine phosphoribosyltransferase* (*hprt*) gene. *Mol Cell Biol* **14**:7975-7983.

Petinga, R.A., A.D. Andrews, R.E. Tarone, and J.H. Robbins (1977) Typical xeroderma pigmentosum complementation group A fibroblasts have detectable ultraviolet light-induced unscheduled DNA synthesis. *Biochim Biophys Acta* **479**:400-410.

Pfeifer, G.P., R. Drouin, A.D. Riggs, and G.P. Holmquist (1991) *In vivo* mapping of a DNA adduct at nucleotide resolution: Detection of pyrimidine (6-4) pyrimidine

photoproducts by ligation-mediated polymerase chain reaction, *Proc Natl Acad Sci USA* **88**:1374-8.

Pfeifer, G.P., R. Drouin, A.D. Riggs, and G.P. Holmquist (1992) Binding of transcription factors creates hot spots of for UV photoproducts *in vivo*. *Mol Cell Biol* **12**:1798-1804.

Piegorsch, W.W., A.C. Lockhart, G.J. Carr, B.H. Margolin, T. Brooks, G.R. Douglas, U.M. Liegibel, T. Suzuki, V. Thybaud, J.H. van Delft, and N.J. Gorelick (1997) Sources of variability in data from a positive selection *lacZ* transgenic mouse mutation assay: an interlaboratory study. *Mutat Res* **388**:249-289.

Piegorsch, W.W., A.M. Lockhart, C.J. Carr, B.H. Margolin, T. Brooks, G.R. Douglas, U.M. Liegibel, T. Suzuki, V. Thybaud, J.H.M. van Delft, and N.J. Gorelick (1995) Sources of variability in data from a positive selection lacZ transgenic mouse assay: An interlaboratory study. *Mutat Res* **388**:249-289.

Piegorsch, W.W., A.M. Lockhart, B.H. Margolin, K.R. Tindall, N.J. Gorelick, J.M. Short, G.J. Carr, E.D. Thompson, and M.D. Shelby (1994) Sources of variability in data from a *lacI* transgenic mouse mutation assay. *Environ Mol Mutagen* **23**:17-31.

Piegorsch, W.W., B.H. Margolin, M.D. Shelby, A. Johnson, J.E. French, R.W. Tennant and K.R. Tindall (1995) Study design and sample sizes for a lacI transgenic mouse mutation assay. *Environ Mol Mutagen* **25**:231-245.

Pienkowska, M., B.W. Glickman, A. Ferreira, M. Anderson, M. and Zielenska (1993) Large-scale mutational analysis of EMS-induced mutation in the *lacI* gene of *Escherichia coli*. *Mutat Res* **288**:123-131.

Pinto, A.L., and S.J. Lipard (1985) Binding of the antitumor drug cis-diaminedichloroplatinum(II) (cisplatin) to DNA. *Biochim Biophys Acta* **780**:167-180.

Porcher, C., M.C. Malinge, C. Picat, and B. Grandchamp (1992) A simplified method for determination of specific DNA or RNA copy number using quantitative PCR and an automated DNA sequencer. *Biotechniques* **13**:106-113.

Pott, P. (1775) Chirurgical Observations relative to the Cataract, the Polypus of the Nose, the Cancer of the Scrotum, the Different Kinds of Ruptures, and the Mortification of the Toes and Feet, Clarke and Collins, London.

Provost, G.S., P.L. Kretz, R.T. Hamner, C.D. Matthews, B.J. Rogers, K.S. Lundberg, M.J. Dycaico, and J.M. Short (1993) Transgenic systems for *in vivo* mutation analysis. *Mutat Res* **288**:133-149.

Quintanilla, M., K. Brown, M. Ransden, and A. Balmain (1986) Carcinogenic-specific mutation and amplification of Ha-ras during mouse skin carcinogenesis. *Nature* **322**:78-83.

Ravanat, J.L., and J. Cadet (1995) Reaction of singlet oxygen with 2'-deoxyguanosine and DNA. Isolation and characterization of the main oxidation products. *Chem Res Toxicol* **8**:379-388.

Reid, T.M., and L.A. Loeb (1993) Tandem double CC-->TT mutations are produced by reactive oxygen species. *Proc Natl Acad Sci USA* **90**:3904-3907.

Robert, C., B. Muel, A. Benoit, L. Dubertret, A. Sarasin, and A. Stary (1996) Cell survival and shuttle vector mutagenesis induced by ultraviolet A and ultraviolet B radiation in a human cell line. *J Invest Dermatol* **106**:721-728.

Roberts, J.J., and A.J. Thomson (1979) The mechanism of action of antitumor platinum compounds. *Prog Nucleic Acids Res Mol Biol* **22**:71-133.

Rodriguez, H., and E.L. Loechler (1993a) Mutational specificity of the dextro anti-diol epoxide of benzo(alpha)-pyrene in a *supF* gene of an *Escherichia coli* plasmid: DNA sequence context influences hotspots, mutagenic specificity and the extent of SOS enhancement of mutagenesis. *Carcinogenesis* **14**:373-383.

Rodriguez, H., and E.L. Loechler (1993b) Mutagenesis by the dextro-anti-diol epoxide of benzo(a)pyrene: What controls mutagenic specificity? *Biochemistry* **32**:1759-1769.

Runger, T.M., B. Epe, and K. Moller (1995) Processing of directly and indirectly ultraviolet-induced DNA damage in human cells. *Recent Results Cancer Res* **139**:31-42.

Rychlik, W., and R.E. Rhoads (1989) A computer program for choosing optimal oligonucleotides for filter hybridization, sequencing and *in vitro* amplification of DNA. *Nucleic Acids Res* **17**:8543-8551.

Sage, E., E. Cramb, and B.W. Glickman (1992) The distribution of UV damage in the *lacI* gene of *Escherichia coli*: Correlation with mutation spectrum. *Mutat Res* **269**:285-299.

Sage, E., and W.A. Haseltine (1984) High ratio of alkali-sensitive lesions to total DNA modification induced by benzo(a)pyrene diol epoxide. *J Biol Chem* **259**:11098-11102.

Sage, E. (1993) Distribution and repair of photolesions in DNA: genetic consequences and the role of sequence context. *Photochem Photobiol* **57**:163-174.

Sage, E., B. Lamolet, E. Brulay, E. Moustacchi, A. Chateauneuf and E.A. Drobetsky (1996) Mutagenic specificity of solar UV light in nucleotide excision repair-deficient rodent cells. *Proc Natl Acad Sci USA* **93**:176-180.

Sanger, F., Nicklen, S., and Coulson, A. R., 1977, DNA sequencing with chain-terminating inhibitors. *Proc Natl Acad Sci USA* **74**:5463-5467.

Sayer, J.M., A. Chadha, S.K. Agarwal, H.J.C. Yeh , H. Yagi, and D.M. Jerina (1991) Covalent nucleoside adducts of benzo(a)pyrene 7,8-diol 9,10-epoxides: Structural reinvestigation and characterization of a novel adenosine adduct on the ribose moiety. *J Organic Chemistry* **56**:20-29.

Schaaper, R.M. and B.W. Glickman (1982) Mutability of bacteriophage M13 by ultraviolet light: role of pyrimidine dimers. *Mol Gen Genet* **185**:404-407.

Schaaper, R.M., R.L. Dunn, and B.W. Glickman (1987) Mechanisms of UV-induced mutation: mutational spectra in the *Escherichia coli lacI* gene for a wild type and excision deficient strain. *J Mol Biol* **198**:187-202.

Schaaper, R.M., and R.L. Dunn (1987) Spectra of spontaneous mutations in *Escherichia coli* strains defective in mismatch correction: the nature of *in vivo* DNA replication errors. *Proc Natl Acad Sci USA* **84:**6220-6224.

Schaaper, R.M., N. Koffel-Schwartz, and R.P.P. Fuchs (1990) N-acetoxy-N-acetyl-2-aminofluroene-induced mutagenesis with the *lacI* gene of *Escherichia coli*. *Carcinogenesis* **11:**1087-1095.

Schorderet, D., and S. Gartler (1992) Analysis of CpG suppression in methylated and non-methylated species. *Proc Natl Acad Sci USA* **89**:957-981.

Segurado, O.G., and D.J. Schendel (1993) Identification of predominant T-cell receptor rearrangements by temperature-gradient gel electrophoresis and automated DNA sequencing. *Electrophoresis* **14**:747-752.

Setlow, R.B., E. Grist, K. Thompson, and A.D. Woodhead (1993) Wavelengths effective in induction of malignant melanoma. *Proc Natl Acad Sci USA* **90**:6666-6670.

Shane, B.S., A.M. Lockhart, G.W. Winston, and K.R. Tindall (1997) Mutant frequency of *lacI* in transgenic mice following benzo[a]pyrene treatment and partial hepatectomy. *Mutat Res* **377**:1-11.

Shane, B.S., J.G. De Boer, K.R. Tindall, and B.W. Glickman (in preparation) Mutational spectra in Big Blue transgenic mice treated with benzo(a)pyrene followed by a partial hepatectomy.

Shennan, M.G., C.M. Palmer, and H.E. Schellhorn (1996) Role of Fapy glycosylase and UvrABC excinuclease in the repair of UVA (320-400 nm)-mediated DNA damage in *Escherichia coli* [published erratum appears in *Photochem Photobiol* (1996) **64**:876]. *Photochem Photobiol* **63**:68-73.

Shibutani, S., and A.P. Grollman (1993a) Nucleotide misincorporation on DNA templates containing N-(deoxyguanosin-N^2-yl)-2-(acetylamino)fluorene. *Chem Res Toxicol* **6**:819-824.

Shibutani, S., and A.P. Grollman (1993b) On the mechanism of frameshift (deletion) mutagenesis *in vitro*. *J Biol Chem* **268**:11703-11710.

Shindo, Y. and T. Hashimoto (1997) Time course of changes in antioxidant enzymes in human skin fibroblasts after UVA irradiation. *J Dermatol Sci* **14**:225-232.

Short, J.M., S.W. Kohler, G.S. Provost, A. Feick, and P.L. Kretz (1990) The use of lambda phage shuttle vectors in transgenic mice for development of a short term mutagenicity assay, in: Anonymous Mutation and the Environment. Part A, Wiley-Liss, Inc., pp. 355-367.

Shoukry, S., M.W. Anderson, and B.W. Glickman (1991) A new technique for determining the distribution of N7-methyl guanine using an automated DNA sequencer. *Carcinogenesis* **12**:2089-2092.

Shoukry, S., M.W. Anderson, and B.W. Glickman (1993) Use of fluorescently tagged DNA and an automated DNA sequencer for the comparison of the sequence selectivity of SN1 and SN2 alkylating agents. *Carcinogenesis* **14**:155-157.

Skopek, T.R., K.L. Kort, and D.R. Marino (1995) Mutation of the endogenous hprt gene and the lacI transgene in ENU-treated Big Blue™ B6C3F1 mice. *Environ Mol Mutagen* **26**:9-15.

Skopek, T.R., K.L. Kort, D.R. Marino, L.V. Mittal, D.R. Umbenhauer, G.M. Laws, and S.P. Adams (1996) Mutagenic response of the endogenous *hprt* gene and *lacI*

transgene in benzo[a]pyrene-treated Big Blue B6C3F1 mice. *Environ Mol Mutagen* **28**:376-384.

Slaga, T.J., W.J. Bracken, G. Gleason, W. Levin, H. Yagi, B.M. Jerina, A.H. Conney (1979) Marked differences in skin tumor-initiating activities of the optical enantiomers of the diastereomeric benzo[a]pyrene-7,8-diol-9,10-epoxides. *Cancer Res* **39**:67-71.

Slaper, H., G.J. Velders, J.S. Daniel, F. R. de Gruijl, and J.C. van der Leun (1996) Estimates of ozone depletion and skin cancer incidence to examine the Vienna Convention achievements. *Nature* **384**:256-258.

Smith, L.M., S. Fung, M.W. Hunkapiller, T.J. Hunkapiller, and L.E. Hood (1985) The synthesis of oligonucleotides containing an aliphatic amino group at the 5' terminus: synthesis of fluorescent DNA primers for use in DNA sequence analysis. *Nucleic Acids Res* **13**:2399-2412.

Smith, L. M., J.Z. Sanders, R.J. Kaiser, P. Hughes, C. Dodd, C.R. Connell, C. Heiner, S.B.H. Kent, and L.E. Hood (1986) Fluorescence detection in automated DNA sequence analysis. *Nature* **321**:674-679.

Stary, A., C. Robert, and A. Sarasin (1997) Deleterious effects of ultraviolet A radiation in human cells. *Mutat Res* **383**:1-8.

Stevens, C.W., N. Bouck, J.A. Burgess, W.E. Fahl (1985) Benzo[a]pyrene diol-epoxides: different mutagenic efficiency in human and bacterial cells. *Mutat Res* **152**:5-14.

Stuart, G.R., N.J. Gorelick, J.L. Andrews, J.G. de Boer, and B.W. Glickman (1996) The genetic analysis of *lacI* mutations in sectored plaques from Big Blue transgenic mice. *Environ Mol Mutagen* **28**:385-392.

Swiger, R.R., L. Cosentino, N. Shima, J.H. Bielas, W. Cruz-Munoz, and J.A. Heddle (1999) The *cII* locus in the MutaMouse system. *Environ Mol Mutagen* **34**:201-207.

Tang, M.S., J.R. Pierce, R.P. Doisy, M.E. Nazimiec, and M.C. Macleod (1992) Differences and similarities in the repair of two benzo(a)pyrene diol epoxide isomers induced DNA adducts by uvrA, uvrB, and uvrC gene products. *Biochemistry* **31**:8429-8436.

Tao, K.S., C. Urlando and J.A. Heddle (1993) Comparison of somatic mutation in a transgenic versus host locus. *Proc Natl Acad Sci USA* **90**:10681-10685.

Tao, K.S., and J.A. Heddle (1994) The accumulation and persistence of somatic mutations *in vivo*. *Mutagenesis* **9**:187-191.

Tebbe, B., S. Wu, C.C. Geilen, J. Eberle, V. Kodelja, and C.E. Orfanos (1997) L-ascorbic acid inhibits UVA-induced lipid peroxidation and secretion of IL-1alpha and IL-6 in cultured human keratinocytes *in vitro*. *J Invest Dermatol* **108**:302-306.

Tennant, R.W. (1993) Stratification of rodent carcinogenicity bioassay results to reflect relative human hazard. *Mutat Res* **286**:111-118.

Tennant, R.W., J.E. French, and J.W. Spalding (1995) Identifying chemical carcinogens and assessing potential risk in short- term bioassays using transgenic mouse models. *Environ Health Perspect* **103**:942-950.

Tessman, I., and M.A. Kennedy (1991) The two-step model of UV mutagenesis reassessed: Deamination of cytosine in cyclobutane dimers as the likely source of the mutations associated with photoreactivation. *Mol Gen Genet* **227**:144-148.

Thakker, D.R., H. Yagi, W. Levin, A.W. Wood , A.H. Conney, and D.M. Jerina (1985) Bay-region diol epoxides, in: A.H. Anders (Ed.), Bioactivation of Foreign Compounds, Academic Press, New York, pp. 177-242.

Thrall, B.D., D.B. Mann, M.J. Smerdon, and D.L. Springer (1992) DNA polymerase, RNA polymerase and exonuclease activities on a DNA sequence modified by benzo[a]pyrene diolepoxide. *Carcinogenesis* **13**:1529-1534.

Tornanen, V.T., and G.P. Pfeifer (1992) Mapping of UV photoproducts within ras proto-oncogenes in UV-irradiated cells: Correlation with mutations in human skin cancer. *Oncogene* **7**:1729-1736.

Tornaletti, S. and G.P. Pfeifer (1994) Slow repair of pyrimidine dimers at p53 mutation hotspots in skin cancer. *Science* **263**:1436-1438.

Tornaletti, S., D. Rozek, and G.P. Pfeifer (1993) The distribution of UV photoproducts along the human *p53* gene and its relation to mutations in skin cancer. *Oncogene* **8**:2051-2058.

Tyrrell, R.M. (1996) Activation of mammalian gene expression by the UV component of sunlight - from models to reality. *Bioessays* **18**:139-148.

Tyrrell, R.M., and M. Pidoux (1987) Action spectra for human skin cells: estimates of the relative cytotoxicity of the middle ultraviolet, near ultraviolet, and violet regions of sunlight on epidermal keratinocytes. *Cancer Res* **47**:1825-1829.

Tyrrell, R.M., and M. Pidoux (1989) Singlet oxygen involvement in the inactivation of cultured human fibroblasts by UVA (334 nm, 365 nm) and near-visible (405 nm) radiations. *Photochem Photobiol* **49**:407-412.

van Duin, M., G. Vredeveldt, L.V. Mayne, H. Odijk, W. Vermeulen, B. Klein, G. Weeda, J.H. Hoeijmakers, D. Bootsma, and A. Westerveld (1989) The cloned human DNA excision repair gene ERCC-1 fails to correct xeroderma pigmentosum complementation groups A through I. *Mutat Res* **217**:83-92.

Veaute, X., and R.P.P. Fuchs (1991) Polymorphism in N-2-acetylaminofluorene induced DNA structure as revealed by DNase I footprinting. *Nucleic Acids Res* **19**:5603-5606.

Verpy, E., M. Biasotto, T. Meo, and M. Tosi (1994) Efficient detection of point mutations on color-coded strands of target DNA. *Proc Natl Acad Sci USA* **91**:1873-1877.

Vrieling, H., L.H. Zhang, A.A. van Zeeland, and M.Z. Zdienicka (1992) UV-induced *hprt* mutations in a UV-sensitive hamster cell line from complementation group 3 are biased towards the transcribed strand. *Mutat Res* **274**:147-155.

Vrieling, H., J. Venema, M.L. Van Rooyen, A. Van Hoffen, and P. Menichini (1991) Strand specificity for UV induced DNA repair and mutations in the Chinese hamster *HPRT* gene. *Nucleic Acids Res* **19**:2411-2416.

Vrieling, H., L.H. Zhang, A.A. Van Zeeland, and M.Z. Zdzienicka (1992) UV-induced hprt mutations in a UV-sensitive hamster cell line from complementation group 3 are biased towards the transcribed strand. *Mutat Res* **274**:147-155.

Wamer, W.G., and R.R. Wei (1997) *In vitro* photooxidation of nucleic acids by ultraviolet A radiation. *Photochem Photobiol* **65**:560-563.

Wang, Y.C., V.M. Maher, D.L. Mitchell, and J.J.Mccormick (1993) Evidence from mutation spectra that the UV hypermutability of Xeroderma pigmentosum variant cells reflects abnormal, error-prone replication on a template containing photoproducts. *Mol Cell Biol* **13**:4276-4283.

Wei, D., V.M. Maher, and J.J. Mccormick (1995) Site-specific rates of excision repair of benzo[a]pyrene diol epoxide adducts in the *hypoxanthine phosphoribosyltransferase* gene of human fibroblasts: Correlation with mutation spectra *Proc Natl Acad Sci USA* **92**:2204-2208.

Weinstein, I.B., A.M. Jeffrey, K.W. Jeanette, S.H. Blobstein, R.G. Harvey, C. Harris, H. Autrup, H. Kasai, and K. Nakanishi (1976) Benzo[a]pyrene diol epoxide intermediates in nucleic acid binding *in vitro* and *in vivo*. *Science* **193**:592-595.

Winegar, R.A., G. Carr and J.C. Mirsalis (1997) Analysis of the mutagenic potential of ENU and MMS in germ cells of male C57BL/6 *lacI* transgenic mice. *Mutat Res* **388**:175-178.

Wlaschek, M., J. Wenk, P. Brenneisen, K. Briviba, A. Schwarz, H. Sies, and K. Scharffetter-Kochanek (1997) Singlet oxygen is an early intermediate in cytokine-dependent ultraviolet-A induction of interstitial collagenase in human dermal fibroblasts *in vitro*. *FEBS Lett* **413**:239-242.

Wood, A.W., R.L. Chang, W. Levin, H. Yagi, D.R. Thakker, D.M. Jerina, and A.H. Conney (1977) Differences in mutagenicity of the optical enantiomers of the diastereoisomeric benzo[a]pyrene 7,8-diol-9,10-epoxides. *Biochem Biophys Res Commun* **77**:1389-1396.

Wyborski, D.L., L.C. DuCoeur, and J.M. Short (1996) Parameters affecting the use of the lac repressor system in eukaryotic cells and transgenic animals. *Environ Mol Mutagen* **28**:447-458.

Yamane, T., B.J. Wylunda, and R.G. Shulman (1967) Dihydrothymine from UV-irradiated DNA. *Proc Natl Acad Sci USA* **58**:439-443.

Yang, J.L., V.M. Maher, and J.J. McCormick (1987) Kinds of mutations formed when a shuttle vector containing adducts of (+/-)-7 beta, 8 alpha-dihydroxy-9 alpha, 10 alpha-epoxy-7,8,9, 10- tetrahydrobenzo[a]pyrene replicates in human cells. *Proc Natl Acad Sci USA* **84**:3787-3791.

Zhang, X., B.S. Rosenstein, Y. Wang, M. Lebwohl, D.M. Mitchell, and H. Wei (1997) Induction of 8-oxo-7,8-dihydro-2'-deoxyguanosine by ultraviolet radiation in calf thymus DNA and HeLa cells. *Photochem Photobiol* **65**:119-124.

Zhang, X.B., C. Urlando, K.S. Tao, and J.A. Heddle (1995) Factors affecting somatic mutation frequencies *in vivo*. *Mutat Res* **338**:189-201.

Zhu, Y., S. Bye, P.J. Stambrook, and J.A. Tischfield (1994) Single-base deletion induced by benzo[a]pyrene diol epoxide at the *adenine phosphoribosyltransferase* locus in human fibrosarcoma cell lines. *Mutat Res* **321**:73-79.

Ziegler, A., A.S. Jonason, D.J. Leffell, J.A. Simon, H.W. Sharma, J. Kimmelman, L. Remington, T. Jacks, and D.E. Brash (1994) Sunburn and p53 in the onset of skin cancer. *Nature* **372**:773-776.

Ziegler, A., D.J. Leffell, S. Kunala, H.W. Sharma, M. Gailani, J.A. Simon, A.J. Halperin, H.P. Baden, P.E. Shapiro, and A.E. Bale (1993) Mutation hotspots due to sunlight in the *p53* gene of nonmelanoma skin cancers. *Proc Natl Acad Sci USA* **90**:4216-4220.

Zwelling, L.A., M.O. Bradley, N.A. Sharkey, T. Anderson, and K.W. Kohn (1979) Mutagenicity, cytotoxicity and DNA crosslinking in V79 Chinese hamster cells treated with cis- and trans-Pt(II) diamminedichloride. *Mutat Res* **67**:271-280.